POLYMER MODIFICATION OF FULLERENE FOR PHOTODYNAMIC TUMOR THERAPY AND TUMOR IMAGING

JIAN LIU

2010

CONTENTS

ABBREVIATIONS

ASGPR	Asialoglycoprotein receptors
BMP	Bone morphogentic protein
BSA	Bovine serum albumin
CDI	N,N'-carbonyldiimidazole
CT	Computed X-ray tomography
DDS	Drug delivery system
DDW	Double-distilled water
DLS	Dynamic light scattering
DMAP	4-(dimethylamino)pyridine
DMSO	Dimethyl sulfoxide
DTPA	Diethylenetriaminepentaacetic acid
EPR	Enhanced permeability and retention
FCS	Fetal calf serum
FITC	Fluorescein isothiocyanate
H&E	Hematoxylin and eosin
HA	Hydroxyapatite
HBSS	Hanks balanced salt solution
HPLC	High performance liquid chromatography
KPB	Potassium phosphate-buffer
MALS	Multi-angle light scattering
MEM	Minimal essential medium
MRI	Magnetic resonance imaging
NIRF	Near-infrared fluorescence

PA	Pamidronic acid sodium salt
PBS	Phosphate-buffered saline solution
PDT	Photodynamic therapy
PEG	Poly(ethylene glycol)
PET	Positron emission tomography
QCM	Quartz crystal microbalance apparatus
R1	Longitudinal relaxation constant
RCA120	Ricinus communis agglutinin I
RI	Refractive index
ROS	Reactive oxygen species
SPECT	Single photon emission computed tomography
T1	Longitudinal relaxation time
TNBS	2, 4, 6-Trinitrobezenesulfonic acid
WST-8	2-(2-methoxy-4-nitrophenyl)-3-(4-nitrophenyl)-5-(2, 4-disulfophenyl)-2*H*-tetrazolium

GENERAL INTRODUCTION

With the recent development of molecular biology, cell biology, and genetic engineering, not only the classic low molecular weight drugs but also macromolecules, such as proteins and nucleic acids, have been used for clinical therapeutic applications [1-4]. To obtain the bioactivities expected, therapeutically sufficient amount of the drugs is required to deliver specifically to the targeting tissue or cells at the right timing. The achievement of this purpose needs to develop drug delivery system (DDS), which is a technology or methodology to enable the drugs of bioactive substance to enhance the therapeutic efficacy through controlled regulation of the release profile, absorption, distribution, and elimination in the body as well as to minimize their side effects [5-10]. The biomaterials to modify the bioactive substances is called drug carrier. For example, drugs are firstly modified with several carriers by a chemical or physical method, which usually enhances the water-solubility and absorption efficiency of drugs after the administration though various routes [11-13]. The carrier modification also increases the half-life period of drugs in the blood circulation [14-16] and promotes their subsequent transport across various biological barriers to the site of action and the consequent accumulation thereat [17-19]. In addition, it can achieve the sustained release of drugs over a period of time in a controlled manner [20-23].

The word of drugs not only means therapeutic substances as the conventional idea, but also includes other bioactive substances, such as diagnostic reagents, prophylactics, and even cosmetics. It should be noted that there are a wide variety of combinational ways between drugs and the carriers. Many carriers have been explored for their DDS application, for example liposomes, micelles, microspheres, capsules, and gels prepared from lipid, ceramics or synthetic and natural polymers [24-31]. Environmentally

responsive materials which can respond to some physical and chemical stimuli (for example, electric field, magnetic field, light, ultrasound, heat, and pH), have also been used for drug modification. It is reported that the DDS applications combined with physical and chemical stimuli artificially regulate the rate and position of drugs released to enhance their therapeutic efficacy [32-37].

One of the promising combination applications is photodynamic therapy (PDT) which is a non-invasive therapeutic treatment applicable for various types of tumor [38-40]. In general, the PDT needs to enhance the localization of a light-sensitive drug (photosensitizer) in the target tissue, followed by the local irradiation of tissue with light. It has been well recognized that reactive oxygen species (ROS) generated from the photosensitizer upon light irradiation acting as an effective cytotoxic agent to kill tumor cells [41, 42]. During last 30 years, the photochemical and photophysical principles of PDT have been extensively investigated, and many photosensitizers have been explored to evaluate the PDT efficacy in the in vitro and in vivo systems [43-46]. However, since the PDT has not always displayed the inherent potential, the clinical availability is still limited. There are some problems to be resolved for the clinical application [47-49]. For example, because most of photosensitizers developed are porphyrin-based dyes with low quantum yields, the exposure of high-power laser light is required to effectively generate ROS even if the laser damages normal tissues [50]. In addition, the poor tumor targetability of photosensitizers sometimes results in their distribution in the healthy tissues, which causes serious side effects [51, 52]. Furthermore, when the site for tumor PDT located at the deep position of body, the low permeation of light irradiated is of practical problem.

To overcome these problems, first of all, it is necessary to develop a photosensitizer with a high ROS generation efficiency. C_{60} is an example of fullerene

compounds which are molecules of pure carbon and characterized by a closed cage structure. Since the discovery in 1985 [53], C_{60} has been a subject of intensively used for various types of researches because of its unique structure, interesting properties, and many potential applications. The biological activity of C_{60} was first reported in 1993 [54], and after that, the characteristic bioactivities, such as the DNA cleavage, enzyme inhibition, antiviral activity, free radical quenching, gene transfection activities, and cytotoxicity, have been investigated [55-59]. It is well known that C_{60} can generate ROS in a high yield even by the exposure of weak visible light [60, 61], which expects us to regard the C_{60} as an excellent photosensitizer candidate for tumor PDT [62, 63].

The second key contributing to the PDT efficacy is to enhance the tumor targetability of photosensitizer. It is known that the solubility of C_{60} in water and most polar solvents is quite low and C_{60} itself has no targetability to tumor [64, 65]. Therefore, if the C_{60} can be used for PDT, the combination with DDS technology mentioned above is practically required. A detergent Tween-20, cyclodextrins, and phospholipids have been used to make C_{60} soluble in water [66-68]. Several water-soluble C_{60} derivatives, such as carboxylic acid derivatives, fullerenols, and amino acid derivatives, have been also prepared [69-73]. Among them, the chemical modification with water-soluble polymers is a promising strategy because in addition to the water solubilization, it can also increase the molecular size of C_{60} to that suitable for the enhanced accumulation in the tumor tissue based on the Enhanced Permeability and Retention (EPR) effect [74, 75]. The EPR effect is the phenomenon where a substance with a certain molecular size is susceptible to accumulation in the tumor tissue due to the anatomical features of blood vessel and lymph vasculatures in the tumor tissue [76-79].

The third important key for the PDT efficacy is the timing of light irradiation to maximize the efficiency of ROS generation at the tumor tissue. This is because the

highest PDT efficacy can be obtained if the light irradiation can be performed at the optimal time period when the concentration of photosensitizer accumulated in the tumor tissue becomes maximum. However, it is practically impossible to predict the optimal irradiation timing because the tumor accumulation pattern of photosensitizers greatly depends on the type, size, site and the malignancy of tumor. As one trial to tackle the problem, the combination of diagnostic technology is a practical promising strategy [75]. The combination of diagnosis and therapy may create a new field to apply not only to the tumor PDT but also to other drug therapies. If it is possible, the time schedule of drug administration may be optimized for every patient to enhance the therapeutic effects and subsequently reduce the side effects. There are clinical diagnoses by use of different imaging technologies, but the combination with therapy is still in infant. Because, so far, the research and development of therapy and diagnosis have been traditionally performed separately while little collaboration between the two research fields has been done. In addition, another reason is that pharmaceutical and medical researchers have scarcely been interested in the diagnostic application of DDS technology.

The noninvasive imaging technologies, such as magnetic resonance imaging (MRI), positron emission tomography (PET), single photon emission computed tomography (SPECT), near-infrared fluorescence (NIRF) imaging, and computed X-ray tomography (CT), have been widely used in clinical diagnosis. During or after the antitumor treatment, the PET can provide quick and accurate information about the treatment effectiveness within few days, while the CT can only show if tumor cells are still active by detecting the size increase of tumor mass over few months. Thus, the diagnosis plays an important role in the clinical tumor treatment [80]. However, each imaging modality is based on quite different principles and has the advantages and disadvantages. A single technique does not possess all the capabilities required for

comprehensive imaging [81]. The MRI and CT have the advantages to enable in vivo noninvasive imaging and high resolution three-dimensional tomography, but their usage is often limited by the low sensitivity of target to be detected. On the other hand, radioactive imaging techniques, such as PET and SPECT, have very high target sensitivity, but poor spatial resolution. An optical imaging method with fluorescence has relatively good sensitivity, but does a large issue to be resolved, so-called the low efficiency of light permeation. Therefore, multimodal imaging methods, which combine different imaging modalities to form a combinational imaging system, can compensate the deficiencies of single imaging modalities while they give useful and new tools to biomedical researches and clinical diagnostics. Currently, some prototypes of multimodal imaging system including MRI–optical, NIRF–SPECT, PET-CT, and SPECT-MRI, have been introduced [82-85]. However, the research and development of multimodal imaging probes are still in an early stage although they are highly required to realize the multimodal imaging. To design and prepare the multimodal imaging system, it is of prime necessity to make use of DDS technology. The main contribution of DDS technology is to enhance the accumulation of imaging agents in the target tissue, resulting in the higher S/N ratio. In addition, it is practically possible to combine different imaging probes by use of DDS carriers. On the other hand, the combination of imaging probes with therapeutic drugs is also possible to design and prepare a hybrid DDS system of diagnosis and therapy.

Currently, the tumor imaging has been popular because of the clinical significance [80]. For example, the molecular imaging technology permits accurate characterization of tumor biological properties and subsequently tumor treatment most effective based on the tumor properties. The imaging technology will be useful for diagnosis of disease other than tumor as well as new therapies, such as therapy of regeneration medicine. The

regenerative therapy is a new strategy to treat diseases based on the natural-healing potential of patients themselves. An injured or defected tissue, such as bone, cartilage, skin, and nerve tissues, are regenerated and repaired by cell transplantation and biomaterials for the DDS of growth factors and cell scaffold [86-89]. However, the process of tissue regeneration cannot always be evaluated by the convention diagnosis. For example, the clinical imaging of bone tissue is normally being performed by CT. However, the imaging method cannot provide detailed information of soft tissue and bone tissues regenerated in the early stage [90, 91]. If a new method to image the bone tissue regenerated is developed, clinical diagnosis for bone regeneration therapy will be more reliable. In addition, it can also give a diagnostic strategy to evaluate whether or not the process of tissue regeneration takes place properly.

The objective of this thesis is to design and prepare various types of water-soluble fullerene (C_{60}) conjugates by taking advantage of DDS technologies and evaluate the effect of their physicochemical properties on the photodynamic antitumor activity (the therapeutic function) as well as the imaging ability (the diagnostic function). In part I, C_{60} was modified with water soluble polymers of varied molecular weights and terminal structures and in various coupling manners to prepare different C_{60} conjugates. The C_{60}-polymer conjugates were evaluated in terms of the material properties, the body distribution, and in vitro or in vivo antitumor activity to obtain the basic knowledge of material design to optimize the tumor PDT efficacy of C_{60}-polymer conjugates. In part II, molecular imaging probes were combined with the C_{60} conjugate for tumor PDT to design a new hybrid DDS with therapeutic and diagnostic functions. In addition, a new multimodal imaging material was designed by the DDS technology of polymer conjugation to image the bone tissue newly regenerated.

Chapter 1 describes the effect of molecular weight and terminal structure of polyethylene glycol (PEG) on the photodynamic antitumor activity of PEG-modified C_{60} (C_{60}-PEG conjugates). The PEG samples with different terminal structures and molecular weights were covalently coupled to C_{60} and their generation of superoxide anion of ROS, in vitro or in vivo antitumor activity, and body distribution were assessed for the photosensitizer of PDT. Irrespective of the molecular weight and terminal structure of PEG used, the C_{60}-PEG conjugates exhibited similar superoxide anion generation ability and in vitro antitumor activity. On the contrary, the strong activity to suppress the in vivo tumor growth was observed for the C_{60}-PEG conjugate prepared by methyl-terminated PEG with the highest molecular weight. The conjugate showed the longest half-life period of blood circulation and the highest tumor accumulation among all the conjugates used. On the other hand, the C_{60}-PEG conjugates prepared from PEG with amino terminal groups showed poor tumor accumulation, resulting in the decreased antitumor activity. It is concluded that a superior tumor targetability of C_{60}-PEG conjugates which can be modified by the type of PEG used is one of the keys to enhance the PDT efficacy.

Chapter 2 describes the preparation and cytospecific photodynamic antitumor activity of C_{60} modified by pullulan (C_{60}-pullulan conjugates). By a reductive amination reaction, ethylene diamine was introduced to the terminal aldehyde group of pullulan, which is a water-soluble polysaccharide with a high affinity for asialoglycoprotein receptors. Pullulan was coupled to C_{60} through the terminal amine group. The C_{60}-pullulan conjugate significantly suppressed the in vitro growth of HepG2 hepatoma cells with asialoglycoprotein receptors, while less suppression activity was observed for HeLa cells without the receptors. The conjugate has a high binding affinity for HepG2 cells, in contrast to HeLa cells. On the contrary, the dependence of cell type on the in vitro cell binding and antitumor activities was not observed for C_{60}-PEG with the similar molecular

weight. Following the intravenous injection of C_{60}-pullulan conjugate to mice carrying a subcutaneous mass of HepG2 cells, significantly stronger antitumor effect was observed than the intravenous injection of C_{60}-PEG conjugates and saline. It is concluded that the pullulan conjugation gave C_{60} the targetability to HepG2 cells, resulting in enhanced photodynamic antitumor activity.

Chapter 3 describes the effect of pullulan molecular weight and the modification manner to C_{60} on the photodynamic antitumor activity of C_{60} modified with pullulan. Two modification manners were performed. First, ethylene diamine was chemically introduced to the hydroxyl groups of pullulan with different molecular weights. Then, C_{60} was coupled to pullulan through the amino group introduced (pendant type). Second, similar to Chapter 2, pullulan with the terminal amino group was coupled to C_{60} (terminal type). Irrespective of the pullulan molecular and the modification manner, the C_{60}-pullulan conjugates exhibited the similar ability to generate superoxide anions upon the irradiation of light. When compared between the C_{60}-pullulan conjugates of pendant and terminal types, a high lectin affinity was observed for the latter conjugates. The conjugates showed a high affinity for HepG2 cells with ASGPR and the consequent strong in vitro antitumor activity on the cells. It is conclude that the manner of pullulan modification is a key factor contributing to the photodynamic antitumor activity of C_{60} modified.

Chapter 4 describes a new DDS conjugate with therapeutic and diagnostic activities. An imaging probe, gadolinium (Gd^{3+}) ions of MRI was combined into the C_{60} modified with PEG as the photosensitizer of PDT. The combination with the MRI function enhanced the tumor PDT efficacy of C_{60}-PEG conjugate. After chemical coupling of PEG with both amino and hydroxyl terminal groups to C_{60}, diethylenetriaminepentaacetic acid (DTPA) was subsequently introduced to the remaining hydroxyl terminal group of PEG to prepare DTPA-introduced C_{60}-PEG conjugates (C_{60}-

PEG-DTPA). The C_{60}-PEG-DTPA was mixed with gadolinium acetate solution to obtain Gd^{3+}-chelated C_{60}-PEG conjugates (C_{60}-PEG-Gd). Following intravenous injection of C_{60}-PEG-Gd into tumor-bearing mice, the tumor PDT efficacy and the MRI tumor imaging were evaluated. Both of the C_{60}-PEG-Gd and Magnevist® of MRI agent clinically used exhibited a similar MRI activity in aqueous solutions. When intravenously injected into tumor-bearing mice, the C_{60}-PEG-Gd maintained an enhanced MRI signal at the tumor tissue for a longer time period than Magnevist®. Injection of C_{60}-PEG-Gd plus light irradiation showed significant tumor PDT efficacy although the effect depended on the timing of light irradiation. The PDT efficacy of C_{60}-PEG-Gd was observed at the time when the tumor accumulation was detected by the enhanced intensity of MRI signal. This therapeutic and diagnostic hybrid system is a promising tool to enhance the PDT efficacy for tumor.

Chapter 5 describes the imaging of bone tissue by a new multimodal imaging DDS system with bone targetability. The objection of this system is to evaluate the process of bone regeneration. Pamidronate, one type of bisphosphonate with a high affinity for the Hydroxyapatite (HA) of bone tissues, was introduced to pullulan (PA-pullulan conjugate). Then, different imaging probes for fluorescence and MRI were introduced into the PA-pullulan conjugate to prepare PA-pullulan conjugate containing two imaging probes (PA-pullulan-F/M conjugate). The PA-pullulan-F/M conjugate had an affinity to HA and the extent increased in the amount of PA conjugated. In aqueous solutions, the PA-pullulan-F/M conjugate showed a similar MRI activity to Magnevist® of MRI agent clinically used. A gelatin hydrogel of biodegradability was prepared and then bone morphogentic protein (BMP)-2 was incorporated into the hydrogel. When implanted subcutaneously into mice, the hydrogel incorporating BMP-2 formed bone tissues around the hydrogel through the BMP-2 release. When the PA-pullulan-F/M

conjugate were intravenously administered into mice with bone tissue newly formed by BMP-2 release to evaluate their imaging effect on the bone tissue, the PA-pullulan-F/M conjugate accumulated in the new generated bone tissue, resulting in a significant detection of fluorescence signal thereat. The fluorescence intensity increased with an increase in the amount of calcium deposited in the new bone tissue during the process of bone regeneration. This indicates that the PA-pullulan-F/M conjugate is a useful multimodal DDS for the noninvasive evaluation of bone regeneration.

In summary, this thesis describes the design and preparation of various types of water-soluble C_{60} conjugates with several water-soluble polymers in different coupling manners. The physicochemical properties of C_{60} conjugates affected their in vitro antitumor activity as well as their body distribution and the consequent in vivo antitumor activity. The results obtained were all important to design the DDS modification of C_{60} for the tumor PDT. Additional, combination with imaging probes significantly improved the PDT efficacy. This finding is one of the researches to map out our future course of therapy-diagnosis hybrid DDS. Co-conjugation of a targeting moiety and imaging probes with pullulan enhanced their ability to visualize the site to be detected. It is concluded that DDS technology was also useful to design a multimodal imaging system of DDS.

REFERENCES

[1] L. Aagaard, J.J. Rossi, RNAi therapeutics: principles, prospects and challenges. Adv Drug Deliv Rev 59(2-3) (2007) 75-86.

[2] M. Rimmele, Nucleic acid aptamers as tools and drugs: recent developments. Chembiochem 4(10) (2003) 963-971.

[3] P. Vermeij, D. Blok, New peptide and protein drugs. Pharm World Sci 18(3) (1996) 87-93.

[4] R. Duncan, The dawning era of polymer therapeutics. Nat Rev Drug Discov 2(5) (2003) 347-360.

[5] Y. Tabata, Biomaterial technology for tissue engineering applications. J R Soc Interface 6 Suppl 3 (2009) S311-324.

[6] Y. Tabata, Nanomaterials of drug delivery systems for tissue regeneration. Methods Mol Biol 300 (2005) 81-100.

[7] A.S. Hoffman, The origins and evolution of "controlled" drug delivery systems. J Control Release 132(3) (2008) 153-163.

[8] M. Yokoyama, Drug delivery system. Mater. Integr. 20(9) (2007) 38-43.

[9] T.G. Park, J.H. Jeong, S.W. Kim, Current status of polymeric gene delivery systems. Adv Drug Deliv Rev 58(4) (2006) 467-486.

[10] H. Shibata, S. Nakagawa, Y. Tsutsumi, Optimization of protein therapies by polymer-conjugation as an effective DDS. Molecules 10(1) (2005) 162-180.

[11] F.M. Veronese, G. Pasut, PEGylation, successful approach to drug delivery. Drug Discov Today 10(21) (2005) 1451-1458.

[12] P. Karande, S. Mitragotri, Enhancement of transdermal drug delivery via synergistic action of chemicals. Biochim. Biophys. Acta, Biomembr. 1788(11) (2009) 2362-2373.

[13] G.N. Patel, G.C. Patel, R.B. Patel, S.S. Patel, J.K. Patel, P.D. Bharadia, M.M. Patel, Oral colon-specific drug delivery: an overview. Drug Delivery Technol. 6(7) (2006) 62-71.

[14] M. Werle, A. Bernkop-Schnurch, Strategies to improve plasma half life time of peptide and protein drugs. Amino Acids 30(4) (2006) 351-367.

[15] J.M. Harris, N.E. Martin, M. Modi, Pegylation: a novel process for modifying pharmacokinetics. Clin Pharmacokinet 40(7) (2001) 539-551.

[16] V. Trubetskoy, V. Torchilin, Use of polyoxyethylene-lipid conjugates as long-circulating carriers for delivery of therapeutic and diagnostic agents. Adv Drug Deliv Rev 16 (1995) 311-320.

[17] R. Juliano, J. Bauman, H. Kang, X. Ming, Biological Barriers to Therapy with Antisense and siRNA Oligonucleotides. Mol. Pharmaceutics 6(3) (2009) 686-695.

[18] R.L. Oostendorp, J.H. Beijnen, J.H.M. Schellens, The biological and clinical role of drug transporters at the intestinal barrier. Cancer Treat. Rev. 35(2) (2009) 137-147.

[19] M.M. Patel, B.R. Goyal, S.V. Bhadada, J.S. Bhatt, A.F. Amin, Getting into the brain: approaches to enhance brain drug delivery. CNS Drugs 23(1) (2009) 35-58.

[20] M. Konishi, Y. Tabata, M. Kariya, A. Suzuki, M. Mandai, K. Nanbu, K. Takakura, S. Fujii, In vivo anti-tumor effect through the controlled release of cisplatin from biodegradable gelatin hydrogel. J Control Release 92(3) (2003) 301-313.

[21] R. Langer, J. Folkman, Polymers for the sustained release of proteins and other macromolecules. Nature 263(5580) (1976) 797-800.

[22] M. Alagusundaram, C.M.S. Chetty, K. Umashankari, V.B. Attuluri, C. Lavanya, S. Ramkanth, Microspheres as a novel drug delivery sytem - a review. Int J ChemTech Res. 1(3) (2009) 526-534.

[23] S.A. Giannos, Pulsatile delivery of drugs and topical actives. Skin Delivery Syst (2006) 327-357.

[24] M.N. Ravi Kumar, Nano and microparticles as controlled drug delivery devices. J Pharm Pharm Sci 3(2) (2000) 234-258.

[25] A. Estella-Hermoso de Mendoza, M.A. Campanero, F. Mollinedo, M.J. Blanco-Prieto, Lipid nanomedicines for anticancer drug therapy. J Biomed Nanotechnol 5(4) (2009) 323-343.

[26] K. Osada, R.J. Christie, K. Kataoka, Polymeric micelles from poly(ethylene glycol)-poly(amino acid) block copolymer for drug and gene delivery. J R Soc Interface 6(Suppl. 3) (2009) S325-S339.

[27] Y. Mizushima, Lipid microspheres (lipid emulsions) as a drug carrier - An overview. Adv Drug Delivery Rev 20(2,3) (1996) 113-115.

[28] C. Dai, B. Wang, H. Zhao, Microencapsulation peptide and protein drugs delivery system. Colloids Surf B Biointerfaces 41(2-3) (2005) 117-120.

[29] S. Bhattacharya, B. Mazumder, Bioceramics: concepts and prospects in drug delivery. Pharma Rev 7(40) (2009) 59-63.

[30] A. Samad, M.I. Alam, K. Saxena, Dendrimers: a class of polymers in the nanotechnology for the delivery of active pharmaceuticals. Curr Pharm Des 15(25) (2009) 2958-2969.

[31] M. Hamidi, A. Azadi, P. Rafiei, Hydrogel nanoparticles in drug delivery. Adv Drug Delivery Rev 60(15) (2008) 1638-1649.

[32] F. Meng, Z. Zhong, J. Feijen, Stimuli-Responsive Polymersomes for Programmed Drug Delivery. Biomacromolecules 10(2) (2009) 197-209.

[33] C. Alvarez-Lorenzo, L. Bromberg, A. Concheiro, Light-sensitive intelligent drug delivery systems. Photochem Photobiol 85(4) (2009) 848-860.

[34] P. Bawa, V. Pillay, Y.E. Choonara, L.C. du Toit, Stimuli-responsive polymers and their applications in drug delivery. Biomed Mater (Bristol, U. K.) 4(2) (2009) 022001/022001-022001/022015.

[35] N. Tirelli, (Bio)Responsive nanoparticles. Curr. Opin. Colloid Interface Sci 11(4) (2006) 210-216.

[36] I. Shubayev Veronica, R. Pisanic Thomas, 2nd, S. Jin, Magnetic nanoparticles for theragnostics. Adv Drug Delivery Rev 61(6) (2009) 467-477.

[37] K. Park, Ultrasound-activatable drug-loaded microbubbles for intracellular targeting. J Controlled Release 132(3) (2008) 151.

[38] Z. Huang, A review of progress in clinical photodynamic therapy. Technol Cancer Res Treat 4(3) (2005) 283-293.

[39] V.F. Dima, M.D. Ionescu, C. Balotescu, S.F. Dima, Photodynamic therapy and some clinical applications in oncology. Roum Arch Microbiol Immunol 61(3) (2002) 159-205.

[40] T.J. Dougherty, C.J. Gomer, B.W. Henderson, G. Jori, D. Kessel, M. Korbelik, J. Moan, Q. Peng, Photodynamic therapy. J Natl Cancer Inst 90(12) (1998) 889-905.

[41] M. Ochsner, Photophysical and photobiological processes in the photodynamic therapy of tumours. J Photochem Photobiol B 39(1) (1997) 1-18.

[42] A. Juarranz, P. Jaen, F. Sanz-Rodriguez, J. Cuevas, S. Gonzalez, Photodynamic therapy of cancer. Basic principles and applications. Clin Transl Oncol 10(3) (2008) 148-154.

[43] M. Kreimer-Birnbaum, Modified Porphyrins, Chlorins, Phthalocyanines, and Purpurins: Second-Generation Photosensitizers for Photodynamic Therapy. Seminars in Hematology 26(2) (1989) 157-173.

[44] M.R. Detty, S.L. Gibson, S.J. Wagner, Current clinical and preclinical photosensitizers for use in photodynamic therapy. J Med Chem 47(16) (2004) 3897-3915.

[45] T. Reynolds, Photodynamic therapy expands its horizons. J Natl Cancer Inst 89(2) (1997) 112-114.

[46] W.L. Nourse, R.M. Parkhurst, W.A. Skinner, R.T. Jordan, Photodynamic toxicity of porphyrins and chlorins for a human tumor cell line: combined light and concentration dose responses for the retained fraction. Biochem Biophys Res Commun 151(1) (1988) 506-511.

[47] N. Razum, O.J. Balchum, A.E. Profio, F. Carstens, Skin photosensitivity: duration and intensity following intravenous hematoporphyrin derivates, HpD and DHE. Photochem Photobiol 46(5) (1987) 925-928.

[48] S.B. Brown, E.A. Brown, I. Walker, The present and future role of photodynamic therapy in cancer treatment. Lancet Oncol 5(8) (2004) 497-508.

[49] D.E. Dolmans, D. Fukumura, R.K. Jain, Photodynamic therapy for cancer. Nat Rev Cancer 3(5) (2003) 380-387.

[50] K.A. Brackett, M.Y. Sankar, S.N. Joffe, Effects of Nd:YAG laser photoradiation on intra-abdominal tissues: a histological study of tissue damage versus power density applied. Lasers Surg Med 6(2) (1986) 123-130.

[51] P. Lehmann, [Side effects of topical photodynamic therapy]. Hautarzt 58(7) (2007) 597-603.

[52] W.G. Roberts, K.M. Smith, J.L. McCullough, M.W. Berns, Skin photosensitivity and photodestruction of several potential photodynamic sensitizers. Photochem Photobiol 49(4) (1989) 431-438.

[53] H.W. Kroto, J.R. Heath, S.C. O'Brien, R.F. Curl, R.E. Smalley, C60: Buckminsterfullerene. Nature 318 (1985) 162-163.

[54] S.H. Friedman, D.L. DeCamp, R.P. Sijbesma, G. Srdanov, F. Wudl, G.L. Kenyon, Inhibition of the HIV-1 protease by fullerene derivatives: model building studies and experimental verification. J Am Chem Soc 115(15) (1993) 6506-6509.

[55] F. Kasermann, C. Kempf, Photodynamic inactivation of enveloped viruses by buckminsterfullerene. Antiviral Res 34(1) (1997) 65-70.

[56] N. Nakajima, C. Nishi, F.-M. Li, Y. Ikada, Photo-induced cytotoxicity of water-soluble fullerene. Fullerene Sci Technol 4(1) (1996) 1-19.

[57] E. Nakamura, H. Isobe, N. Tomita, M. Sawamura, S. Jinno, H. Okayama, Functionalized Fullerene as an Artificial Vector for Transfection. Angewandte Chemie International Edition 39(23) (2000) 4254-4257.

[58] K. Okuda, T. Mashino, M. Hirobe, Superoxide radical quenching and cytochrome C peroxidase-like activity of C60-dimalonic acid, C62(COOH)4. Bioorganic and Medicinal Chemistry Letters 6(5) (1996) 539-542.

[59] H. Tokuyama, S. Yamago, E. Nakamura, T. Shiraki, Y. Sugiura, Photoinduced biochemical activity of fullerene carboxylic acid. J Am Chem Soc 115(17) (1993) 7918-7919.

[60] J.W. Arbogast, A.P. Darmanyan, C.S. Foote, F.N. Diederich, R.L. Whetten, Y. Rubin, M.M. Alvarez, S.J. Anz, Photophysical properties of sixty atom carbon molecule (C60). J Phys Chem 95(1) (1991) 11-12.

[61] C.S. Foote, Photophysical and Photochemical Properties of Fullerenes. Top. Curr Chem 169 (1994) 347-363.

[62] T. Tsuchiya, I. Oguri, Y.N. Yamakoshi, N. Miyata, Novel harmful effects of [60]fullerene on mouse embryos in vitro and in vivo. FEBS Lett 393(1) (1996) 139-145.

[63] F. Cheng, X. Yang, H. Zhu, J. Sun, Y. Liu, Synthesis of oligoadducts of malonic acid C60 and their scavenging effects on hydroxyl radical. J Phys Chem 61 (2000) 1145-1148.

[64] R.S. Ruoff, D.S. Tse, R. Malhotra, D.C. Lorents, Solubility of C60 in a variety of solvents. J Phys Chem 97 (1993) 3379-3383.

[65] G.V. Andrievsky, M.V. Kosevich, O.M. Vovk, V.S. Shelkovsky, L.A. Vashchenko, Are fullerenes soluble in water? Proc. Electrochem Soc 95 (1995) 1591-1602.

[66] F. Moussa, F. Trivin, R. Ceolin, M. Hadchouel, P.Y. Sizaret, V. Greugny, C. Fabre, A. Rassat, H. Szwarc, Early effects of C60 administration in Swiss mice: a preliminary account for in vivo C60 toxicity. Fullerene Sci Technol 4(1) (1996) 21-29.

[67] K.C. Hwang, D. Mauzerall, Vectorial electron transfer from an interfacial photoexcited porphyrin to ground-state fullerene C60 and C70 and from ascorbate to triplet C60 and C70 in a lipid bilayer. J Am Chem Soc 114(24) (1992) 9705-9706.

[68] T. Andersson, K. Nilsson, M. Sundahl, G. Westman, O. Wennerstroem, C60 embedded in gamma -cyclodextrin: a water-soluble fullerene. J Chem Soc, Chem Commun(8) (1992) 604-606.

[69] L.Y. Chiang, R.B. Upasani, J.W. Swirczewski, Versatile nitronium chemistry for C60 fullerene functionalization. J Am Chem Soc 114(26) (1992) 10154-10157.

[70] I. Lamparth, A. Hirsch, Water-soluble malonic acid derivatives of C60 with a defined three-dimensional structure. J Chem Soc, Chem Commun (14) (1994) 1727-1728.

[71] D.M. Guldi, H. Hungerbuehler, K.-D. Asmus, Unusual redox behavior of a water soluble malonic acid derivative of C60: evidence for possible cluster formation. J Phys Chem 99(36) (1995) 13487-13493.

[72] Y.Z. An, J.L. Anderson, Y. Rubin, Synthesis of alpha -amino acid derivatives of C60 from 1,9-(4-hydroxycyclohexano)buckminsterfullerene. J Org Chem 58(18) (1993) 4799-4801.

[73] A. Skiebe, A. Hirsch, A facile method for the synthesis of amino acid and amido derivatives of C60. J Chem Soc, Chem Commun (3) (1994) 335-336.

[74] Y. Tabata, Y. Murakami, Y. Ikada, Photodynamic effect of polyethylene glycol-modified fullerene on tumor. Jpn J Cancer Res 88(11) (1997) 1108-1116.

[75] J. Liu, S. Ohta, A. Sonoda, M. Yamada, M. Yamamoto, N. Nitta, K. Murata, Y. Tabata, Preparation of PEG-conjugated fullerene containing Gd3+ ions for photodynamic therapy. J Control Release 117(1) (2007) 104-110.

[76] Y. Matsumura, H. Maeda, A new concept for macromolecular therapeutics in cancer chemotherapy: mechanism of tumoritropic accumulation of proteins and the antitumor agent smancs. Cancer Res 46(12 Pt 1) (1986) 6387-6392.

[77] H. Maeda, J. Wu, T. Sawa, Y. Matsumura, K. Hori, Tumor vascular permeability and the EPR effect in macromolecular therapeutics: a review. J Control Release 65(1-2) (2000) 271-284.

[78] V.P. Torchilin, Drug targeting. Eur J Pharm Sci 11 Suppl 2 (2000) S81-91.

[79] T. Yamaoka, Y. Tabata, Y. Ikada, Distribution and tissue uptake of poly(ethylene glycol) with different molecular weights after intravenous administration to mice. J Pharm Sci 83(4) (1994) 601-606.

[80] R. Weissleder, Molecular imaging in cancer. Science 312(5777) (2006) 1168-1171.

[81] T.F. Massoud, S.S. Gambhir, Molecular imaging in living subjects: seeing fundamental biological processes in a new light. Genes Dev 17(5) (2003) 545-580.

[82] K. Chtourou, M. Maloul, F. Kallel, S. Charfedine, F. Hamza, F. Guermazi, SPECT and MRI fusion for an extended bilateral osteonecrosis. Eur J Nucl Med Mol Imaging 35(12) (2008) 2343.

[83] V. Ntziachristos, A.G. Yodh, M. Schnall, B. Chance, Concurrent MRI and diffuse optical tomography of breast after indocyanine green enhancement. Proc Natl Acad Sci U S A 97(6) (2000) 2767-2772.

[84] T. Beyer, D.W. Townsend, T. Brun, P.E. Kinahan, M. Charron, R. Roddy, J. Jerin, J. Young, L. Byars, R. Nutt, A combined PET/CT scanner for clinical oncology. J Nucl Med 41(8) (2000) 1369-1379.

[85] O. Veiseh, C. Sun, J. Gunn, N. Kohler, P. Gabikian, D. Lee, N. Bhattarai, R. Ellenbogen, R. Sze, A. Hallahan, J. Olson, M. Zhang, Optical and MRI multifunctional nanoprobe for targeting gliomas. Nano Lett 5(6) (2005) 1003-1008.

[86] Y. Tabata, Tissue regeneration based on growth factor release. Tissue Eng 9 Suppl 1 (2003) S5-15.

[87] Y. Tabata, Regenerative inductive therapy based on DDS technology of protein and gene. J Drug Target 14(7) (2006) 483-495.

[88] D.J. Mooney, H. Vandenburgh, Cell delivery mechanisms for tissue repair. Cell Stem Cell 2(3) (2008) 205-213.

[89] J.A. Hubbell, Biomaterials in tissue engineering. Biotechnology (N Y) 13(6) (1995) 565-576.

[90] D. Berthoty, P. Haghighi, D.J. Sartoris, D. Resnick, Osseous invasion by soft-tissue sarcoma seen better on MR than on CT. AJR Am J Roentgenol 152(5) (1989) 1131.

[91] J.J. Peterson, L.W. Bancroft, M.J. Kransdorf, Principles of bone and soft tissue imaging. Hand Clin 20(2) (2004) v, 147-166.

PART I.

ANTITUMOR ACTIVITY OF FULLERENE MODIFIED WITH WATER-SOLUBLE POLYMERS

Chapter 1

Photodynamic antitumor activity of fullerene modified by polyethylene glycol with different molecular weights and terminal structures

INTRODUCTION

PDT is one of the non-invasive treatments applicable for various types of tumor [1-3]. During last 30 years, many photosensitizers have been explored to evaluate the PDT effect in vitro as well as in vivo systems [4-7]. However, most of the photosensitizers developed are porphyrin-based dyes and there are some problems to be resolved for the clinical application [8]. For example, because of their low quantum yield, the exposure of high-power laser light is required to generate ROS even if it damages normal tissues. In addition, the lack of tumor targetability results in their distribution in the healthy tissues, which causes serious side effects. To overcome these problems, it is necessary to develop a photosensitizer with a high ROS generation efficiency and tumor targetability.

It is well known that C_{60} can generate ROS in a high yield when exposed to visible light [9, 10]. Since the first report on the biological activity of C_{60} in 1993, water-soluble derivatives of C_{60} have been prepared by various methods and their characteristic bioactivities, such as the DNA cleavage, enzyme inhibition, antiviral activity, free radical quenching, gene transfection activities, and cytotoxicity, have been reported [11-16]. It is reported that C_{60} is an excellent photosensitizer for PDT [17, 18].

To make water-insoluble C_{60} soluble in water, chemical modification with water-soluble PEG (PEGylation) is a promising strategy. It has been demonstrated that PEG is a non-toxic, non-immunogenic, and non-antigenic amphiphilic polymer which is approved by FDA [19, 20]. The PEGylation has been widely used to prolong the in vivo half-life

period of drugs [21], increase the resistance against the hydrolysis caused by proteases or nucleases [22, 23], and reduce the immunogenicity [24]. In addition, it is well recognized that there are leaky vasculature with increased material permeability and poor lymphatic drainage in the tumor tissue (EPR effect). Based on the EPR effect, substances with a high molecular weight is susceptible to preferential extravasation from blood vessels and the subsequent accumulation in the tumor compared with in the normal tissue [25, 26]. It has been experimentally confirmed that PEGylation enables drugs to target to the tumor based on the EPR effect, resulting in their enhanced antitumor activity [24, 27-29]. The PEGylation of C_{60} also enhanced the in vivo efficacy of antitumor PDT [17].

This study is undertaken to obtain the basic knowledge of material design about the antitumor PDT of C_{60}-PEG conjugates. The first objective of this study is to investigate the influence of the PEG molecular weight on the PDT effect of PEG-modified C_{60}. The second objective is to evaluate the effect of the terminal structure of PEG on the bioactivity of C_{60}. Various types of PEG with different molecular weights and terminal groups were covalently conjugated to C_{60} to prepare various C_{60}-PEG conjugates. The properties of C_{60}-PEG conjugates were examined in terms of their ROS generation efficiency, the in vitro antitumor activity, and the profile of body distribution. The in vivo photodynamic antitumor activity of C_{60}-PEG conjugates was studied to evaluate the influence of PEG structures on the activity.

EXPERIMENTAL

Materials and reagents

C_{60} was purchased from SES Research Co. (Houston, lot No. BT-6906, Mw= 720, purity 99.9%.), Various PEG samples with different terminal structures and molecular weights were purchased from Nippon Oil & Fats Co., Ltd., Japan (**Table 1**). $Na^{125}I$ (20

mCi/ml, 0.1N NaOH aqueous solution) and cytochrome C (horse heart, Mw=12,384) were purchased from NEN Research Products, Dupont, Wilmington, DE and Nakalai Tesque Inc., Kyoto, Japan, respectively. Other chemicals were used without further purification.

Table 1. Preparation and characterization of C_{60}-PEG conjugates

Code of conjugates	Chemical structure	Weight-average molecular weight of PEG	Weight-average molecular weight of C_{60}-PEG conjugates	Apparent molecular size (nm)
C_{60}-MEPA20	C_{60} -NH-$(CH_2CH_2O)_n$-OCH_3	2,000	9,300	14.9±2.9
C_{60}-MEPA50	C_{60} -NH-$(CH_2CH_2O)_n$-OCH_3	5,000	22,000	30.6±4.4
C_{60}-MEPA120	C_{60} -NH-$(CH_2CH_2O)_n$-OCH_3	12,000	51,000	42.6±3.5
C_{60}-AMPA50	C_{60} -NH-$(CH_2CH_2O)_n$-NH_2	5,000	22,000	28.3±4.9
C_{60}-HOPA50	C_{60} -NH-$(CH_2CH_2O)_n$-OH	5,000	21,000	29.8±4.5
C_{60}-CAPA50	C_{60} -NH-$(CH_2CH_2O)_n$-COOH	5,000	21,000	31.2±5.3

Chemical conjugation of PEG to C_{60}

Chemical conjugation of PEG to C_{60} was carried out based on the high coupling reactivity of amines to C_{60} [30]. Briefly, 7.2 mg of C_{60} and different amounts of PEG were dissolved in 10 ml of dehydrated benzene, and the reaction mixture was stirred with magnetic agitation at room temperature for various time periods up to 24 hr in a dark or light irradiated place with an incandescent lamp (60W, 400-700 nm). When PEG was chemical conjugated to C_{60}, the color of C_{60} benzene solution changed from violet to brown. After the conjugation, the reaction solution was mixed with 20 ml of double-distilled water (DDW) to extract water-soluble C_{60}-PEG conjugates into the water phase. The amount of un-reacted C_{60} remained in the benzene phase was determined by absorptiometry and the amount of C_{60} conjugated to PEG was calculated from that of un-reacted C_{60} and that of C_{60} initially used. To quantitatively evaluate the effect of PEG concentration and terminal structure on the conjugation reaction to C_{60}, the T50 value, which is defined as the time period to reduce the concentration of unreacted C_{60} to half,

was obtained from the time course plot of PEG coupling reaction to C_{60} (Fig. 1). The water containing water-soluble C_{60}-PEG conjugates was further purified by gel filtration with a column filled with Sephacryl S-200 (Pharmacia Biotech, Uppsala, Sweden. elution buffer: 0.4 M CH_3COONH_4). C_{60}-PEG conjugates obtained were freeze-dried and stored in dark.

Characterization of C_{60}-PEG conjugates

The weight-average molecular weight of C_{60}-PEG conjugates was determined by a High Performance Liquid Chromatography (HPLC) system (TOSOH Corporation, Tokyo, Japan) equipped with variable-wavelength UV-vis, Refractive Index (RI), and Multi-Angle Light Scattering (MALS) triplex detectors. Analysis was performed by using SK-GEL PW2000xl plus PW4000xl column. The elution buffer was 20 vol% of acetonitrile in 0.2 M phosphate-buffered solution (pH 6.9) and the flow-rate was 0.8 ml/min.

The apparent molecular size of C_{60}-PEG conjugates was estimated by Dynamic Light Scattering (DLS) measurement at 37 ˚C and a fixed scattered angle of 90° (DLS-6000 system, Otsuka Electronics, Osaka, Japan), equipped with 10mW He-Ne laser (vertically polarized, 633 nm).

Measurement of superoxide anion generation efficiency of C_{60}-PEG conjugates

Superoxide anion generation efficiency of C_{60}-PEG conjugates was evaluated by the conventional cytochrome C method [31]. Briefly, 100 μl of Hanks Balanced Salt Solution (HBSS, pH=7.4, Life Technologies Oriental, Inc, Tokyo, Japan) containing 20 μM of cytochrome C was added to 100 μl HBSS containing 10 μM of C_{60}-PEG conjugates, and the mixed solution was placed into each well of 96-well multi-well culture plate (COSTAR® 3595, Corning Inc, NY). The plate was then exposed to a visible light supplied from a fluorescence lamp (8 W, 400 nm-700 nm, 2 cm from the plate bottom) for up to 60 min. The absorbance increase of solution at 550 nm was measured

by a microplate reader (VERSAmax, Molecular device corporation, California) to evaluate the superoxide anion generation efficiency.

Assessment of photo-induced in vitro antitumor activity of C_{60}-PEG conjugates

The in vitro antitumor activity of C_{60}-PEG conjugates was evaluated in terms of the suppression activity of tumor cells growth. Meth AR1 fibrosarcoma cells were suspended in RPMI-1640 medium (COSMO BIO Co., Ltd., Tokyo, Japan) supplemented with 10 v/v% of Fetal Calf Serum (FCS) to give a final density of 1×10^5 cells/ml. Then, 1 ml of the cell suspension was mixed with 100 μl medium containing 10 μM of C_{60}-PEG conjugates and the mixture was placed into each well of 24-well multi-well culture plate (COSTAR® 3526, Corning Inc, NY). The plate was fixed on a shaker and exposed to a visible light supplied from a fluorescence lamp (8 W, 400 nm-700 nm, 2 cm from the plate bottom) for 20 or 40 min with gentle shaking. After light irradiation, cells were further cultured for 3 days in dark, and the number of cells grown was determined by Cell Counting Kit (Dojindo Molecular Technologies, Inc., Kumamoto, Japan). The percent cell viability was expressed as 100% for control, non-treated cells.

Radioiodination of C_{60}-PEG conjugates

Radioiodination was carried out according to a chloramine T method [32]. Firstly, tyramine was introduced into the C_{60}-PEG conjugates. Briefly, tyramine was added to 10 ml of dehydrated dimethyl sulfoxide (DMSO) solution containing 0.2 mM of C_{60}-PEG conjugates at a tyramine/C_{60} molar ratio of 100. After the introduction reaction at room temperature for 24 hr, the resulting solution was dialyzed against DDW using a dialysis membrane (Spectra/Pore® 3.1, MWCO: 3,500, Spectrum Laboratories Inc., CA) to exclude non-coupled tyramine, followed by freeze-drying to obtain the tyramine-introduced C_{60}-PEG conjugates. Next, the tyramine-introduced C_{60}-PEG conjugates were dissolved in 150 μl of 0.5 M potassium phosphate-buffered (KPB) solution (pH 7.5) to

give a final concentration of 50 μM. Then, 5 μl of $Na^{125}I$ solution (20 mCi/ml) and 100 μl of 0.5 M KPB solution containing 0.02 mg of chloramine T were added. After agitation for 2 min, 100 μl of phosphate-buffered saline solution (PBS, pH 7.4) containing 0.4 mg of sodium pyrosulfite was added to stop the reaction. The resulting mixture was allowed to pass through the PD-10 column (Pharmacia Biotech Inc, Sweden) to separate ^{125}I-labeled C_{60}-PEG conjugates from unbound ^{125}I.

Preparation of tumor-bearing mice

Meth AR1 fibrosarcoma cells were maintained by repeated intraperitoneal passage in CDF1 mice (Japan SLC, Inc, Shizuoka, Japan) before subcutaneously inoculated into the back of 6-week-old CDF1 mice (1×10^7 cells/ml, 100 μl/mouse). When the tumor mass grew to 5 mm in average diameter about 1 week after the inoculation, the tumor-bearing mice were used for the following in vivo experiments.

Evaluation of body distribution of C_{60}-PEG conjugates

Tumor-bearing mice received the intravenous injection of 100 μl of PBS solution containing ^{125}I -labeled C_{60}-PEG conjugates. At various time intervals, blood samples were collected directly from the heart by syringe aspiration, and the tumor tissue, normal muscle, and normal skin were taken out. After weighing, the radioactivity of excised tissue and blood samples was measured with a gamma counter (Autowell gamma system Aloka ARC-301B, Aloka Company, Ltd, Tokyo, Japan). The body distribution data were expressed as the percentage of radioactivity remaining which is calculated by dividing the percentage of radioactivity measured to that injected initially per mouse, and the percentage divided by the weight of each tissue (percent remaining/ g tissue).

Interaction evaluation of C_{60}-PEG conjugates with protein

The interaction of C_{60}-PEG conjugates with a serum protein in physiological saline solution was evaluated by a quartz crystal microbalance apparatus (QCM) (Affinix Q, Initium Co., Tokyo, Japan). According to the manual procedure, a 27 MHz QCM sensor chip was immersed in aqueous solution of bovine serum albumin (BSA, fraction V, Nakalai Tesque Inc, Kyoto, Japan) to allow the gold surface of sensor chip to coat with BSA. The BSA coated sensor was placed in 8 ml of physiological saline solution at 37 ˚C for 30 min until its frequency became stable. After 8 μl of C_{60}-PEG solution (0.2 mM) was added to the solution, the frequency change was continually recorded. Based on the assumption that the absorption of 30 pg protein on the chip surface bring about 1.0 Hz decrease in the frequency, the amount of C_{60}-PEG conjugates adsorbed on the sensor (W) was calculated by the following formula: $W=\Delta\nu\times30$ pg/Hz, where $\Delta\nu$ is the frequency change.

Photodynamic effect of C_{60}-PEG conjugates on tumor

To evaluate the antitumor PDT effect of C_{60}-PEG conjugates, 100 μl of conjugate solution in saline (0.3 mM) was intravenously injected into the tail vein of tumor-bearing mice. Six h latter the tumor tissue was exposed to visible light (400-505 nm) from a light probe of 7 mm active diameter using a Heliomat Multifunction Halogen-Light (Vivadent Co. Ltd, Lichtenstein). The irradiation was carried out for 10 min at an output power of 89.2 mW/cm^2 (53.5 J/cm^2). Then, mice were fed in dark during the experiment. At different time intervals, the tumor volume (V) was calculated according to the formula of $V=\pi/6\times a\times b^2$ (where a and b is the length of long axis and short axis of tumor mass, respectively) [33] and expressed as the volume ratio of the tumor to that before conjugates injection.

RESULTS

Preparation and characterization of C_{60}-PEG conjugates

Figure 1 shows a representative time course of MEPA120 coupling reaction to C_{60}. The reaction was accelerated with an increase in the concentration of PEG, while light irradiation was necessary to make the reaction proceed. **Table 2** shows the effect of PEG concentration on the conjugation reaction to C_{60}. The T50 value is defined as the time period to reduce the concentration of unreacted C_{60} to half. Except for AMPA50, the similar T50 value was observed when the initial concentration of PEG was similar, irrespective of the molecular weight and terminal structure of PEG. The value decreased with an increase in the concentration of PEG. The AMPA50 has amine groups on the both ends and consequently the T50 value is about half.

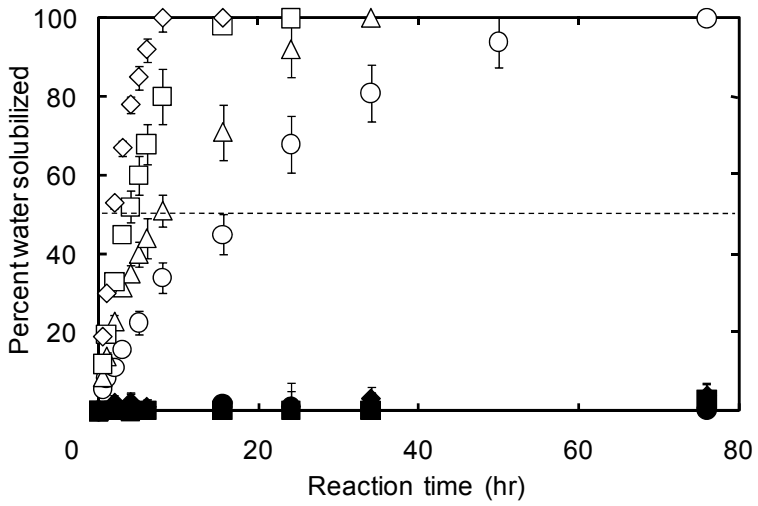

Figure 1. Time course of MEPA120 coupling reaction to C_{60} under the light (open marks) and dark conditions (closed marks) The concentration of C_{60} is 1 mM and the concentration of MEPA50 is 5 (○ and ●·), 10 (△ and ▲), 20 (□ and ■) or 50 mM (◇ and ◆).

The DLS measurement revealed that the apparent molecular size of C_{60}-PEG conjugates increased with an increase in the molecular weight of PEG conjugated.

Irrespective of the terminal structure of PEG, the molecular size of conjugates prepared by PEG with the molecular weight of 5,000 was about 30 nm in diameter (**Table 1**).

Table 2. Effect of PEG amount on the conjugation reaction rate of PEG to C_{60}

Code of conjugates	Amount of PEG added (mM)			
	5	10	20	50
C_{60}-MEPA20	16.0 [a)]	7.6	3.5	1.5
C_{60}-MEPA50	15.1	7.3	3.3	1.4
C_{60}-MEPA120	15.3	7.5	3.8	1.6
C_{60}-AMPA50	7.4	3.4	1.4	-
C_{60}-HOPA50	14.7	6.9	3.1	1.3
C_{60}-CAPA50	15.6	7.2	3.2	1.5

[a)] Defined as the time period (hr) when the concentration of unreacted C_{60} in benzene decreased to 50% of the initial concentration.

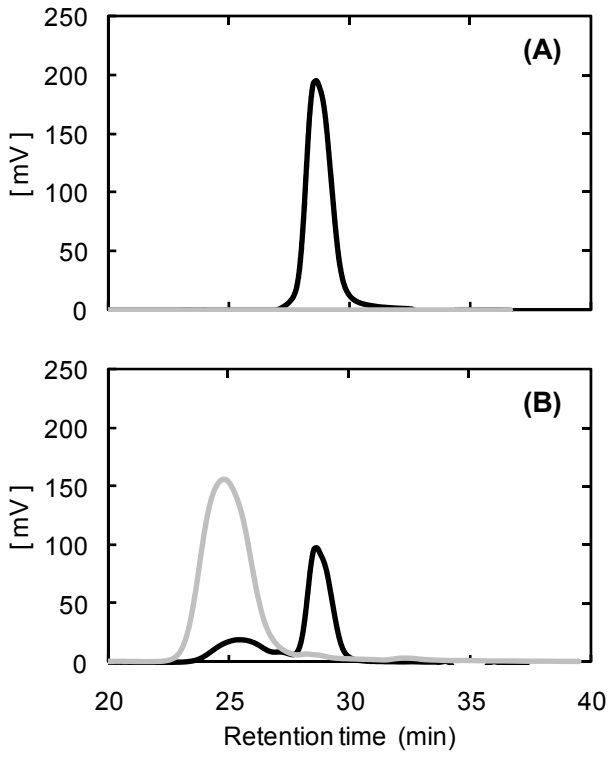

Figure 2. Representative chromatograms of original MEPA120 (A) and reaction product after 24 hr conjugation at C_{60} and MEPA120 concentrations of 1 and 20 mM (B). The samples were measured by the UV (gray line) and refractive (black line) detectors.

Figure 2 shows representative HPLC chromatograms of PEG and C_{60}-PEG conjugates. By C_{60} conjugation, a new peak was RI detected at a shorter retention time and the peak had the UV absorption of C_{60}. The molecular weight of C_{60}-PEG conjugates also increased with increased molecular weight of PEG. On the other hand, no dependence of the PEG terminal structure on the molecular weight of conjugates was observed (**Table 1**). Comparing the molecular weight of C_{60}-PEG conjugates with original PEG, it was found that 4 of PEG molecules covalently conjugated to one molecule of C_{60} for any type of C_{60}-PEG conjugates.

Superoxide anion generation of C_{60}-PEG conjugates

Figure 3 shows the absorbance increase of cytochrome C solution containing different C_{60}-PEG conjugates after light irradiation. In the present of C_{60}-PEG conjugates, the absorbance increased with the irradiation period, in marked contrast to that of saline solution. The similar increase pattern was observed for all types of C_{60}-PEG conjugates. The results indicate that every C_{60}-PEG conjugate had the similar nature of ROS generation.

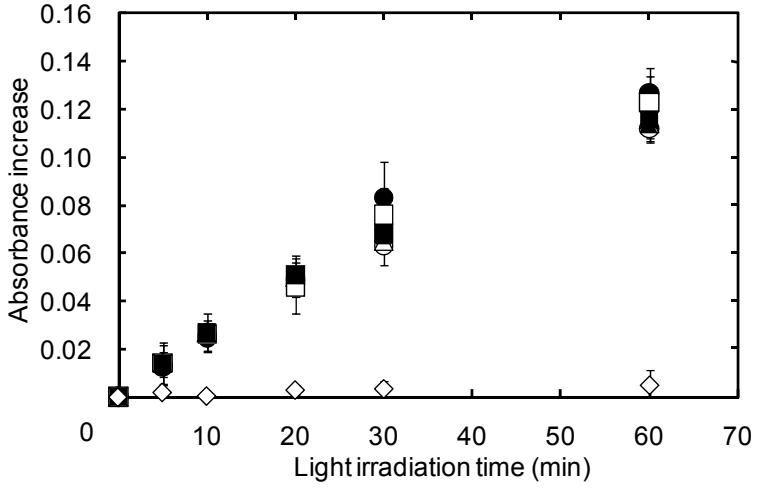

Figure 3. Absorbance increase of cytochrome C solution after light irradiation in the present of C_{60}-MEPA20 (○), C_{60}-MEPA50 (●), C_{60}-MEPA120 (△), C_{60}-AMPA50 (▲), C_{60}-HOPA50 (□), and C_{60}-CAPA50 conjugates (■) or absence of conjugates (◇).

Photo-induced in vitro antitumor activity of C_{60}-PEG conjugates

Figure 4 shows the in vitro antitumor activity of C_{60}-PEG conjugates with or without light irradiation. Combination of C_{60}-PEG conjugates and light irradiation exhibited significant in vitro growth of tumor cells, while light irradiation alone or the C_{60}-PEG conjugates alone under the dark condition did not decrease the cell number. There was no significant difference in the antitumor activity among all C_{60}-PEG conjugates. Irrespective of the conjugates type, the survival cell number decreased to about 40 % by light irradiation for 20 min and more cells died with the increased irradiation period.

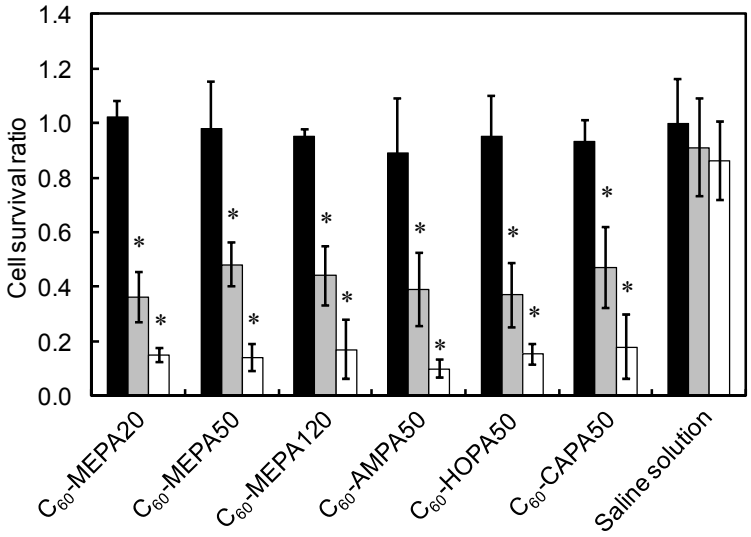

Figure 4. The number of MethAR1 cells growth 3 days after culturing in the presence of different C_{60}-PEG conjugates in dark (black bars) or with light irradiation for 20 (gray bars), and 40 min (white bars). The C_{60} concentration is 3.44 mg/ml. *, $p<0.05$: significance against the number ratio of cells grown in dark at the corresponding conjugate.

Body distribution of C_{60}-PEG conjugates

Figure 5 shows the time-course of radioactivity remaining in the blood circulation after intravenous injection of radiolabeled C_{60}-PEG conjugates. Among the C_{60}-PEG conjugates with the methoxy terminal group (**Figure 5A**), the serum half-life period of

C_{60}-PEG conjugates tended to become longer with an increase in the molecular weight of PEG conjugated. On the other hand, the terminal structure of PEG greatly affect the serum half-life period of C_{60}-PEG conjugates (**Figure 5B**). The C_{60}-AMPA50 conjugate with the amino terminal group was eliminated fastest from the blood circulation.

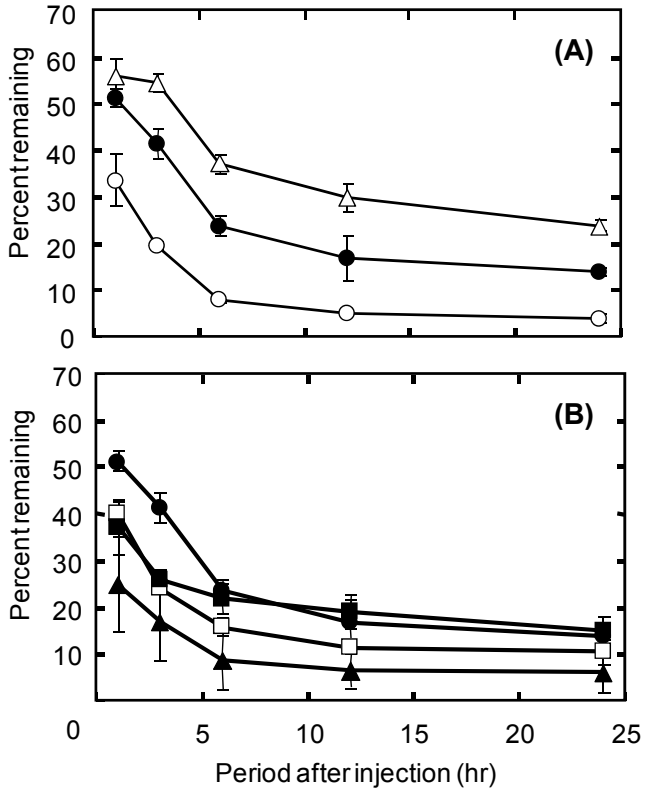

Figure 5. Time course of radioactivity remaining in the blood circulation of tumor-bearing mice after intravenous injection of ^{125}I-labeled different C_{60}-PEG conjugates: C_{60}-MEPA20 (○), C_{60}-MEPA50 (●), C_{60}-MEPA120 (△), C_{60}-AMPA50 (▲), C_{60}-HOPA50 (□), and C_{60}-CAPA50 conjugates (■)

Figure 6 shows the time courses of ^{125}I-labeled C_{60}-PEG conjugates accumulation in the tumor, normal skin, and normal muscle. After intravenously injected to tumor-bearing mice, the conjugate was accumulated in the tumor tissue with time, and significant difference in the accumulation amount from the normal tissues was detected, even 3 hr after injection. The conjugate was retained in the tumor tissue at a significantly larger amount and for a longer time period. The similar tendency was observed for all

types of C_{60}-PEG conjugates although their tumor accumulation amounts were depended on the molecular weight and terminal structure of PEG conjugated (**Figure 7**). When compared among the C_{60}-MEPA conjugates, the amount of tumor accumulation became larger with increasing molecular weight of PEG. On the other hand, the conjugates prepared from PEG with the same molecular weight but with different terminal groups tended to accumulate in the tumor tissue with time in the similar pattern. Among them, the C_{60}-AMPA50 conjugate with amino terminal group showed the lower accumulation.

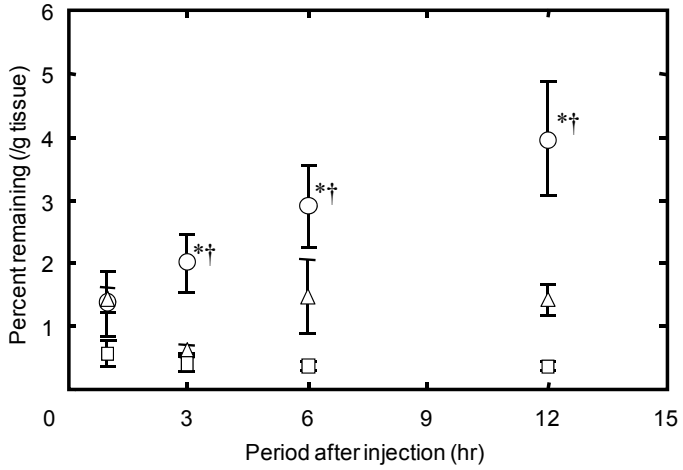

Figure 6. Time course of radioactivity remaining in the tumor (○), normal skin (△), and normal muscle (□) of tumor-bearing mice after intravenous injection of the ^{125}I-labeled C_{60}-MEPA120 conjugate. *, $p<0.05$: significance against the percent radioactivity of normal skin at the corresponding time period. †, $p<0.05$: significance against the percent radioactivity of normal muscle at the corresponding time period.

Interaction of C_{60}-PEG conjugates with serum protein

Figure 8 shows the adsorption amounts of C_{60}-PEG conjugates with different terminal groups on the BSA-coated QCM sensor chip. For the C_{60} conjugates prepared from PEG with the amino terminal group, significant high adsorption on the sensor chip was observed. However, there is no difference in the adsorption profile among other types of C_{60}-PEG conjugates.

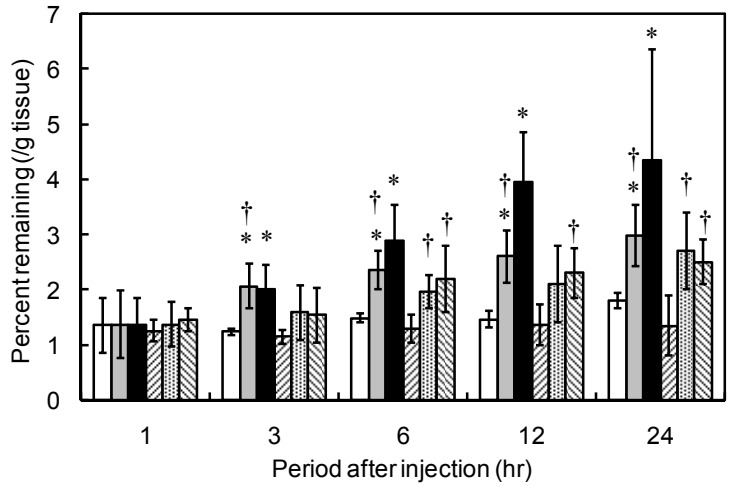

Figure 7. Time course of radioactivity remaining in the tumor tissue of tumor-bearing mice after intravenous injection of ^{125}I-labeled C_{60}-PEG conjugates: C_{60}-MEPA20 (□), C_{60}-MEPA50 (▒), C_{60}-MEPA120 (■), C_{60}-AMPA50 (▨), C_{60}-HOPA50 (⁙), and C_{60}-CAPA50 conjugates (▩). *, $p<0.05$: significance against the percent remaining of mice injected with C_{60}-MEPA20 at the corresponding time period. †, $p<0.05$: significance against the percent remaining of mice injected with C_{60}-AMPA50 at the corresponding time period.

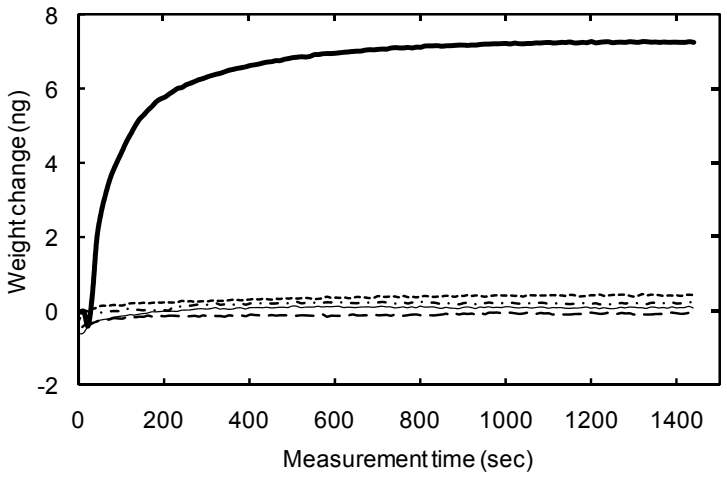

Figure 8. QCM measurement of BSA interaction with different C_{60}-PEG conjugates: C_{60}-MEPA50 (thin lines), C_{60}-AMPA50 (thick lines), C_{60}-HOPA50 (dotted line), C_{60}-CAPA50 (broken lines), and C_{60}-MEPA120 (alternate long and short dash line) conjugates.

Photodynamic effect of C_{60}-PEG conjugates on tumor

Figure 9 shows the in vivo photodynamic effect of different C_{60}-PEG conjugates. Different from the in vitro antitumor activity, in vivo antitumor activity of C_{60}-PEG conjugates greatly depended on the molecular weight and terminal structure of PEG. The

in vivo suppression of tumor growth by the C_{60}-MEPA conjugates increased with increasing molecular weight (**Figure 9A**). On the other hand, when comparing the C_{60}-PEG conjugates prepared from PEG with different terminal groups (**Figure 9B**), the similar effect of tumor suppression was observed for conjugates prepared from PEG with methoxyl, hydroxyl, and carboxylic groups, while the conjugate from PEG with the amino terminal group showed significantly lower antitumor activity. In the case of no light irradiation, no suppression effect was observed, irrespective of C_{60}-PEG conjugates type. The time profiles of tumor growth were similar to that of saline-injected, control mice (data not shown).

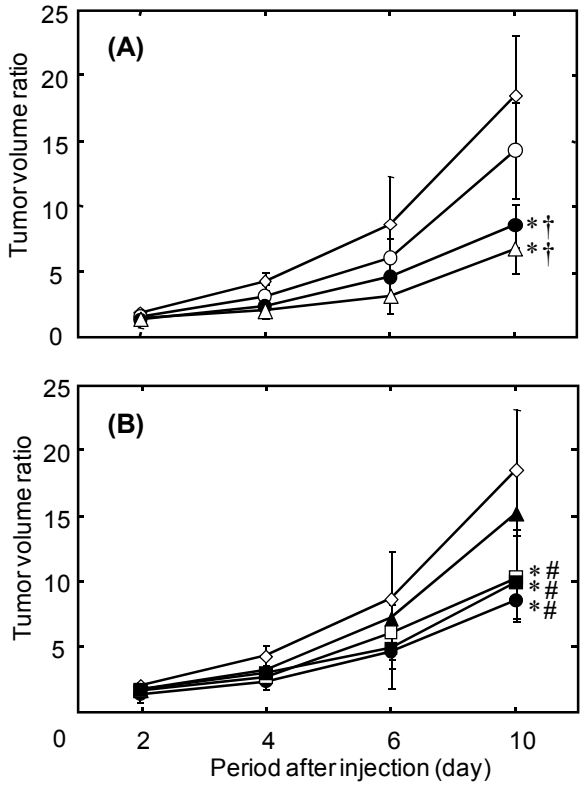

Figure 9. Photodynamic effect on the Meth AR1 tumor-bearing mice after intravenous injection of different C_{60}-PEG conjugates: C_{60}-MEPA20 (○), C_{60}-MEPA50 (●), C_{60}-MEPA120 (△), C_{60}-AMPA50 (▲), C_{60}-HOPA50 (□), and C_{60}-CAPA50 conjugates (■) or saline (◇). *, $p<0.05$: significance against the tumor size ratio of mice injected with saline at the corresponding time period. †, $p<0.05$: significance against the tumor size ratio of mice injected with C_{60}-MEPA20 at the corresponding time period. #, $p<0.05$: significance against the tumor size ratio of mice injected with C_{60}-AMPA50 at the corresponding time period.

DISCUSSION

In the present paper, several kinds of water-soluble C_{60}-PEG conjugates were prepared from PEG with different molecular weights and terminal structures. Every C_{60}-PEG conjugate showed similar ROS generation efficiency and in vitro antitumor activity (**Figures 3** and **4**). However, the in vivo antitumor activity of C_{60}-PEG conjugates depended on the type of PEG used for C_{60} conjugation. This phenomenon can be explained in term of body distribution of conjugates injected. It is likely that the in vitro properties of C_{60}-PEG conjugates one-to-one correspond to the inherent physicochemical nature of C_{60} molecule itself. Irrespective of the molecular weight and terminal group of PEG used, once the number of PEG molecules conjugated to one C_{60} molecule is fixed, the in vitro properties of PEG-conjugated C_{60} consequently is determined. When exposed to visible light, every C_{60}-PEG conjugate generated superoxide anions, a kind of ROS, which results in the antitumor effect in vitro as well as in vivo. Both the ROS generation and in vitro antitumor activity of C_{60}-PEG conjugates were observed only by the light irradiation while they depended on the time period of light irradiation. It is conceivable that the in vitro antitumor activity of C_{60}-PEG conjugates is mainly due to the ROS generated by the conjugates in light irradiation. Taken together, the ability of C_{60} derivatives to generation ROS is a fixed nature which can be unconditionally regulated only by designing the chemical structure of C_{60}. The ability is not influenced by the molecular weight and terminal structure of PEG, but by the style of PEG binding to C_{60}. It is apparent that the binding style was similar, irrespective of the PEG type.

It has been known that amines can react to C_{60} based on the nucleophilic attack mechanism to the π-electron of C_{60} [34]. In this study, it was found that the conjugation reaction of amine to C_{60} proceeded very slowly in dark, while it could be dramatically accelerated by light irradiation. It is likely that light irradiation can excite the electron

state of C_{60} molecules from the singlet to a long life-time triplet with higher reduction potentials [10], which enhances the reactivity of amines to C_{60}. In previous researches, preparation of C_{60}-amine conjugates was carried out in dark [15, 17]. The difference from this study may be caused by an incomplete shading condition during the conjugation. An increase in the PEG concentration accelerates the conjugation reaction, irrespective of the PEG molecular weights and terminal structure. This indicates that in the range of molecular weight from 2,000 to 12,000, the amine group of PEG could conjugate to C_{60} molecules in a similar reaction rate. Crosslink reaction sometimes occurs when a low concentration of AMPA was used. Therefore, in this study, an excess of AMPA (20 times to C_{60}) was used for the C_{60} conjugation. Under this condition, no crosslink product was observed. From the molecular weight date in **Table 1**, the pattern of molecular weight increase by C_{60} conjugation has something in common, where the molecular weight of PEG is increased by 4 times, irrespective of the PEG type. Based on the simple calculation from this molecular weight of PEG in conjugates, we may reasonably conclude that 4 of PEG molecules conjugated to one molecule of C_{60} for any C_{60}-PEG conjugate.

In contrast to the in vitro results, the in vivo photodynamic effect of C_{60}-PEG conjugates on tumor strongly depended on the type of PEG. This is because the in vivo activity is due to the extent that the C_{60} is accumulated in the tumor tissue. It is apparent from **Figures 7** and **9** that the antitumor activity of C_{60}-PEG conjugates correlated well with their tumor accumulation. The higher the amount of C_{60}-PEG conjugates accumulated in the tumor tissue, the greater their antitumor activity. The accumulation of C_{60}-PEG conjugates in tumor increased over time in 24 hr after the intravenous injection. However, 6 hr after injection, the difference in the accumulation of C_{60}-PEG conjugates

was observed and after that the trend was not changed. Based on the results, the light irradiation 6 hr after intravenous injection was selected in this study.

Influence of molecular size of C_{60}-PEG conjugates on their tumor accumulation can be explained from two viewpoints. The first point is the half-life time period in the blood circulation (**Figure 5A**). The C_{60}-MEPA20 conjugate with the smallest molecular size of about 16 nm disappeared from the blood circulation very quickly, consequently the low tumor accumulation was observed. On the other hand, the C_{60}-MEPA120 conjugate with the largest molecular size showed the longest half-life time period in the blood circulation which may due to the suppressed kidney excretion. The elimination of C_{60}-PEG conjugates from the blood circulation occurred primarily in the first one hour after the intravenous injection. After that, there was no big difference in the elimination rate. It should be noted that the amount of C_{60}-PEG conjugates in the blood continuously decreased to a lower level even after one hour although the decrease pattern seems to be different. This may be due to the difference in the organ distribution of conjugates. On the other hand, it is apparent in **Figure 7** that difference in the tumor accumulation was not observed one hour after conjugates injection, but after that. We think that the phenomenon can be explained in the terms of difference in the absolute amount of C_{60}-PEG conjugates remaining in the blood circulation.

Secondly, it is necessary to consider the pattern of tumor accumulation according to the EPR effect. It is reported that the tumor accumulation of poly(vinyl alcohol) after intravenous injection depended on their molecular size and the maximum EPR effect was observed at about 60 nm [35]. It is possible that this EPR effect also help the C_{60}-PEG conjugates to accumulate in the tumor tissue. Considering the molecular size of C_{60}-MEPA120, it was about 43 nm, which is larger than that of C_{60}-MEPA20 and C_{60}-

MEPA50 conjugates. It is possible that the conjugate with the largest molecular size is more susceptible to tumor accumulation.

PEG is a biocompatible material and has been widely used for chemical modification of DDS [21-24, 36]. However, few studies have been performed to evaluate the effect of terminal structure of PEG on the pattern of body distribution. Except for the C_{60}-AMPA50 conjugate, other types of conjugates with the similar molecular weight showed a similar pattern of blood clearance and tumor accumulation. The QCM measurement demonstrated that the conjugate interacted with albumin of serum protein strongly compared with other conjugates (**Figure 8**). It is possible that amino groups are localized on the surface of C_{60}-AMPA50 conjugate. The positive surface due to the presence of amino groups would result in strong interaction with BSA through the electrostatic interaction force. In addition, the positive charged conjugate may interact with the endothelial cells of blood vessels with a negative charge. It is conceivable that such interaction suppresses the tumor accumulation of conjugate. The low tumor accumulation of C_{60}-AMPA50 conjugates would result in the lower photodynamic effect on tumor.

In conclusion, the present study indicates that the tumor targetability of C_{60}-PEG conjugates is a key factor contributing to the PDT ability for tumor. Conjugation by PEG with an appropriate molecular weight and terminal group could enable C_{60} to solubilize in water and become an optimal size susceptible to tumor accumulation, which consequently enhanced photodynamic effect of C_{60}-PEG conjugates on tumor.

REFERENCES

[1] Z. Huang, A review of progress in clinical photodynamic therapy. Technol Cancer Res Treat 4(3) (2005) 283-293.

[2] V.F. Dima, M.D. Ionescu, C. Balotescu, S.F. Dima, Photodynamic therapy and some clinical applications in oncology. Roum Arch Microbiol Immunol 61(3) (2002) 159-205.

[3] T.J. Dougherty, C.J. Gomer, B.W. Henderson, G. Jori, D. Kessel, M. Korbelik, J. Moan, Q. Peng, Photodynamic therapy. J Natl Cancer Inst 90(12) (1998) 889-905.

[4] W.L. Nourse, R.M. Parkhurst, W.A. Skinner, R.T. Jordan, Photodynamic toxicity of porphyrins and chlorins for a human tumor cell line: combined light and concentration dose responses for the retained fraction. Biochem Biophys Res Commun 151(1) (1988) 506-511.

[5] M.R. Detty, S.L. Gibson, S.J. Wagner, Current clinical and preclinical photosensitizers for use in photodynamic therapy. J Med Chem 47(16) (2004) 3897-3915.

[6] M. Kreimer-Birnbaum, Modified Porphyrins, Chlorins, Phthalocyanines, and Purpurins: Second-Generation Photosensitizers for Photodynamic Therapy. Seminars in hematology 26(2) (1989) 157-173.

[7] T. Reynolds, Photodynamic therapy expands its horizons. J Natl Cancer Inst 89(2) (1997) 112-114.

[8] N. Razum, O.J. Balchum, A.E. Profio, F. Carstens, Skin photosensitivity: duration and intensity following intravenous hematoporphyrin derivates, HpD and DHE. Photochem Photobiol 46(5) (1987) 925-928.

[9] J.W. Arbogast, A.P. Darmanyan, C.S. Foote, F.N. Diederich, R.L. Whetten, Y. Rubin, M.M. Alvarez, S.J. Anz, Photophysical properties of sixty atom carbon molecule (C60). J Phys Chem 95(1) (1991) 11-12.

[10] C.S. Foote, Photophysical and Photochemical Properties of Fullerenes. Top Curr Chem 169 (1994) 347-363.

[11] H. Tokuyama, S. Yamago, E. Nakamura, T. Shiraki, Y. Sugiura, Photoinduced biochemical activity of fullerene carboxylic acid. J Am Chem Soc 115(17) (1993) 7918-7919.

[12] E. Nakamura, H. Isobe, N. Tomita, M. Sawamura, S. Jinno, H. Okayama, Functionalized Fullerene as an Artificial Vector for Transfection. Angewandte Chemie International Edition 39(23) (2000) 4254-4257.

[13] S.H. Friedman, D.L. DeCamp, R.P. Sijbesma, G. Srdanov, F. Wudl, G.L. Kenyon, Inhibition of the HIV-1 protease by fullerene derivatives: model building studies and experimental verification. J Am Chem Soc 115(15) (1993) 6506-6509.

[14] F. Kasermann, C. Kempf, Photodynamic inactivation of enveloped viruses by buckminsterfullerene. Antiviral Res 34(1) (1997) 65-70.

[15] N. Nakajima, C. Nishi, F.-M. Li, Y. Ikada, Photo-induced cytotoxicity of water-soluble fullerene. Fullerene Sci Tech 4(1) (1996) 1-19.

[16] K. Okuda, T. Mashino, M. Hirobe, Superoxide radical quenching and cytochrome C peroxidase-like activity of C60-dimalonic acid, C62(COOH)4. Bioorg Medi Chem Lett 6(5) (1996) 539-542.

[17] Y. Tabata, Y. Murakami, Y. Ikada, Photodynamic effect of polyethylene glycol-modified fullerene on tumor. Jpn J Cancer Res 88(11) (1997) 1108-1116.

[18] T. Tsuchiya, I. Oguri, Y.N. Yamakoshi, N. Miyata, Novel harmful effects of [60]fullerene on mouse embryos in vitro and in vivo. FEBS Lett 393(1) (1996) 139-145.

[19] U. Wattendorf, H.P. Merkle, PEGylation as a tool for the biomedical engineering of surface modified microparticles. J Pharm Sci 97(11) (2008) 4655-4669.

[20] A. Jain, S.K. Jain, PEGylation: an approach for drug delivery. A review. Crit Rev Ther Drug Carrier Syst 25(5) (2008) 403-447.

[21] J.M. Harris, N.E. Martin, M. Modi, Pegylation: a novel process for modifying pharmacokinetics. Clin Pharmacokinet 40(7) (2001) 539-551.

[22] T. Merdan, K. Kunath, H. Petersen, U. Bakowsky, K.H. Voigt, J. Kopecek, T. Kissel, PEGylation of poly(ethylene imine) affects stability of complexes with plasmid DNA under in vivo conditions in a dose-dependent manner after intravenous injection into mice. Bioconjug Chem 16(4) (2005) 785-792.

[23] J. Ramon, V. Saez, R. Baez, R. Aldana, E. Hardy, PEGylated interferon-alpha2b: a branched 40K polyethylene glycol derivative. Pharm Res 22(8) (2005) 1374-1386.

[24] F.M. Veronese, G. Pasut, PEGylation, successful approach to drug delivery. Drug Discov Today 10(21) (2005) 1451-1458.

[25] Y. Matsumura, H. Maeda, A new concept for macromolecular therapeutics in cancer chemotherapy: mechanism of tumoritropic accumulation of proteins and the antitumor agent smancs. Cancer Res 46(12 Pt 1) (1986) 6387-6392.

[26] V.P. Torchilin, Drug targeting. Eur J Pharm Sci 11 Suppl 2 (2000) S81-91.

[27] H. Maeda, The enhanced permeability and retention (EPR) effect in tumor vasculature: the key role of tumor-selective macromolecular drug targeting. Adv Enzyme Regul 41 (2001) 189-207.

[28] K. Greish, Enhanced permeability and retention of macromolecular drugs in solid tumors: a royal gate for targeted anticancer nanomedicines. J Drug Target 15(7-8) (2007) 457-464.

[29] T. Tanaka, S. Shiramoto, M. Miyashita, Y. Fujishima, Y. Kaneo, Tumor targeting based on the effect of enhanced permeability and retention (EPR) and the mechanism of receptor-mediated endocytosis (RME). Int J Pharm 277(1-2) (2004) 39-61.

[30] N. Manolova, I. Rashkov, F. Beguin, H. Vandamme, Amphiphilic Derivatives Of Fullerenes Formed By Polymer Modification. Chem Comm (1993) 1725-1727.

[31] B.M. Babior, R.S. Kipnes, J.T. Curnutte, Biological defense mechanisms. The production by leukocytes of superoxide, a potential bactericidal agent. J Clin Invest 52(3) (1973) 741-744.

[32] T. Yamaoka, Y. Tabata, Y. Ikada, Distribution and tissue uptake of poly(ethylene glycol) with different molecular weights after intravenous administration to mice. J Pharm Sci 83(4) (1994) 601-606.

[33] H. Winn, Journal of the National Cancer Institute Monographs 2 (1959) 113.

[34] A. Skiebe, A. Hirsch, H. Klos, B. Gotschy, [DBU]C60. Spin pairing in a fullerene salt. Chem Phys Lett 220(1-2) (1994) 138-140.

[35] Y. Tabata, Y. Murakami, Y. Ikada, Tumor accumulation of poly(vinyl alcohol) of different sizes after intravenous injection. J Control Release 50(1-3) (1998) 123-133.

[36] N.V. Katre, The conjugation of proteins with polyethylene glycol and other polymers : Altering properties of proteins to enhance their therapeutic potential. Adv Drug Delivery Review 10(1) (1993) 91-114.

Chapter 2

Photodynamic antitumor activity of fullerene modified with pullulan on hepatoma cells

INTRODUCTION

From the therapeutic viewpoint of tumor PDT, photosensitizers with a high light-induced ROS generation efficiency and tumor targetability are expected to design. Previous researches show that fullerene (C_{60}) can generate ROS in a high yield even by the exposure of weak visible light, and functions as a potential photosensitizer for PDT [1, 2]. In **Chapter 1**, we have demonstrated that chemical conjugation with PEG enabled C_{60} to dissolve in water and accumulate in the tumor tissue [3-5] based on the EPR effect [6-8]. The EPR effect is one of the pharmaceutical strategies to increase the accumulation of drugs in the tumor, but the tumor accumulation of C_{60} modified with PEG should be improved in terms of tumor targeting.

To enhance the tumor targetability of C_{60} and the consequently promoted photodynamic tumor therapy effect, active targeting approaches are expected. The active targeting approach is based on the ability of specific molecular recognition [9, 10]. Several researches on the active targeting of drugs have been widely demonstrated by making use of biospecific ligands, such as antibodies and peptides [11-13].

Pullulan is a water-soluble polysaccharide with a repeated unit of maltotriose bound through α-1, 6 linkage and has an inherent affinity for the asialoglycoprotein receptors (ASGPR) expressed on the surface of hepatocytes [14, 15]. In our previously studies, we have shown that pullulan was accumulated in liver several times higher than PEG and other water-soluble polymers [16]. Based on the nature, modification with

pullulan enabled drugs of interferon [17] and plasmid DNA [18, 19] to deliver to liver and enhance the biological activities thereat.

In this study, a chemical conjugation with pullulan is applied to the C_{60} of a photosensitizer to enhance the targetability to hepatoma cells. Amino groups were introduced to the terminal aldehyde group of pullulan and the chemical conjugation to C_{60} was achieved through the terminal amino group of pullulan. The in vitro and in vivo photodynamic tumor therapy effects of C_{60}-pullulan conjugates with or without light irradiation were evaluated. We examine the binding affinity of C_{60}-pullulan conjugates for HepG2 cells with the ASGPR and the receptor-free HeLa cells.

EXPERIMENTAL

Materials and reagents

Pullulan with a weight-average molecular weight of 200,000 was purchased from Tokyo Kasei Kogyo Co., Ltd., Tokyo, Japan. PEG with one terminal amine group (PEG-NH_2, molecular weights 12,000) was purchased from Nippon Oil & Fats Co., Ltd., Japan. C_{60} was purchased from the SES Research Co. Ltd., Houston, (Lot BT-6906, purity=99.9%). Fluorescein isothiocyanate (FITC) and asialofetuin were purchased from the Sigma Chemical Co., St. Louis, MO. Dibutyltin dilaurate was purchased from Wako Pure Chemical Industries, Ltd., Osaka, Japan. 2, 4, 6-Trinitrobezenesulfonic acid (TNBS), β-alanine, and cytochrome C (horse heart, Mw=12,384) were purchased from Nakalai Tesque Inc., Kyoto, Japan and was used as obtained. Other chemicals were used without further purification.

Terminal amination of pullulan

To decrease the molecular weight of pullulan, 1wt% of original pullulan solution in 0.01M HCl was heated at 98°C for 120 min. The weight average molecular weight of pullulan hydrolyzed was determined by HPLC system with SK-GEL PW4000xl column (TOSOH Corporation, Tokyo, Japan). The final hydrolysate was purified by ultrafiltration (Amicon® Ultra, 20,000 MWCO, and 5000 MWCO, Millipore Corporation, Bedford) and freeze-dried.

Introduction of amino groups to the terminal aldehyde groups of pullulan was performed by the conventional reductive amination reaction [20]. Briefly, ethylene diamine (120 mg) and sodium cyanoborohydride (125 mg) as a reductant were resolved in pullulan solution (0.1 mmol) in DMSO. After reaction for 48 hr at 60°C, the reaction mixture was cooled down to room temperature and precipitated by absolute ethanol. The precipitate was washed with absolute ethanol, redissolved in 20 ml of double-distilled water (DDW) and freeze-dried to obtain terminal aminized pullulan (pullulan-NH_2). The pullulan-NH_2 was characterized by dinitrosalicylate [21] and TNBS methods [22] to determine the amount of terminal aldehyde and amino groups, respectively.

Chemical conjugation of pullulan-NH_2 and PEG-NH_2 to C_{60}

C_{60} (7.2 mg) was dissolved in 10 ml of chlorobenzene and 20 ml of DMSO containing 0.1mmole of pullulan-NH_2 was added. The reaction mixture was stirred with a magnetic agitation at room temperature for 24 hr in a light irradiated place (incandescent lamp, 60W, 400-700 nm). After the conjugation, the reaction product was precipitated with 200 ml of absolute ethanol and recovered by centrifugation (5,000rpm, 4°C, and 10 min). The precipitate was redissolved in DDW, dialyzed against DDW for 2 days with a dialysis membrane (cut-off molecular weight: 14,000, Viskase Companies, Inc, Willowbrook, Illinois) and freeze-dried to obtain powdered C_{60}-pullulan conjugates.

C_{60}-PEG conjugates were prepared as reported previously [4, 5]. Briefly, 7.2 mg of C_{60} and 1 g of PEG-NH_2 were dissolved in 10 ml of benzene, and the reaction mixture was stirred with magnetic agitation at room temperature for 24 hr in a light irradiated place. After the conjugation, the reaction solution was mixed with 20 ml of DDW to extract the water-soluble fraction of C_{60}-PEG conjugate into the water phase. The resulting C_{60}-PEG conjugates were dialyzed against DDW for 2 days with a dialysis membrane (cut-off molecular weight: 14,000) and freeze-dried.

The C_{60}-pullulan and C_{60}-PEG conjugates were characterized by the HPLC system with SK-GEL PW4000xl column at a flow-rate of 1 ml/min. The elution buffer was 20 vol% of acetonitrile in 0.2 M phosphate-buffered solution (pH 6.9). The apparent molecular size and weight-average molecular weight of C_{60}-pullulan conjugates was determined by a MALS detector (DAWN® EOS, Wyatt Technology Co., CA).

Measurement of superoxide anion generation of C_{60}-pullulan and C_{60}-PEG conjugates

Superoxide anion generation efficiency of C_{60}-pullulan and C_{60}-PEG conjugates was evaluated by the conventional cytochrome C method [23] with a slight modification. Briefly, 100 μl of HBSS (pH=7.4, Life Technologies Oriental, Inc, Tokyo, Japan) containing 20 μM of cytochrome C was added to 100 μl HBSS containing 10 μM of C_{60} conjugates, and the mixed solution was placed into each well of 96 well cell culture cluster (COSTAR® 3595, Corning Inc, NY). The plate was then exposed to a visible light supplied from a fluorescence lamp (8 W, 400 nm-700 nm, 2 cm from the plate bottom) for up to 60 min. The absorbance increase of solution at 550 nm was measured by a microplate reader (VERSAmax, Molecular device corporation, California) to evaluate the superoxide anion generation efficiency.

Affinity evaluation of C_{60}-pullulan and C_{60}-PEG to lectin

The affinity of C_{60}-pullulan and C_{60}-PEG conjugates to lectin was demonstrated by a column binding experiment [24, 25]. Briefly, C_{60}-pullulan or C_{60}-PEG was dissolved in 25 mM Tris–HCl (pH 7.4) containing 0.3 M NaCl (buffer A) and applied on a column filled with 0.5ml of agarose-Ricinus communis agglutinin I (agarose-RCA120, vector Laboratories, inc., Burlingame, USA). After adding 2 ml of buffer A, an elution buffer of 25 mM Tris–HCl (pH 7.4) containing 0.3 M NaCl and 0.2 M of galactose (buffer B) was applied to the column. The amount of C_{60} in each fraction was determined by the absorbance measurement at a wavelength of 400 nm.

Assessment of photo-induced in vitro antitumor activity of C_{60}-pullulan and C_{60}-PEG conjugates

HepG2 cells of a human hepatoma cell line with the ASGPR were purchased from American Type Culture Collection, Manassas VA, and maintained in Minimal Essential Medium (MEM) supplemented with 1 mM sodium pyruvate, 0.1 mM non-essential amino acid solution (Invitrogen Corp., Carlsbad, CA), and 10 vol% fetal calf serum (Hyclone laboratories, Inc., Utah) at 37 °C. As a control, non-ASGPR-expressing HeLa cells which are human cervical cancer cells of a cell line, were cultured under the same conditions.

The in vitro antitumor activity of C_{60}-pullulan and C_{60}-PEG conjugates was evaluated in terms of the suppression activity of tumor cells growth using a cell counting kit (Nacalai Tesque, Inc., Kyoto, Japan). HepG2 and HeLa cells were seeded on each well of 96 well cell culture cluster (COSTAR® 3595, Corning Inc, NY, USA) at a density of 1×10^4 cells/well and cultivated in MEM overnight. The medium was changed by the fresh MEM medium containing C_{60}-pullulan or C_{60}-PEG conjugates at the C_{60} concentration of 1 μM, and incubated for 6 hr in dark. Then, the plate was exposed to a visible light supplied from a fluorescence lamp (8 W, 400 nm-700 nm, 2 cm from the

plate bottom) for 5 min. After changing the medium to fresh MEM, cells were incubated further for 48 hr. Then, 100 μl of 2-(2-methoxy-4-nitrophenyl)-3-(4-nitrophenyl)-5-(2, 4-disulfophenyl)-2*H*-tetrazolium (WST-8) solution was added and the cells were incubated further for 3 hr. The absorbance of samples was measured at 450 nm by a microplate reader (VERSAmax, Molecular device corporation, California) and the percent cell viability was expressed as 100 % for control, non-treated cells.

An inhibition experiment with asialofetuin was performed to evaluate the influence of the ASGPR on the antitumor activity of C_{60} conjugates according to the method previously reported [19, 26]. Briefly, asialofetuin which is a natural ligand for the ASGPR was added to cells to give a final concentration of 1mg/ml and pre-incubated for 1 hr before the addition of C_{60} conjugates. Then, the similar experiment was performed to evaluate the inhibition effect of asialofetuin on the in vitro antitumor activity of C_{60}-pullulan and C_{60}-PEG conjugates.

Binding affinity evaluation of C_{60}-pullulan conjugates to tumor cells.

FITC-labeled C_{60}-pullulan was prepared as previously described [27] with a slight modification. Briefly, 0.1 g of C_{60}-pullulan was dissolved in 1 ml of DMSO, and 10 mg of FITC and 2 mg of dibutyltin dilaurate were added to the solution, followed by heating for 2 hr at 95 °C. The reaction mixture was dialyzed against DDW for 2 days, purified by a gel filtration of a PD-10 column (GE healthcare UK ltd., Buckinghamshire, UK) with DDW, and then freeze-dried to obtain the FITC-labeled C_{60}-pullulan conjugates.

The cell binding experiments were performed independently in triplicate. HepG2 and HeLa cells were seeded on each well of 6 well cell culture cluster (COSTAR® 3516, Corning Inc, NY) at a density of 4×10^5 cells/well and cultivated in 2 ml of MEM for 24 hr. Then, FITC-labeled C_{60}-pullulan conjugates was added to each well and further incubated for 6 hr. All of the operations were performed in dark. Cells were washed with

10 mM PBS (pH 7.4) twice, lysed in 200 μl of a cell culture lysis reagent (Promega Corp., Madison, WI, USA) and transferred into a micro reaction tube while the cell debris was separated by centrifugation (14,000 rpm, 4 °C, and 20 min). The fluorescence intensity of supernatants was measured by SpectraMax Gemini EM Fluorescence Microplate reader (Molecular Devices, sunnyvale CA, USA).

An inhibition experiment with asialofetuin was performed to evaluate the influence of the ASGPR on the cell binding affinity of C_{60}-pullulan conjugate. Briefly, asialofetuin was added to cells to give a final concentration of 1mg/ml and pre-incubated for 1 hr before the addition of C_{60}-pullulan conjugates. Then, the similar experiment was performed to evaluate the inhibition effect of asialofetuin on the cell binding affinity of C_{60}-pullulan conjugates.

Photodynamic effect of C_{60}-pullulan and C_{60}-PEG conjugates on tumor

To prepare a mouse hepatoma xenograft model, 100 μl of HepG2 cells suspension in HBSS (1×10^8 cells/ml) was subcutaneously inoculated into the back of each nude mice aged 6 weeks (Balb/C nu/nu, Japan SLC, Inc, Shizuoka, Japan). When the tumor mass grew to 4 mm in average diameter, the tumor-bearing mice were used for the following in vivo experiments.

To evaluate the photodynamic effect of C_{60}-pullulan and C_{60}-PEG conjugates on tumor, 100 μl of conjugates solution in saline (0.3 mM) was intravenously injected to the tumor-bearing mice from the tail vein. The tumor tissue was exposed 6 hr later to visible light (400-505 nm) from a light probe of 7 mm active diameter by Heliomat Multifunction Halogen-Light (Vivadent Co. Ltd, Lichtenstein). The irradiation was carried out for 10 min at an output power of 89.2 mW/cm^2 (53.5 J/cm^2). Then, mice were fed in dark during the experiment. At different time intervals, the tumor volume (V) was

calculated according to the formula of $V=\pi/6\times a\times b^2$ (a and b is the length of long axis and short axis of tumor mass, respectively) [28].

Statistical analysis

All the data were expressed as the mean ± the standard deviation of the mean. Statistical analysis was performed based on the ANOVA, followed by Fisher's PLSD and significance was accepted at $p<0.05$.

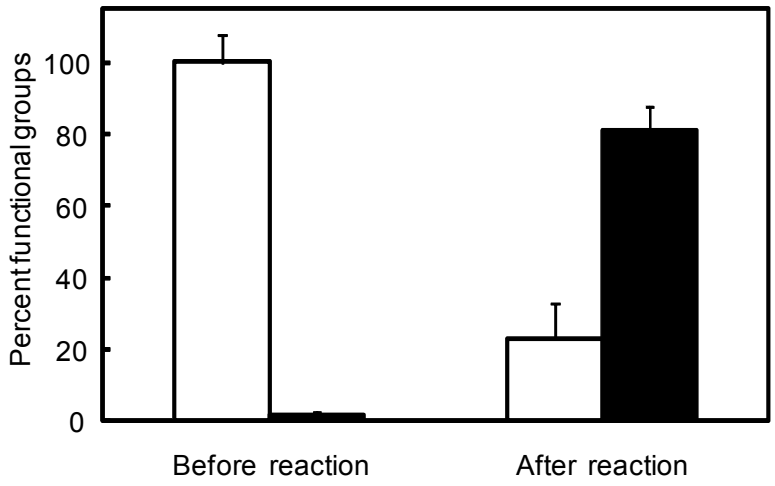

Figure 1. Percentage of terminal aldehyde (white bars) and amino groups (black bars) in pullulan before and after reductive amination reaction. The aldehyde and amino groups were determined by the dinitrosalicylate and TNBS methods, respectively.

RESULTS

Preparation and characterization of C_{60}-pullulan conjugates

The molecular weight of pullulan was decreased by the acidic hydrolysis for 120 min to about 12,000 which is similar to that of PEG-NH_2 used for C_{60} conjugation. **Figure 1** shows the percent substitution of terminal amino groups of pullulan before and after the reductive amination reaction. The percentage of terminal aldehyde group was decreased and subsequently that of amino groups introduced was increased.

Figure 2 shows the HPLC chromatograms of pullulan-NH_2 before and after C_{60} conjugation. The chromatographic peak of pullulan-NH_2 was shifted to the position at a shortened retention time by the C_{60} conjugation. When detected by UV absorbance, C_{60} was detected at the fraction of C_{60}-pullulan (data not shown). These findings indicate the conjugation of C_{60} with pullulan. When the molecular weight of C_{60}-pullulan conjugates was compared with that of original pullulan, it was found that 4 pullulan molecules were covalently conjugated to one molecule of C_{60}. The number of pullulan conjugated was similar to that of C_{60}-PEG conjugates used as the control sample in this study.

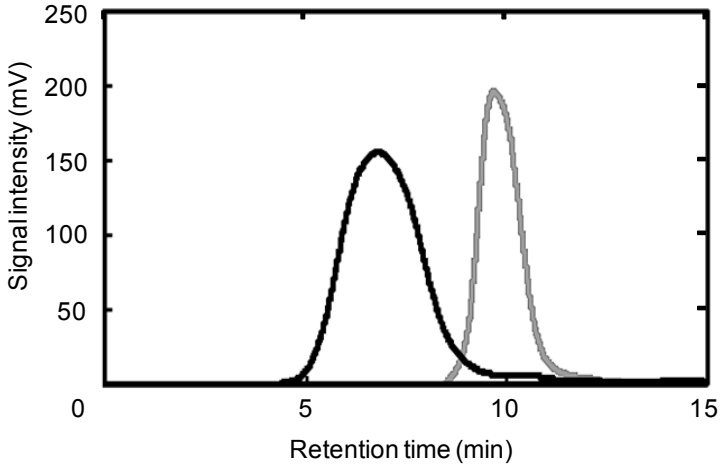

Figure 2. HPLC chromatograms of pullulan-NH_2 before (gray line) and after C_{60} conjugation (black line).

Superoxide anion generation of C_{60}-pullulan and C_{60}-PEG conjugates

Figure 3 shows the absorbance increase of cytochrome C solution containing C_{60}-pullulan and C_{60}-PEG conjugates with light irradiation for various time periods. In the presence of C_{60} conjugates, the absorbance increase became higher with the irradiation period. The similar increase pattern was observed for both the C_{60} conjugates. This indicates that the C_{60}-pullulan and C_{60}-PEG conjugates had a similar property to generate ROS.

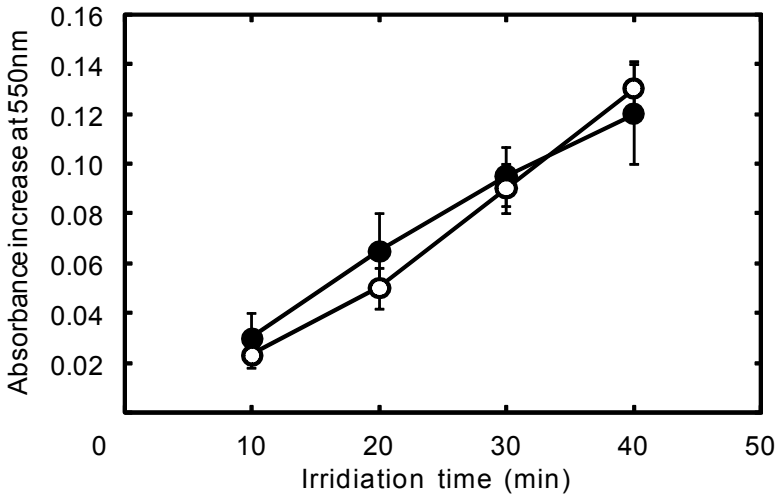

Figure 3. Absorbance increase of cytochrome C solution containing C_{60}-pullulan (○) and C_{60}-PEG conjugates (●) with light irradiation for various time periods. The absorbance increase is expressed as the difference in the absorbance value against the cytochrome C solution.

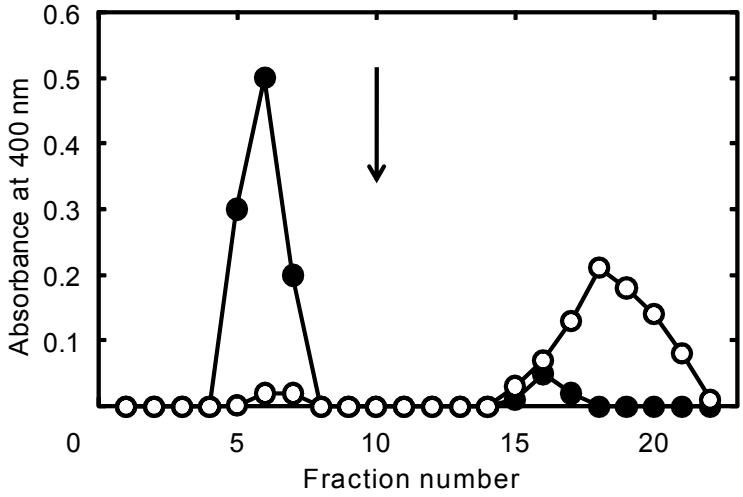

Figure 4. Gel filtration patterns of C_{60}-pullulan (○) and C_{60}-PEG conjugates (●) by RCA120-Agarose column. An arrow mark indicates the change point of elution buffer from buffer A (25 mM Tris–HCl (pH 7.4) containing 0.3 M NaCl) to buffer B (25 mM Tris–HCl (pH 7.4) containing 0.3 M NaCl and 0.2 M of galactose).

Affinity evaluation of C_{60}-pullulan and C_{60}-PEG conjugates to lectin

Figure 4 shows the elution curve of C_{60}-pullulan and C_{60}-PEG conjugates from a RCA120-Agarose column. The elution pattern was different between the C_{60}-pullulan and

C_{60}-PEG conjugates. The C_{60}-pullulan conjugates were almost completely trapped in the column equilibrated by the buffer A, whereas by washing with the buffer B containing a high concentration of galactose, they were eluted. This indicated that the C_{60}-pullulan conjugates were strongly interacted with the RCA120-Agarose. On the contrary, the C_{60}-PEG conjugates were not trapped, but eluted in the buffer A, indicating no affinity for the RCA120 lectin.

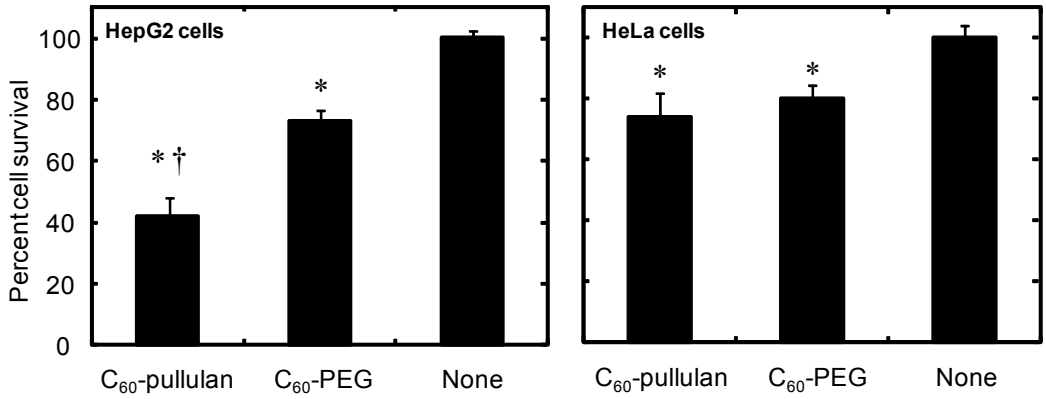

Figure 5. The survival percentage of HepG2 and HeLa cells 2 days after co-culture with C_{60}-pullulan or C_{60}-PEG conjugates plus light irradiation for 5 min. The concentration of C_{60} added is 1 μM. *, $p<0.05$: significance against the percentage of group without C_{60} conjugates (None). †, $p<0.05$: significance against the percentage of group treated with the C_{60}-PEG conjugates.

Photo-induced in vitro antitumor activity of C_{60}-pullulan and C_{60}-PEG conjugates

Figure 5 shows the photo-induced in vitro antitumor activity of C_{60}-pullulan and C_{60}-PEG conjugates on HepG2 and HeLa cells with light irradiation. Although both of the C_{60} conjugates showed photo-induced antitumor activity, the suppression activity of C_{60}-pullulan conjugates on HepG2 cells growth was significantly stronger than that of C_{60}-PEG conjugate. On the contrary, such dependence of conjugates type on the antitumor activity was not observed for HeLa cells. Irrespective of the conjugates type, the percent survival of HeLa cells was 70-80 % of control cells number by light irradiation for 5min.

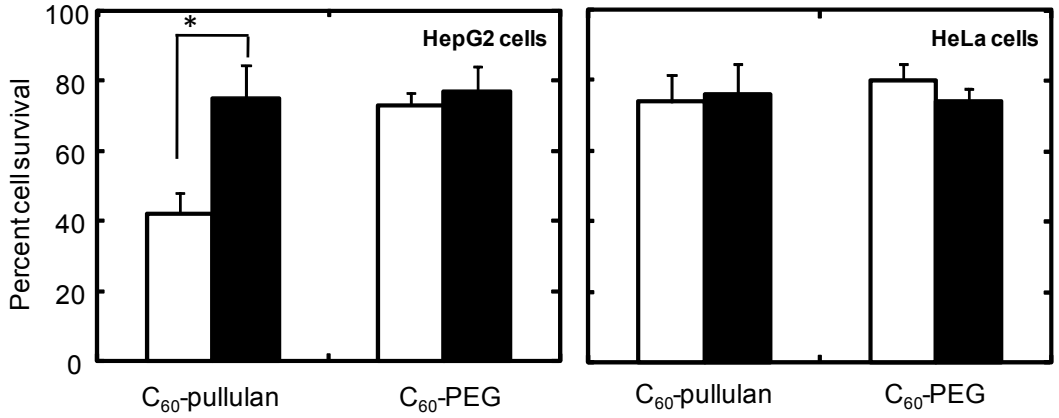

Figure 6 The survival percentage of HepG2 and HeLa cells 2 days after co-culture with of C_{60}-pullulan or C_{60}-PEG conjugates plus light irradiation for 5 min with (black bars) or without (white bars) asialofetuin pretreatment. The concentration of C_{60} added is 1 μM. *, $p<0.05$: significance against the percentage of group with asialofetuin pretreatment.

Figure 6 shows the inhibition effect of asialofetuin on the in vitro antitumor activity of C_{60}-pullulan conjugate. Pre-incubation of HepG2 cells with asialofetuin decreased the antitumor activity of C_{60}-pullulan conjugates on the HepG2 cells to the same level of C_{60}-PEG conjugate, whereas the present of asialofetuin did not affect the antitumor activity of C_{60} conjugates for HeLa cells.

Binding affinity of C_{60}-pullulan conjugates to tumor cells

Figure 7 shows the fluorescence intensity of cell lysis solution after the incubation of HepG2 and HeLa cells with FITC-labeled C_{60}-pullulan conjugates with or without asialofetuin pretreatment. The fluorescent intensity of HepG2 cells incubated with FITC-labeled C_{60}-pullulan conjugates was significant higher than that of HeLa cells. However, the increased intensity decreased by pretreatment with asialofetuin. On the other hand, for HeLa cells, pretreatment with asialofetuin had no influence on the binding behavior.

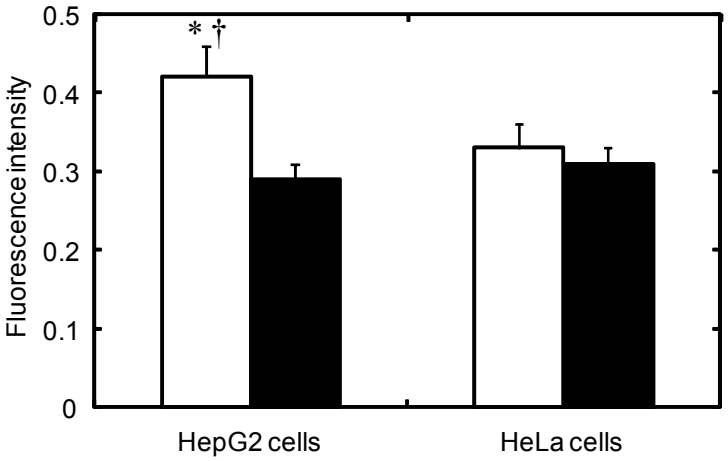

Figure 7. The fluorescence intensity of cell lysis solution after the incubation of HepG2 and HeLa cells with fluorescence-labeled C_{60}-pullulan conjugates at 37 °C for 6 hr in dark conditions with (black bars) or without (white bars) asialofetuin pretreatment. * $p<0.05$: significant against the fluorescence intensity of lysis solution for HeLa cells pretreated with asialofetuin. † $p<0.05$: significant against the fluorescence intensity of lysis solution for HepG2 cells pretreated with asialofetuin.

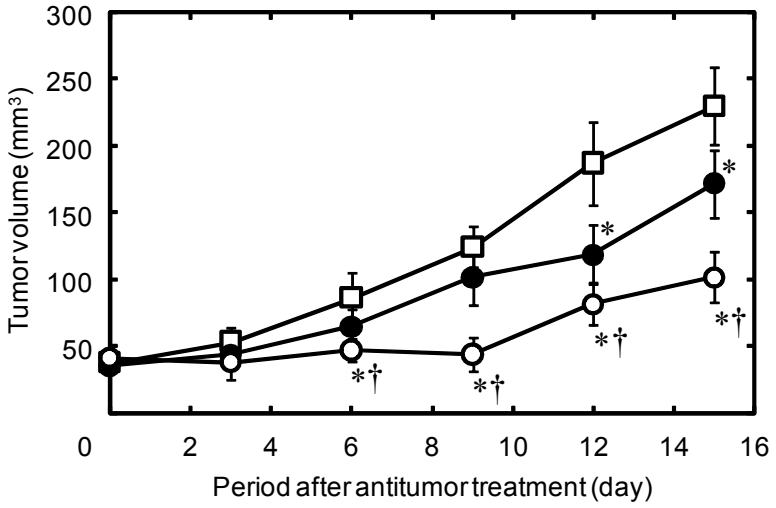

Figure 8. Photodynamic antitumor effect of C_{60}-polymer conjugates on HepG2 tumor-bearing mice after intravenous injection of C_{60}-pullulan (○), and C_{60}-PEG conjugates (●) or saline (□). * $p<0.05$: significant against the tumor volume of saline-injected group at the corresponding time point. † $p<0.05$: significant against the tumor volume of C_{60}-PEG injected group at the corresponding time point.

Photodynamic effect of C_{60}-pullulan and C_{60}-PEG conjugates on tumor

Figure 8 shows the in vivo photodynamic effect of C_{60}-pullulan and C_{60}-PEG conjugates on tumor. After the PDT treatment, both of the C_{60} conjugates showed tumor suppression effect to a significantly great extent compared with the treatment of saline. However, the tumor suppression effect of C_{60}-pullulan conjugates was significantly higher than that of C_{60}-PEG conjugates over the whole time period studied.

DISCUSSION

The present study demonstrated that C_{60}-pullulan conjugates showed an enhanced antitumor activity on HepG2 cells of hepatoma both in the in vitro and in vivo systems compared with the C_{60}-PEG conjugates. To modify C_{60} for a drug effective in the PDT, there are two points to be resolved: one is to make C_{60} water-soluble, and the other is to give C_{60} a tumor targetability. Our previous studies experimentally demonstrated that C_{60} chemically modified with PEG was dissolved in water and accumulated in the tumor tissue to a higher extent than in other normal tissues. It is likely that this is based on the EPR effect [3-5]. However, this C_{60} modification is not always sufficient in terms of tumor targetability. The objective of this study is to give C_{60} a tumor targetability through the conjugation with pullulan. It is found that pullulan of a water-soluble polysaccharide was accumulated in the liver at significantly higher amounts than other water-soluble polymers probably due to the inherent nature to be recognized by ASGPR [14-16]. The pullulan conjugation succeeded in the liver targeting of drugs [17-19, 29, 30].

Our previous studies demonstrated that C_{60}-PEG conjugates prepared by PEG-NH_2 with a molecular weight of 12,000 showed a high tumor PDT effect compared with that of other molecular weights. Based on the result, in this study, pullulan with the molecular weight of 12,000 was selected for comparison. In addition, to make the

chemical structure of C_{60}-pullulan conjugates correspond to that of C_{60}-PEG conjugates, pullulan was required to conjugate to C_{60} in the end-on fashion. Therefore, amino groups were chemically introduced to the terminal of pullulan by the reductive amination reaction [31]. A quantitative analysis (**Figure 1**) indicated that the amino groups were one-to-one introduced to the terminal aldehyde groups of pullulan. From the chromatographic study, it was experimentally confirmed that the number of pullulan introduced to C_{60} was similar to that of C_{60}-PEG conjugates which is used as the control sample in this study. The similar increase pattern in the cytochrome C absorbance for C_{60}-PEG and C_{60}-pullulan conjugates (**Figure 3**) indicated that both of the C_{60} conjugates had a similar efficiency of ROS generation. The lectin affinity test (**Figure 4**) of C_{60}-pullulan and C_{60}-PEG conjugates with a RCA120-Agarose column revealed that the C_{60}-pullulan conjugates had a lectin affinity, but the C_{60}-PEG conjugates did not. The RCA120 was a kind of lectin and widely used for the detection of galactose-containing oligosaccharides [32]. Taken together, the C_{60}-PEG and C_{60}-pullulan conjugates had the similar molecular structure where one C_{60} molecular is covered with 4 molecules of pullulan or PEG and the similar ROS generation efficiency. More importantly, the pullulan molecules localized on the surface of C_{60}-pullulan conjugates can be recognized by the sugar-recognizable lectin.

The in vitro antitumor activity experiments with or without asialofetuin pretreatment clearly indicated that the photo-induced antitumor activity of C_{60}-pullulan was specific for HepG2 cells with the ASGPR on the surface (**Figure 5 and Figure 6**). It is reported that the ASGPR which belongs to the c-type lectin family and recognizes galactose or N-acetylgalactosamine residues of desialylated glycoproteins, are expressed on the surface of HepG2 cells, but not on HeLa cells. As shown in **Figure 7**, the binding of C_{60}-pullulan conjugates onto HepG2 cells was significant higher than that of HeLa

cells, but the difference disappeared when the cells were pretreated with asialofetuin to block the ASGPR. On the other hand, pretreatment of HeLa cells with asialofetuin did not affect the binding property. We can say with fair certainty that the C_{60}-pullulan conjugates were recognized by the ASGPR on the surface of HepG2 cells, resulting in cell-specifically enhanced PDT antitumor effect.

The in vivo antitumor experiments demonstrated that the C_{60}-pullulan conjugates showed higher photodynamic effect on tumor in vivo than the C_{60}-PEG conjugates (**Figure 8**). Since both the C_{60}-PEG and C_{60}-pullulan conjugates had the similar structure, molecular weight, and ROS generation efficiency (**Figure 2**), it is highly conceivable that the enhanced in vivo photodynamic effect on tumor was due to the effective accumulation in the tumor tissue due to the EPR effect and subsequently the higher binding affinity to hepatoma cells mediated by the specific interaction with ASGPR.

It should be noted that in this study, the in vivo treatment of C_{60}-pullulan conjugates was applied for a subcutaneous tumor model, but not for liver tumor model due to the transparent limitation of light permeation. As a recent trial to tackle this issue, most of the recent photosensitizer studies focused on the compounds with absorbance peak in the near-infrared wavelength range. However, such an approach cannot always come to the clitical applications because the human tissue is generally thicker than the animal one. It was known that ultrasound with a higher permeability can induce a luminescence in the body (sonoluminescence), which is a new candidate of physical stimulus for PDT applications [33]. One of the problems is that the light generated by the sonoluminescence mechanism is too weak to induce the photodynamic effect for most photosensitizers. It should be noted that the C_{60}-based photosensitizers possesses a high quantum yield, which means the photodynamic effect can be induced even by a weak light [34]. An ultrasound irradiation was performed instead of light irradiation for the C_{60}-

pullulan conjugates to evaluate the in vitro antitumor activity on HepG2 cells. It was experimentally demonstrated that the ultrasound irradiation also worked well to induce C_{60}-pullulan-based antitumor activity (data not shown). Sonodynamic therapy by C_{60}-pullulan conjugates combined with ultrasound may be promising for liver cancer therapy.

REFERENCE

[1] J.W. Arbogast, A.P. Darmanyan, C.S. Foote, F.N. Diederich, R.L. Whetten, Y. Rubin, M.M. Alvarez, S.J. Anz, Photophysical properties of sixty atom carbon molecule (C60). The Journal of Physical Chemistry 95(1) (1991) 11-12.

[2] T. Tsuchiya, I. Oguri, Y.N. Yamakoshi, N. Miyata, Novel harmful effects of [60]fullerene on mouse embryos in vitro and in vivo. FEBS Lett 393(1) (1996) 139-145.

[3] Y. Tabata, Y. Murakami, Y. Ikada, Photodynamic effect of polyethylene glycol-modified fullerene on tumor. Jpn J Cancer Res 88(11) (1997) 1108-1116.

[4] J. Liu, S. Ohta, A. Sonoda, M. Yamada, M. Yamamoto, N. Nitta, K. Murata, Y. Tabata, Preparation of PEG-conjugated fullerene containing Gd3+ ions for photodynamic therapy. J Control Release 117(1) (2007) 104-110.

[5] J. Liu, M. Yamamoto, Y. Tabata, Antitumor activity of fullerene modified by polyethylene glycol with different molecular weights and terminal structures.

[6] H. Maeda, J. Wu, T. Sawa, Y. Matsumura, K. Hori, Tumor vascular permeability and the EPR effect in macromolecular therapeutics: a review. J Control Release 65(1-2) (2000) 271-284.

[7] T. Yamaoka, Y. Tabata, Y. Ikada, Distribution and tissue uptake of poly(ethylene glycol) with different molecular weights after intravenous administration to mice. J Pharm Sci 83(4) (1994) 601-606.

[8] V.P. Torchilin, Drug targeting. Eur J Pharm Sci 11 Suppl 2 (2000) S81-91.

[9] Y.H. Bae, Drug targeting and tumor heterogeneity. J Control Release 133(1) (2009) 2-3.

[10] C.S.S.R. Kumar, Nanomaterials for cancer diagnosis, Wiley-VCH, 2007.

[11] M. Pagé, Tumor targeting in cancer therapy Humana Press, 2002.

[12] P.A. McCarron, W.M. Marouf, D.J. Quinn, F. Fay, R.E. Burden, S.A. Olwill, C.J. Scott, Antibody targeting of camptothecin-loaded PLGA nanoparticles to tumor cells. Bioconjug Chem 19(8) (2008) 1561-1569.

[13] F. Danhier, B. Vroman, N. Lecouturier, N. Crokart, V. Pourcelle, H. Freichels, C. Jerome, J. Marchand-Brynaert, O. Feron, V. Preat, Targeting of tumor endothelium by RGD-grafted PLGA-nanoparticles loaded with Paclitaxel. J Control Release (2009).

[14] Y. Kaneo, T. Tanaka, T. Nakano, Y. Yamaguchi, Evidence for receptor-mediated hepatic uptake of pullulan in rats. J Control Release 70(3) (2001) 365-373.

[15] T. Tanaka, Y. Fujishima, S. Hanano, Y. Kaneo, Intracellular disposition of polysaccharides in rat liver parenchymal and nonparenchymal cells. Int J Pharm 286(1-2) (2004) 9-17.

[16] T. Yamaoka, Y. Tabata, Y. Ikada, Body distribution profile of polysaccharide after intravenous administration. Drug Deliv. 1 (1993).

[17] K. Xi, Y. Tabata, K. Uno, M. Yoshimoto, T. Kishida, Y. Sokawa, Y. Ikada, Liver targeting of interferon through pullulan conjugation. Pharm Res 13(12) (1996) 1846-1850.

[18] H. Hosseinkhani, T. Aoyama, O. Ogawa, Y. Tabata, Liver targeting of plasmid DNA by pullulan conjugation based on metal coordination. J Control Release 83(2) (2002) 287-302.

[19] J. Jo, T. Ikai, A. Okazaki, M. Yamamoto, Y. Hirano, Y. Tabata, Expression profile of plasmid DNA by spermine derivatives of pullulan with different extents of spermine introduced. J Control Release 118(3) (2007) 389-398.

[20] R.F. Borch, M.D. Bernstein, H.D. Durst, Cyanohydridoborate anion as a selective reducing agent. Journal of the American Chemical Society 93(12) (1971) 2897-2904.

[21] G.L. Miller, Use of dinitrosalicylic acid reagent for determination of reducing sugar. Analytical Chemistry 31(3) (1959) 426-428.

[22] T.G.M. Schalkhammer, Analytical biotechnology Springer, 2002.

[23] B.M. Babior, R.S. Kipnes, J.T. Curnutte, Biological defense mechanisms. The production by leukocytes of superoxide, a potential bactericidal agent. J Clin Invest 52(3) (1973) 741-744.

[24] Y. Ohyama, K. Kasai, H. Nomoto, Y. Inoue, Frontal affinity chromatography of ovalbumin glycoasparagines on a concanavalin A-sepharose column. A quantitative study of the binding specificity of the lectin. J Biol Chem 260(11) (1985) 6882-6887.

[25] W. Bessler, P. Schindler, Purification of 2-deoxy-2-dansylamido-D-glucose by affinity chromatography on a lectin-loaded agarose column. Experientia 35(10) (1979) 1292-1293.

[26] I. Kanatani, T. Ikai, A. Okazaki, J. Jo, M. Yamamoto, M. Imamura, A. Kanematsu, S. Yamamoto, N. Ito, O. Ogawa, Y. Tabata, Efficient gene transfer by pullulan-spermine occurs through both clathrin- and raft/caveolae-dependent mechanisms. J Control Release 116(1) (2006) 75-82.

[27] A.N. Belder, K. Granath, Preparation and properties of fluorescein-labelled dextrans. Carbohydr. Res. 30 (1973) 375–378.

[28] H. Winn, The Immune Response and the Homograft Reaction. Journal of the National Cancer Institute Monographs 2 (1959) 113.

[29] Y. Suginoshita, Y. Tabata, T. Matsumura, Y. Toda, M. Nabeshima, F. Moriyasu, Y. Ikada, T. Chiba, Liver targeting of human interferon-beta with pullulan based on metal coordination. J Control Release 83(1) (2002) 75-88.

[30] Y. Suginoshita, Y. Tabata, F. Moriyasu, Y. Ikada, T. Chiba, Liver targeting of interferon-beta with a liver-affinity polysaccharide based on metal coordination in mice. J Pharmacol Exp Ther 298(2) (2001) 805-811.

[31] M. Yalpani, A survey of recent advances in selective chemical and enzymic polysaccharide modifications. Tetrahedron 41(15) (1985) 2957-3020.

[32] Y. Itakura, S. Nakamura-Tsuruta, J. Kominami, N. Sharon, K. Kasai, J. Hirabayashi, Systematic comparison of oligosaccharide specificity of Ricinus communis agglutinin I and Erythrina lectins: a search by frontal affinity chromatography. J Biochem 142(4) (2007) 459-469.

[33] L.A. Crum, R.A. Roy, Sonoluminescence. Science 266(5183) (1994) 233-234.

[34] Y. Tabata, T. Ishii, T. Aoyama, R. Oki, Y. Hirano, O. Ogawa, Y. Ikada, Sonodynamic effect of polyethylene glycol-conjugated fullerene on tumor. Perspectives of Fullerene Nanotechnology (2002) 185-196.

Chapter 3

Effect of modification manner on photodynamic antitumor activity of fullerene modified with pullulan

INTRODUCTION

In **Chapter 1**, we have demonstrated that chemical conjugation with PEG enabled C_{60} to dissolve in water and accumulate in the tumor tissue [1-3] based on the EPR effect [4-7]. In addition, **Chapter 2** showed that the tumor targetability can be further enhanced by the modification with pullulan which is a water-soluble polysaccharide with a repeated unit of maltotriose bound through α-1, 6 linkage and has an inherent affinity for the ASGPR expressed on the surface of hepatocytes [8, 9]. The pullulan conjugation gave C_{60} the active targetability to HepG2 cells, resulting in enhanced photodynamic antitumor effect.

The objective of this study is to obtain the basic knowledge about the tumor affinity and the photodynamic antitumor therapy effect of C_{60} modified with pullulan. It is highly conceivable that the physicochemical structure of C_{60}-pullulan conjugates is an important key for their photodynamic antitumor therapy effect. To evaluate the effect of pullulan molecular weight and the modification manner to C_{60} on the photodynamic antitumor activity of C_{60} conjugates, two modification manners were performed. C_{60} was conjugated to pullulan through the hydroxyl groups of main chain (pendant type) and the terminal aldehyde groups (terminal type). Their affinity for tumor cells as well as the in vitro antitumor activities of C_{60}-pullulan conjugates was examined in terms of the molecular weights and modification manner of pullulan.

EXPERIMENTAL

Materials and reagents

Pullulan with different weight-average molecular weights of 6,000, 12,000, 23,000, 47,000, and 112,000 were purchased from Hayashibara Biochemical Laboratories, Inc., Okayama, Japan. C_{60} was purchased from the SES Research Co. Ltd., Houston, (Lot BT-6906, purity=99.9%). FITC and asialofetuin were purchased from the Sigma Chemical Co., St. Louis, MO. Dibutyltin dilaurate was purchased from Wako Pure Chemical Industries, Ltd., Osaka, Japan. TNBS, β-alanine, and cytochrome C (horse heart, Mw=12,384) were purchased from Nakalai Tesque Inc., Kyoto, Japan and was used as obtained. Other chemicals were used without further purification.

Introduction of amino groups to pullulan

Amino groups were introduced to the terminal aldehyde and hydroxyl groups of pullulan to allow C_{60} to conjugate in different modification manners. First, introduction of amino groups to the terminal aldehyde groups of pullulan was performed by the conventional reductive amination reaction [10]. Briefly, ethylene diamine (120 mg) and sodium cyanoborohydride (125 mg) as a reductant were resolved in pullulan solution (0.1 mmol) in DMSO. After reaction for 48 hr at 60°C, the reaction mixture was cooled down to room temperature and precipitated by absolute ethanol. The precipitate was washed with absolute ethanol, redissolved in 20 ml of DDW and freeze-dried to obtain terminal aminized pullulan. The terminal aminized pullulan prepared was characterized by the dinitrosalicylate [11] and TNBS methods [12] to determine the amount of terminal aldehyde and amino groups, respectively.

Next, ethylene diamine was introduced to the hydroxyl groups of pullulan by a N,N'-carbonyldiimidazole (CDI) activation method [13]. Ethylene diamine and CDI were

added to 50 ml of dehydrated DMSO containing 500 mg of pullulan. Following agitation using a magnetic stirrer at 35 °C for 20 hr, the pullulan with OH groups aminized (pendant) was separated and purified by the procedure above mentioned. The amino groups introduced were determined by the TNBS method.

Chemical conjugation of pullulan-NH_2 to C_{60}

C_{60} (7.2 mg) was dissolved in 10 ml of chlorobenzene and 20 ml of DMSO containing 0.1mmole of pullulan aminized was added. The reaction mixture was stirred with a magnetic agitation at room temperature for 24 hr in a light irradiated place (incandescent lamp, 60W, 400-700 nm). After the conjugation, the reaction product was precipitated with 200 ml of absolute ethanol and collected by centrifugation (5,000 rpm, 4 °C, and 10 min). The precipitate was redissolved in DDW, further purified by gel filtration with a column filled with Sephacryl S-200 (Pharmacia Biotech, Uppsala, Sweden. elution buffer: 0.4 M CH_3COONH_4) and freeze-dried to obtain powdered C_{60}-pullulan conjugates with terminal (C_{60}-t-pullulan) or pendant (C_{60}-p-pullulan) modification manners.

The C_{60}-pullulan conjugates were characterized by the HPLC system with SK-GEL PW4000xl column (TOSOH Corporation, Tokyo, Japan) at a flow-rate of 1 ml/min. The elution buffer was 20 vol% of acetonitrile in 0.2 M phosphate-buffered solution (pH 6.9). The apparent molecular size and weight-average molecular weight of C_{60}-pullulan conjugates was determined by a MALS detector (DAWN® EOS, Wyatt Technology Co., CA).

Measurement of superoxide anion generation of C_{60}-pullulan conjugates

Superoxide anion generation efficiency of C_{60}-pullulan conjugates was evaluated by the conventional cytochrome C method [14] with a slight modification. Briefly, 100 μl of HBSS (pH=7.4, Life Technologies Oriental, Inc, Tokyo, Japan) containing 20 μM of

cytochrome C was added to 100 μl HBSS containing 10 μM of C_{60}-pullulan conjugates, and the mixed solution was placed into each well of 96-well multi-well culture plate (COSTAR® 3595, Corning Inc, NY). The plate was then exposed to a visible light supplied from a fluorescence lamp (8 W, 400 nm-700 nm, 2 cm from the plate bottom) for up to 60 min. The absorbance increase of solution at 550 nm was measured by a microplate reader (VERSAmax, Molecular device corporation, California) to evaluate the superoxide anion generation efficiency.

Affinity evaluation of C_{60}-pullulan for lectin

Agarose beads (100 μl) immobilized with galactose-specific recinus communis agglutinin (agarose-RCA120, vector Laboratories, inc., Burlingame, USA) were mixed with 200 μl phosphate-buffer solution (PBS, 10 mM, pH 7.4) containing C_{60}-pullulan conjugates and incubated at room temperature for 30 min with continuous shaking. After centrifugation, C_{60}-pullulan in the supernatant was determined by measuring the absorbance of solution at 400 nm. As an inhibition experiment, 60 μmol of galactose was added to the pullulan PBS solution before mixing with agarose-RCA120 beads. Then, the similar binding experiment was performed to evaluate the addition effect of galactose on the binding affinity of C_{60}-pullulan conjugates for agarose-RCA120 beads.

Assessment of photo-induced in vitro antitumor activity of C_{60}-pullulan conjugates

HepG2 cells of a human hepatoma cell line with the ASGPR were purchased from American Type Culture Collection, Manassas VA, and maintained in MEM supplemented with 1 mM sodium pyruvate, 0.1 mM non-essential amino acid solution (Invitrogen Corp., Carlsbad, CA), and 10 vol% fetal calf serum (Hyclone laboratories, Inc., Utah) at 37 °C.

The in vitro antitumor activity of C_{60}-pullulan conjugates was evaluated in terms of the suppression activity of tumor cells growth using a cell counting kit (Nacalai Tesque, Inc., Kyoto, Japan). HepG2 cells were seeded on each well of 96 well cell culture plate

(COSTAR® 3595, Corning Inc, NY) at a density of 1×10^4 cells/well and cultivated in the MEM medium overnight. The medium was changed by the fresh MEM medium containing C_{60}-pullulan at the C_{60} concentration of 1 μM, and incubated for 1 hr in dark. Then, the plate was exposed to a visible light supplied from a fluorescence lamp (8 W, 400 nm-700 nm, 2 cm from the plate bottom) for 5 min. After changing the medium to fresh MEM, cells were incubated further for 48 hr. Then, 100 μl of WST-8 solution was added and the cells were incubated further for 3 hr. The absorbance of samples was measured at 450 nm with the microplate reader (VERSAmax, Molecular Device Corporation, California) and the percent cell viability was expressed as 100 % for control, non-treated cells.

Binding affinity evaluation of C_{60}-pullulan conjugates for tumor cells.

FITC-labeled C_{60}-pullulan was prepared as previously described [15] with a slight modification. Briefly, 0.1 g of C_{60}-pullulan was dissolved in 1 ml of DMSO, and 10 mg of FITC and 2 mg of dibutyltin dilaurate were added to the solution, followed by heating for 2 hr at 95 °C. The reaction mixture was dialyzed against DDW for 2 days, purified by a gel filtration of a PD-10 column (GE healthcare UK ltd., Buckinghamshire, UK) with DDW, and then freeze-dried to obtain the FITC-labeled C_{60}-pullulan conjugates.

The cell binding experiments were performed independently in triplicate. HepG2 and HeLa cells were seeded on each well of 6 well cell culture plate (COSTAR® 3516, Corning Inc, NY) at a density of 4×10^5 cells/well and cultivated in 2 ml of MEM for 24 hr. Then, FITC-labeled C_{60}-pullulan conjugates were added to each well and further incubated for 1 or 6 hr. All of the operations were performed in dark. Cells were washed with 10 mM PBS (pH 7.4) twice, lysed in 200 μl of a cell culture lysis reagent (Promega Corp., Madison, WI, USA) and transferred into a micro reaction tube while the cell debris was separated by centrifugation (14,000 rpm, 4 °C, and 20 min). The fluorescence

intensity of supernatants was measured by SpectraMax Gemini EM Fluorescence Microplate reader (Molecular Devices, sunnyvale CA, USA).

An inhibition experiment with asialofetuin was performed to evaluate the influence of the ASGPR on the antitumor activity of C_{60}-pullulan conjugates according to the method previously reported [16, 17]. Briefly, asialofetuin which is a natural ligand for the ASGPR was added to cells to give a final concentration of 1mg/ml and pre-incubated for 1 hr before the addition of C_{60} conjugates. Then, the similar experiment was performed to evaluate the inhibition effect of asialofetuin on the in vitro antitumor activity of C_{60}-pullulan conjugates.

Statistical analysis

All the data were expressed as the mean ± the standard deviation of the mean. Statistical analysis was performed based on the ANOVA, followed by Fisher's PLSD and significance was accepted at $p < 0.05$.

RESULTS

Preparation and characterization of C_{60}-pullulan conjugates

Ethylene diamine was introduced to the hydroxyl groups of pullulan by the CDI activation method (**Figure 1A**). The extent of ethylene diamine introduced could be changed by altering the amount of CDI added initially, irrespective of the pullulan molecular weight. On the other hand, ethylene diamine was introduced to the terminal aldehyde groups of pullulan by the reductive amination reaction (**Figure 1B**). The terminal aldehyde groups were converted to amino groups by the reaction although the reaction ratio decreased when the molecular weight of pullulan increased to 112,000.

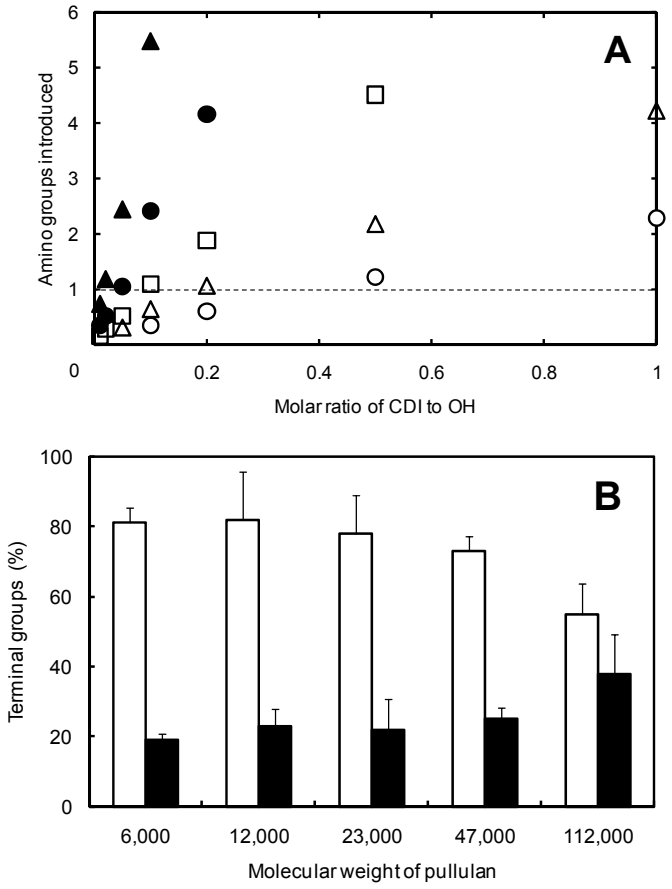

Figure 1. (A) Introduction efficiency of ethylene diamine to the hydroxyl groups of pullulan with molecular weights of 6,000 (○), 12,000 (△), 23,000 (□), 47,000 (●), and 112,000 (▲) by the CDI activation method. (B) Percentage of terminal amino (white bars) and aldehyde groups (black bars) in pullulan after the reductive amination reaction.

Figure 2 shows the apparent molecular size and weight average molecular weight of C_{60}-t-pullulan and C_{60}-p-pullulan conjugates. Irrespective of the modification manner, both of the apparent molecular size and molecular weight of C_{60}-pullulan conjugates increased with an increase in the molecular weight of pullulan conjugated. **Table 1** shows the number of pullulan conjugated to one C_{60} molecule calculated from comparing the molecular weight of C_{60}-pullulan conjugates with that of original pullulan. Irrespective of the pullulan modification manner, the amount of pullulan molecules covalently conjugated to one molecule of C_{60} ranged from 3 to 5 for C_{60}-pullulan conjugates, although it tended to decrease with an increase in the molecular weight of pullulan.

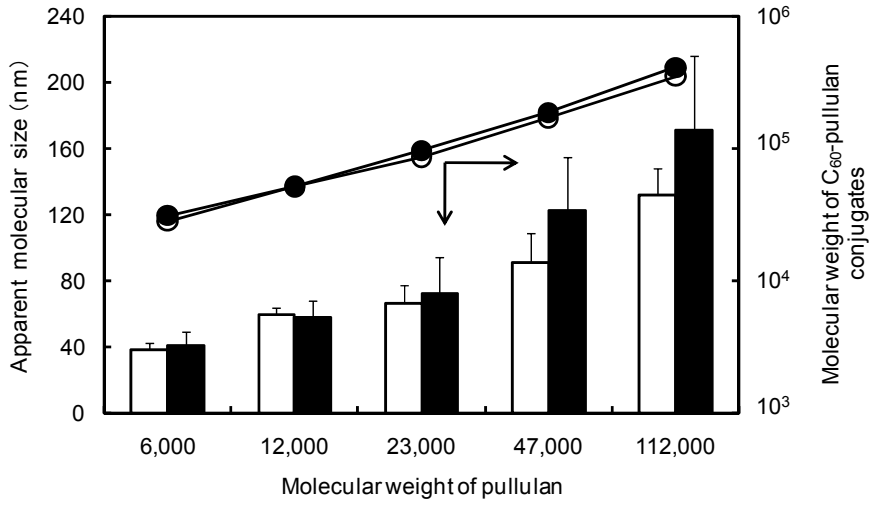

Figure 2. The apparent molecular size and weight-average molecular weight of C_{60}-t-pullulan (white marks) and C_{60}-p-pullulan (black marks).

Superoxide anion generation of C_{60}-pullulan conjugates

Figure 3 shows the absorbance increase of cytochrome C solution containing C_{60}-t-pullulan and C_{60}-p-pullulan conjugates with light irradiation for various time periods. In the presence of C_{60}-pullulan conjugates, the absorbance increase became higher with the irradiation period. The similar increase pattern was observed for all of the C_{60}-pullulan

conjugates. This indicates that every C_{60}-pullulan conjugate had a similar property to generate ROS.

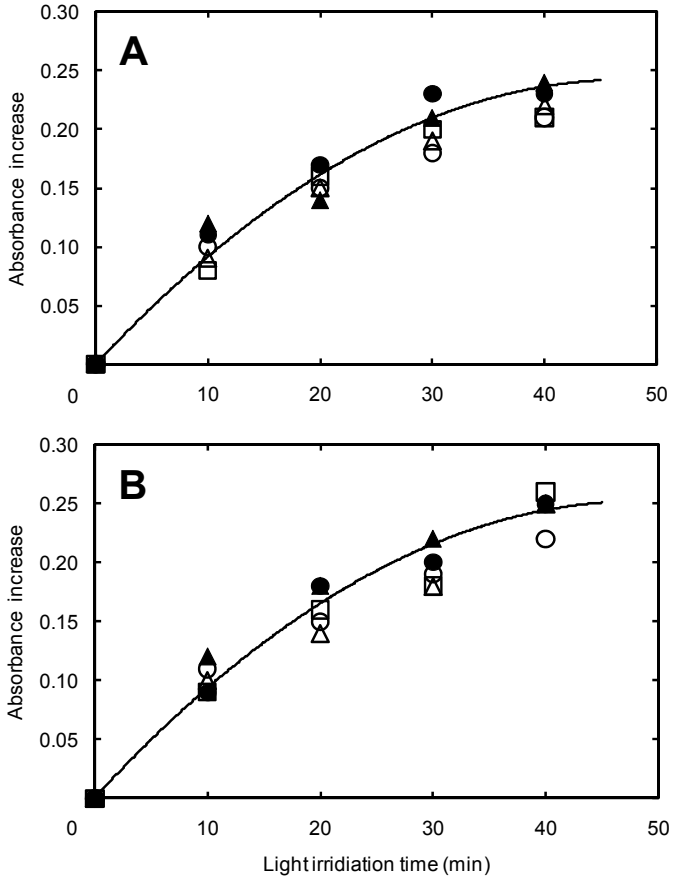

Figure 3. Absorbance increase of cytochrome C solution containing C_{60}-t-pullulan with molecular weights of 6,000 (○), 12,000 (△), 23,000 (□), 47,000 (●), and 112,000 (▲) (A) and C_{60}-p-pullulan conjugates with molecular weights of 6,000 (○), 12,000 (△), 23,000 (□), 47,000 (●), or 112,000 (▲) with light irradiation for various time periods (B). The absorbance increase is expressed as the difference in the absorbance value against that of cytochrome C solution.

Affinity of C_{60}-pullulan conjugates for lectin

Figure 4 shows the adsorption patterns of C_{60}-t-pullulan and C_{60}-p-pullulan conjugates onto RCA120-Agarose beads. The amount of C_{60}-t-pullulan conjugates adsorbed increased with the increase of pullulan molecular weight, while the C_{60}-p-pullulan conjugates showed an invariable adsorption. When compared the adsorption amount among C_{60}-pullulan conjugates with the same molecular weight, a higher

adsorption was observed for the C_{60}-t-pullulan conjugates although the extent increased with the increased molecular weight of pullulan. The similar adsorption was observed for both the C_{60}-t-pullulan and C_{60}-p-pullulan conjugates compared with pullulan molecular weights of 6,000, 12,000, and 23,000. For the pullulan with the molecular weights of 47,000 and 112,000, the lectin affinity of C_{60}-t-pullulan conjugates was significantly higher than that of C_{60}-p-pullulan conjugates. On the other hand, the adsorption amount reduced to a very low level by galactose addition in a similar fashion for the two types of pullulan conjugates although the reduced level was higher with an increase in the molecular weight of pullulan.

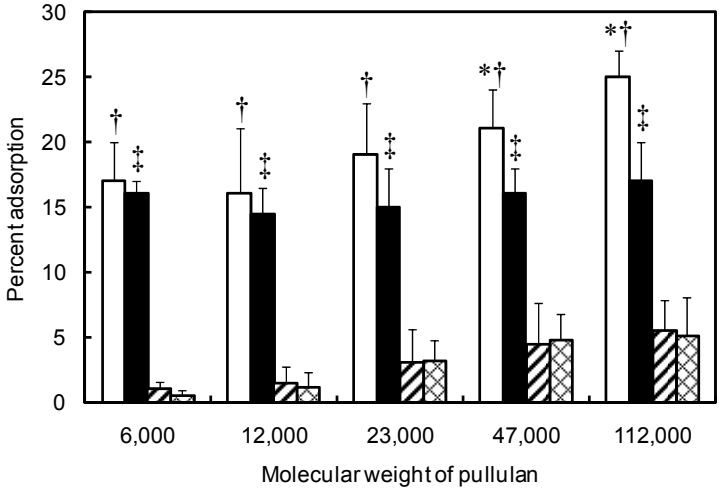

Figure 4. Adsorption patterns of C_{60}-t-pullulan (□ and ▨) and C_{60}-p-pullulan (■ and ▩) conjugates onto RCA120-Agarose beads in PBS (□ and ■) or that containing 0.2 M of galactose (▨ and ▩). *, $p<0.05$: significance against the percent adsorption of C_{60}-p-pullulan conjugates in PBS at the corresponding molecular weight of pullulan. †, $p<0.05$: significance against the percent adsorption of C_{60}-t-pullulan conjugates in PBS containing 0.2 M of galactose at the corresponding molecular weight of pullulan. ‡, $p<0.05$: significance against the percent adsorption of C_{60}-p-pullulan conjugates in PBS containing 0.2 M of galactose at the corresponding molecular weight of pullulan.

Photo-induced in vitro antitumor activity of C_{60}-pullulan conjugates

Figure 5 shows the photo-induced in vitro antitumor activity of C_{60}-t-pullulan and C_{60}-p-pullulan conjugates on HepG2 cells with or without the pretreatment of asialofetuin.

Although both of the C_{60}-pullulan conjugates showed photo-induced antitumor activity, the suppression activity of C_{60}-t-pullulan conjugates on HepG2 cells growth was stronger than that of C_{60}-p-pullulan conjugate. The increase of pullulan molecular weight decreased the in vitro antitumor activity of C_{60}-p-pullulan conjugate. On the contrary, such the molecular weight dependence on the antitumor activity was not observed for C_{60}-t-pullulan conjugates. Irrespective of the molecular weight, the percent survival of cells decreased to the level lower than 50 % of control cells number even by light irradiation for 5min. In addition, pre-incubation of HepG2 cells with asialofetuin decreased the in vitro antitumor activity of C_{60}-t-pullulan conjugates on the HepG2 cells to the same level of C_{60}-p-pullulan conjugates.

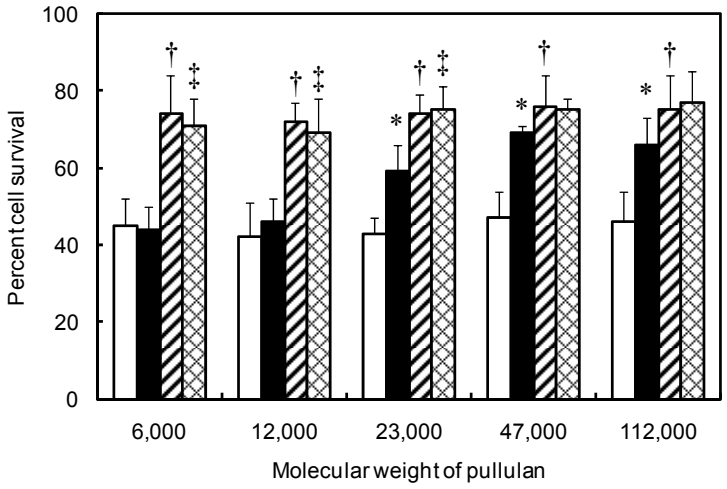

Figure 5. The survival percentage of HepG2 cells 2 days after co-culture with C_{60}-t-pullulan (□ and ▨) or C_{60}-p-pullulan (■ and ▩) conjugates plus light irradiation for 5 min with (▨and ▩) or without (□ and ■) the pretreatment of asialofetuin. The concentration of C_{60} added is 1 μM. *, $p<0.05$: significance against the survival percentage of group co-cultured with C_{60}-p-pullulan conjugates at the corresponding molecular weight of pullulan. †, $p<0.05$: significance against the survival percentage of group co-cultured with C_{60}-t-pullulan conjugates without asialofetuin pretreatment at the corresponding molecular weight of pullulan. ‡, $p<0.05$: significance against the survival percentage of group co-cultured with C_{60}-p-pullulan conjugates without asialofetuin pretreatment at the corresponding molecular weight of pullulan.

Binding affinity of C_{60}-pullulan conjugates for HepG2 cells

Figure 6 shows the fluorescence intensity of cell lysis solution after the incubation of HepG2 cells with FITC-labeled C_{60}-t-pullulan and C_{60}-p-pullulan conjugates for different time periods. The fluorescent intensity of HepG2 cells incubated for 1 hr with FITC-labeled C_{60}-t-pullulan conjugates was significant higher than that of C_{60}-p-pullulan conjugates (**Figure 6A**). However, the intensity difference disappeared when the time period of co-incubation was 6 hr (**Figure 6B**). On the other hand, the fluorescent intensity of C_{60}-p-pullulan conjugates decreased with the increase of pullulan molecular weight at the co-incubation time of 1 hr, whereas no molecular weight dependence was observed for C_{60}-t-pullulan conjugates. However, this phenomenon disappeared for 6 hr co-incubation.

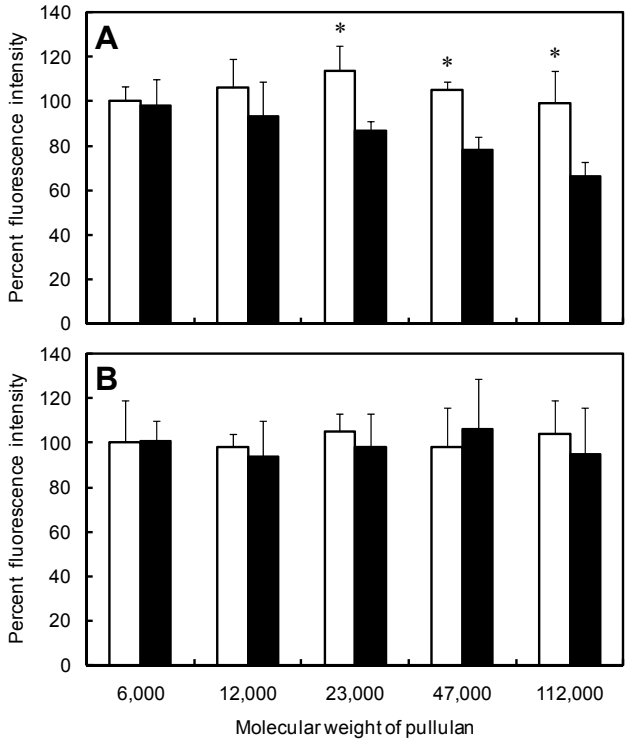

Figure 6. The fluorescence intensity of cell lysis solution after the incubation of HepG2 cells with fluorescence-labeled C_{60}-t-pullulan (white bars) or C_{60}-p-pullulan (black bars) conjugates at 37 °C for 1 (A) and 6 hr (B). * $p<0.05$: significant against the percent fluorescence intensity of cell lysis solution after culture with fluorescence-labeled C_{60}-p-pullulan.

DISCUSSION

In the present paper, several types of water-soluble C_{60}-pullulan conjugates were prepared from pullulan with different molecular weights in different modification manners. Every C_{60}-pullulan conjugate showed similar ROS generation efficiency. However, C_{60}-t-pullulan conjugates showed an enhanced antitumor activity on HepG2 cells with ASGPR both the in vitro and in vivo systems compared with the C_{60}-p-pullulan conjugates. In addition, the in vivo antitumor activity of C_{60}-pulluan conjugates also depended on the molecular weight of pullulan used for C_{60} conjugation. To modify C_{60} for a drug effective for PDT, there are two points to be resolved: one is to make C_{60} water-soluble, and the other is to give C_{60} tumor targetability. Our previous studies experimentally demonstrated that C_{60} chemically modified with PEG of an optimal molecular weight was dissolved in water and accumulated in the tumor tissue to a higher extent than in other normal tissues based on the EPR effect [1-3]. It is also found that pullulan of a water-soluble polysaccharide was accumulated in the liver at significantly higher amounts than other water-soluble polymers probably due to the nature to be recognized by ASGPR [8, 9, 18]. The pullulan conjugation succeeded in the liver targeting of drugs [16, 19-22] and the tumor targetability of C_{60} can be further enhanced by the modification with pullulan. The pullulan conjugation gave C_{60} the active targetability to HepG2 cells, resulting in enhanced photodynamic antitumor effect. In an in vivo system, the C_{60}-pullulan conjugates must reach the tumor tissue before it can interact with the tumor cells. It is highly conceivable that the pullulan molecular weight and modification manners of C_{60} contribute to the antitumor activity of C_{60}-pullulan conjugates.

To evaluate the effect of pullulan molecular weight and the modification manner to C_{60} on the photodynamic antitumor activity of C_{60} conjugates, two different

modification manners were performed by changing the introduction manners of amino groups to pullulan. The reaction mechanism of reductive amination ensure that there is only one amino group can be introduced to the reducing end of one pullulan molecule. On the contrary, for CDI activation method, the large amount of hydroxyl group on pullulan makes it practically hard to control the introduction place and amount accurately. However, it is apparent in **Figure 1A** that the extent of ethylene diamine introduced could be artificially regulated. By selecting an adequate amount of CDI added initially for a pullulan with a given molecular weight, one amino group was introduced to one pullulan molecular in average and the pullulan was used for the following conjugation with C_{60}. High molecular weight reduced the introduction ratio of the reductive amination reaction. This is likely due to the steric hindrance and decreased flexibility of the reducing end of pullulan chain, while the large amount of hydroxyl group allowed the CDI activation method less sensitive to the molecular weight.

When exposed to visible light, every C_{60}-pullulan conjugate generated superoxide anions, a kind of ROS, which results in the antitumor effect in vitro as well as in vivo. The generation of superoxide anions can be detected by cytochrome C. The similar increase pattern in the cytochrome C absorbance was observed for different C_{60}-pullulan conjugates (**Figure 3**). It is likely that such a generation property of C_{60}-pullulan conjugates one-to-one correspond to the inherent physicochemical nature of C_{60} molecule itself. Irrespective of the molecular weight and modification manner, there are no markedly different in the number of pullulan molecules conjugated to one C_{60} molecule (**Table 1**). As a result, the integrality of C_{60} cage and subsequently the ROS generation efficiency were similar for all the C_{60}-pullulan conjugates. Both the ROS generation and in vitro antitumor activity of C_{60}-pullulan conjugates were observed only by the light irradiation while they depended on the time period of light irradiation. It is conceivable

that the in vitro antitumor activity of C_{60}-pullulan conjugates is mainly due to the ROS generated by the conjugates in light irradiation. Taken together, the ability of C_{60} derivatives to generation ROS is a fixed nature which can be unconditionally regulated only by designing the chemical structure of C_{60}. We can say with fair certainty that the ROS generation ability of C_{60}-pullulan conjugates was not influenced by the molecular weight and modification manner.

The lectin affinity test of C_{60}-pullulan conjugates with RCA120-Agarose beads (**Figure 4**) indicates that all of the C_{60}-pullulan conjugates had a lectin affinity although the extent greatly depend on the molecular weight of pullulan and the modification manner. The RCA120 was a kind of lectin and widely used for the detection of galactose-containing oligosaccharides [23]. The pullulan molecules localized on the surface of C_{60}-pullulan conjugates can be recognized by the sugar-recognizable lectin through the non-reducing end. For the C_{60}-t-pullulan conjugates, when the molecular weight of pullulan increased, the flexibility of pullulan chains conjugated on the surface of C_{60} molecule will increase compared with that of C_{60}-p-pullulan conjugates, resulting in an increased absorption (**Figure 4**). It is possible that pullulan with more flexibility of chains increases the frequency of lectin binding, resulting in the enhanced lectin affinity. However, the story is quite different for the C_{60}-p-pullulan conjugates. No effect of the molecular weight of pullulan on the lectin affinity was observed. However, the affinity of C_{60}-p-pullulan conjugates for HepG2 cells tended to decrease with an increased molecular weight of pullulan when the cells were incubated for 1 hr, but no effect of molecular weight on the conjugates affinity was observed for 6 hr incubation. With the increase in the pullulan molecular weight, it is highly conceivable that the density of pullulan chains conjugated on the surface of C_{60} molecule increase, resulting in the reduced flexibility of pullulan chain. This reduced chain flexibility would decrease the possibility of the non-

reducing end of pullulan to meet the ASGPR of cells and lead to the decreased affinity for HepG2 cells. When the incubation time became longer, the chain flexibility influence disappeared, resulting in no effect of the molecular weight on the affinity for the lectin and HepG2 cells. The affinity was specifically reduced by the galactose addition and both C_{60}-t-pullulan and C_{60}-p-pullulan conjugates showed similar adsorption. It is likely that low percent adsorption and fluorescence in the presence of galactose is due to a non-specific interaction other than between the C_{60}-pullulan conjugates and agarose beads or cells surface. The increase of lectin affinity by the pullulan molecular weight will result in an increased non-specific interaction although the detail is unclear at present.

The in vitro antitumor activity experiments with or without asialofetuin pretreatment clearly indicate that the photo-induced antitumor activity of C_{60}-pullulan was specific for HepG2 cells with the ASGPR on the surface (**Figure 5**). It is reported that the ASGPR which belongs to the c-type lectin family and recognizes galactose or N-acetylgalactosamine residues of desialylated glycoproteins, are expressed on the surface of HepG2 cells. The binding of C_{60}-t-pullulan conjugates onto HepG2 cells was higher than that of C_{60}-p-pullulan conjugates, but the difference disappeared when the cells were pretreated with asialofetuin to block the ASGPR. It is likely that the non-reducing end of C_{60}-t-pullulan conjugates was easily recognized by the ASGPR on the surface of HepG2 cells, resulting cell-specifically enhanced in vitro antitumor activity than that of C_{60}-p-pullulan conjugates. An increase of pullulan molecular weight decreased the in vitro antitumor activity of C_{60}-p-pullulan conjugates (**Figure 5**) is due to their decreased affinity for cells with the increase of molecular weight (**Figure 6**). When HepG2 cells incubated with FITC-labeled C_{60}-t-pullulan conjugates for 1 hr, the binding amount of C_{60}-t-pullulan conjugates was significant higher than that of C_{60}-p-pullulan conjugates (**Figure 6A**). The extent was high for C_{60}-pullulan conjugates with higher molecular

weights. When the time period of co-incubation with the C_{60}-pullulan conjugates was 6 hr, it is possible that it takes enough time to allow C_{60}-pullulan conjugates to reach an equilibrium state for binding to HepG2 cells even though their affinity is different (**Figure 6B**), resulting in the similar fluorescence intensity.

REFERENCE

[1] Y. Tabata, Y. Murakami, Y. Ikada, Photodynamic effect of polyethylene glycol-modified fullerene on tumor. Jpn J Cancer Res 88(11) (1997) 1108-1116.

[2] J. Liu, S. Ohta, A. Sonoda, M. Yamada, M. Yamamoto, N. Nitta, K. Murata, Y. Tabata, Preparation of PEG-conjugated fullerene containing Gd3+ ions for photodynamic therapy. J Control Release 117(1) (2007) 104-110.

[3] J. Liu, M. Yamamoto, Y. Tabata, Antitumor activity of fullerene modified by polyethylene glycol with different molecular weights and terminal structures.

[4] H. Maeda, J. Wu, T. Sawa, Y. Matsumura, K. Hori, Tumor vascular permeability and the EPR effect in macromolecular therapeutics: a review. J Control Release 65(1-2) (2000) 271-284.

[5] V.P. Torchilin, Drug targeting. Eur J Pharm Sci 11 Suppl 2 (2000) S81-91.

[6] Y. Matsumura, H. Maeda, A new concept for macromolecular therapeutics in cancer chemotherapy: mechanism of tumoritropic accumulation of proteins and the antitumor agent smancs. Cancer Res 46(12 Pt 1) (1986) 6387-6392.

[7] T. Yamaoka, Y. Tabata, Y. Ikada, Distribution and tissue uptake of poly(ethylene glycol) with different molecular weights after intravenous administration to mice. J Pharm Sci 83(4) (1994) 601-606.

[8] Y. Kaneo, T. Tanaka, T. Nakano, Y. Yamaguchi, Evidence for receptor-mediated hepatic uptake of pullulan in rats. J Control Release 70(3) (2001) 365-373.

[9] T. Tanaka, Y. Fujishima, S. Hanano, Y. Kaneo, Intracellular disposition of polysaccharides in rat liver parenchymal and nonparenchymal cells. Int J Pharm 286(1-2) (2004) 9-17.

[10] R.F. Borch, M.D. Bernstein, H.D. Durst, Cyanohydridoborate anion as a selective reducing agent. Journal of the American Chemical Society 93(12) (1971) 2897-2904.

[11] G.L. Miller, Use of dinitrosalicylic acid reagent for determination of reducing sugar. Analytical Chemistry 31(3) (1959) 426-428.

[12] T.G.M. Schalkhammer, Analytical biotechnology Springer, 2002.

[13] G.T. Hermanson, Bioconjugate techniques, Academic Press, 1996.

[14] B.M. Babior, R.S. Kipnes, J.T. Curnutte, Biological defense mechanisms. The production by leukocytes of superoxide, a potential bactericidal agent. J Clin Invest 52(3) (1973) 741-744.

[15] A.N. Belder, K. Granath, Preparation and properties of fluorescein-labelled dextrans. Carbohydr. Res. 30 (1973) 375–378.

[16] J. Jo, T. Ikai, A. Okazaki, M. Yamamoto, Y. Hirano, Y. Tabata, Expression profile of plasmid DNA by spermine derivatives of pullulan with different extents of spermine introduced. J Control Release 118(3) (2007) 389-398.

[17] I. Kanatani, T. Ikai, A. Okazaki, J. Jo, M. Yamamoto, M. Imamura, A. Kanematsu, S. Yamamoto, N. Ito, O. Ogawa, Y. Tabata, Efficient gene transfer by pullulan-spermine occurs through both clathrin- and raft/caveolae-dependent mechanisms. J Control Release 116(1) (2006) 75-82.

[18] T. Yamaoka, Y. Tabata, Y. Ikada, Body distribution profile of polysaccharide after intravenous administration. Drug Deliv. 1 (1993).

[19] K. Xi, Y. Tabata, K. Uno, M. Yoshimoto, T. Kishida, Y. Sokawa, Y. Ikada, Liver targeting of interferon through pullulan conjugation. Pharm Res 13(12) (1996) 1846-1850.

[20] Y. Suginoshita, Y. Tabata, T. Matsumura, Y. Toda, M. Nabeshima, F. Moriyasu, Y. Ikada, T. Chiba, Liver targeting of human interferon-beta with pullulan based on metal coordination. J Control Release 83(1) (2002) 75-88.

[21] Y. Suginoshita, Y. Tabata, F. Moriyasu, Y. Ikada, T. Chiba, Liver targeting of interferon-beta with a liver-affinity polysaccharide based on metal coordination in mice. J Pharmacol Exp Ther 298(2) (2001) 805-811.

[22] H. Hosseinkhani, T. Aoyama, O. Ogawa, Y. Tabata, Liver targeting of plasmid DNA by pullulan conjugation based on metal coordination. J Control Release 83(2) (2002) 287-302.

[23] Y. Itakura, S. Nakamura-Tsuruta, J. Kominami, N. Sharon, K. Kasai, J. Hirabayashi, Systematic comparison of oligosaccharide specificity of Ricinus communis agglutinin I and Erythrina lectins: a search by frontal affinity chromatography. J Biochem 142(4) (2007) 459-469.

PART II.

IMAGING ACTIVITY OF BIOACTIVE SUBSTANCES

MODIFIED WITH WATER-SOLUBLE POLYMERS

Chapter 4

Tumor imaging and photodynamic antitumor activities of fullerene modified with polyethylene glycol containing Gd^{3+} ions

INTRODUCTION

Previous researches showed that fullerene (C_{60}) could generate the ROS in a high yield even by exposure of weak visible light, and functions as a potential photosensitizer for PDT [1-3]. **Chapter 1** demonstrated that chemical conjugation with PEG enabled C_{60} not only to dissolve in water but also to accumulate in the tumor tissue according to the EPR effect [2, 4, 5]. PEG with an appropriate molecular weight and the terminal residue could enhance the tumor targeting ability of C_{60}, resulting in promoted tumor suppression in vivo.

Successful PDT depends on the body distribution of phtosensitizer after administration. The highest PDT effect can be obtained just if light irradiation is performed at the time when the concentration of photosensitizer in the tumor reaches its maximum [6, 7]. To realize this, combination of photosensitizer with an in vivo imaging technology will be promising. If the therapeutically acceptable time when the tumor concentration of photosensitizer is significantly higher than the normal tissue one, is visualized, the PDT can be carried out in a more scheduled fashion to enhance the therapeutic efficacy.

Among non-invasive techniques having developed to diagnose the tumor tissue, MRI is a promising visualization technique in terms of its high spatial resolution and involving no radiation exposure [8, 9]. However, the photosensitizers current available cannot be visualized by MRI. In this study, a novel photosensitizer with both the tumor targetability and MRI activity was prepared from C_{60} for the efficient PDT of tumor. Gd^{3+}

was selected as the MRI contrast agent and introduced to the PEG terminal of C_{60}-PEG through metal chelation. Following intravenous injection of Gd^{3+}-chelated C_{60}-PEG into tumor-bearing mice, the tumor PDT effect and the MRI tumor imaging were evaluated to compare the correlation.

EXPERIMENTAL

Materials and reagents

C_{60} was purchased from the SES Research Co. Ltd., Houston (Lot BT-6906, purity=99.9%). Heterofunctional PEG with an amino and hydroxyl terminal groups (weight-average molecular weights=5,000) was obtained from Nippon Oil & Fats Co., Ltd., Japan. Cytochrome C (from horse heart, Mw=12,384) was purchased from Nakalai Tesque Inc., Kyoto, Japan. All of organic solvents were pretreated with molecular sieves (3A, 1/8, Nakalai Tesque Inc., Kyoto, Japan) to dehydrate before using. Other chemicals were used without further purification.

Preparation and characterization of C_{60}-PEG-DTPA conjugates

C_{60}-PEG conjugation was performed as previously reported [10]. Briefly, 7.2 mg of C_{60} and 1 g of PEG were dissolved in 10 ml of benzene, and the reaction mixture was stirred with magnetic agitation at room temperature for 24 hr in a light irradiated place. After the conjugation, the reaction solution was mixed with 20 ml of DDW to extract the water-soluble fraction of C_{60}-PEG conjugate into the water phase. The resulting conjugate was separated from unreacted PEG by gel filtration with Sephacryl S-200 (Pharmacia Biotech, Uppsala, Sweden, elution buffer: 0.4 M CH_3COONH_4) and freeze-dried to obtain the hydroxyl terminated C_{60}-PEG conjugate.

The purified C_{60}-PEG conjugate was dissolved in 10 ml of dioxane at a final concentration of 10 mg/ml and dropped into 5 ml of DMSO containing 143 mg of DTPA

anhydride and 24 mg of 4-(dimethylamino)pyridine (DMAP). The reaction solution was magnetically stirred at 40 ˚C for 6 hr, followed by precipitation by diethyl ether. The precipitate was collected by centrifugation (5,000 rpm, 20 ˚C, 10 min), and dissolved in dioxane. This process was repeated 3 times to obtain DTPA-introduced C_{60}-PEG (C_{60}-PEG-DTPA). The C_{60}-PEG-DTPA was dissolved in DDW and freeze-dried.

The C_{60}-PEG-DTPA was dissolved in 10 ml of DDW at a final concentration of 10 mg/ml and the solution pH was adjusted at 6.5 by 1N NaOH. Then, 16 mg of powdered gadolinium acetate was added to the C_{60}-PEG-DTPA solution, followed by 6 hr leaving for Gd^{3+} chelation to obtain Gd^{3+}-chelated C_{60}-PEG-DTPA (C_{60}-PEG-Gd). Free Gd^{3+} ions were removed from the C_{60}-PEG-Gd by ultrafiltration (Amicon® Utra, 10,000 MWCO, Millipore Corporation, Bedford). The amount of Gd^{3+} chelated was measured by atomic absorption spectrophotometer (AA-6800, Shimazu, Kyoto,. Japan).

Preparation of radiolabeled C_{60}-PEG-DTPA conjugates

For the radiolabeling of C_{60}-PEG-DTPA, 10 mg of C_{60}-PEG-DTPA was dissolved in 1 ml of physiological saline solution and mixed with 5 μl of $^{59}FeCl_3$ solution (15.83 mCi/ml, 0.5M HCl aqueous solution, PerkinElmer Life Analytical Sciences, Boston) for 5 min. The resulting mixture was allowed to pass through a PD-10 column (Pharmacia Biotech Inc, Sweden) to separate unbound ^{59}Fe from ^{59}Fe-labeled C_{60}-PEG.

Cells and mouse tumor model

Meth AR1 fibrosarcoma cells used for in vitro experiments were cultured in RPMI-1640 medium (COSMO BIO Co., Ltd., Tokyo, Japan) supplemented with 10 v/v% of FCS, 0.25 w/v% of sodium hydrogen bicarbonate at 37°C in a 5% CO_2-95% air atmosphere.

To prepare a mouse tumor model, Meth AR1 cells were acclimatized to the in vivo condition by their intraperitoneal growth of CDF1 mice (Japan SLC, Inc, Shizuoka,

Japan). The cells were inoculated into the back subcutis of CDF1 mice aged 6 weeks (1×10^7 cells/ml, 100 μl/mouse). The tumor mass grew to 10 mm in average diameter about 10 days after inoculation. These tumor-bearing mice were used for the following in vivo experiments.

Measurement of superoxide anion generation efficiency of C_{60}-PEG-DTPA conjugates

Superoxide anion generation efficiency of C_{60}-PEG-Gd was evaluated by the conventional cytochrome C method [11]. Briefly, 100 μl of HBSS (pH=7.4, Life Technologies Oriental, Inc, Tokyo, Japan) containing 80 μM of cytochrome C was mixed with 100 μl of HBSS containing 20 μM of C_{60}-PEG, C_{60}-PEG-DTPA, C_{60}-PEG-Gd conjugates, or Gd^{3+}-chelated PEG-DTPA (PEG-Gd). The solution was placed into each well of a 96-well multi-culture plate (COSTAR® 3595, Corning Inc, NY), and then the plate was exposed to a visible light supplied from a fluorescence lamp (8 W, 400 nm-700 nm, 2 cm from the plate bottom). An increase in the absorbance at 550 nm was measured by a microplate reader (VERSAmax, Molecular device corporation, California) to evaluate the generation efficiency of superoxide anions.

Assessment of photo-induced in vitro antitumor activity of C_{60}-PEG-DTPA conjugates

The in vitro cytotoxicity of C_{60}-PEG conjugates was evaluated in terms of the suppression activity of tumor cells growth. Briefly, Meth AR1 cells were suspended in RPMI-1640 medium to give a final density of 1×10^5 cells/ml. Then, 1 ml of the cell suspension was mixed with 100 μl of PBS (pH 7.4) and PBS containing 100 μM of C_{60}-PEG, C_{60}-PEG-DTPA, or C_{60}-PEG-Gd conjugates, and the mixture was placed into each well of 24-well multi-culture plate (COSTAR® 3526, Corning Inc, NY). The plate was fixed on a shaker and exposed to a visible light supplied from a fluorescence lamp (8 W, 400 nm-700 nm, 2 cm from the plate bottom) for 20 or 40 min with gentle shaking. After light irradiation, cells were further cultured for 3 days and the number of cells grown was

determined by a Cell Counting Kit (Dojindo Molecular Technologies, Inc., Kumamoto, Japan). The number of cells was compared with that cultured in the medium containing saline to calculate the cell number ratio. Experiment for each sample was performed with three wells.

In vitro and in vivo MRI studies

All the MRI studies were performed with a 7-T MRI apparatus (VARIAN, Inc.). To evaluate the MRI activity of C_{60}-PEG-Gd, the PBS at Gd^{3+} concentrations of 0.2, 0.5, 1, 2, and 5 mM were prepared and their T1 relaxation time was determined in vitro based on the inversion recovery method. The longitudinal relaxation constant ($R1$) of C_{60}-PEG-Gd was determined from the slope of the linear regression of 1/T1 versus contrast agent concentration. The R1 of Magnevist®, a MRI contrast agent commercially available (Japan Schering Inc., Osaka, Japan), was calculated in the same way for comparison.

In vivo MRI activity of C_{60}-PEG-Gd was evaluated with tumor-bearing mice described previously. After intravenous injection of 200 μl of saline solution containing either C_{60}-PEG-Gd or Magnevist® (100 μmole Gd^{3+}/kg bodyweight), tumor-bearing mice were fixed in a rat-head coil and the T1-weighted gradient echo images were taken at different time intervals for 24 hr (TR=300 ms, TE=12 ms, 256×128 image matrix, field of view of 40×40 mm, and slice thickness of 2 mm). Gd^{3+}-free DDW and DDW of 0.2 mM Gd^{3+} were used for the standard in each image. The MRI signal intensity in the tumor and muscle tissues was normalized based on the assumption that the signal intensity of Gd^{3+}-free DDW and DDW of 0.2 mM Gd^{3+} were 0 and 100%, respectively.

Evaluation of tumor accumulation of C_{60}-PEG-DTPA conjugates

Tumor-bearing mice received intravenous injection of physiological saline solution containing of ^{59}Fe-labeled C_{60}-PEG (100 μl). At different time intervals, the tumor and normal muscle tissues were taken out. After weighing, the radioactivity of the

tissue taken was measured with a gamma counter (Autowell gamma system Aloka ARC-301B, Aloka Company, Ltd, Tokyo, Japan). The body distribution data were expressed as the percent dose per g tissue which is calculated by dividing the percentage of radioactivity measured to that injected initially per mouse with the weight of each tissue.

Photodynamic effect of C_{60}-PEG-DTPA on tumor

To evaluate the tumor PDT effect of C_{60}-PEG-Gd, 100 μl of conjugate solution in saline (2.78 mM) was intravenously injected to the tumor-bearing mice from the tail vein. The tumor tissue was exposed 1, 3, 6, and 12 hr later to visible light (400-505 nm) from a light probe of 7 mm active diameter by Heliomat Multifunction Halogen-Light (Vivadent Co. Ltd, Lichtenstein). The irradiation was carried out for 10 min at an output power of 89.2 mW/cm^2 (53.5 J/cm^2), and then, mice were fed in dark. The tumor volume (V) was periodically calculated according to the formula of $V=\pi/6\times a\times b^2$ (a and b is the length of long axis and short axis of tumor mass, respectively) [12] and expressed as the volume ratio of the tumor to that before conjugates injection. Each experiment group consists of 3 mice.

RESULTS

Preparation and characterization of C_{60}-PEG-DTPA conjugates

The introduction of DTPA residues to the terminal hydroxyl groups of C_{60}-PEG increased with an increase in the molar ratio of DTPA anhydride added (**Figure 1**). A chromatographic study revealed that at a low ratio, the molecular weight of C_{60}-PEG increased with the reaction. This is because intermolecular crosslinking of C_{60}-PEG by the DTPA anhydride of bifunction compound. To avoid the crosslinking, C_{60}-PEG-DTPA used for the following experiments was prepared at a ratio of 20. The C_{60}-PEG-Gd

prepared contained 3 Gd^{3+} ions per one molecule. Liquid chromatography studies showed that 4 PEG chains were coupled to one C_{60} molecule [2].

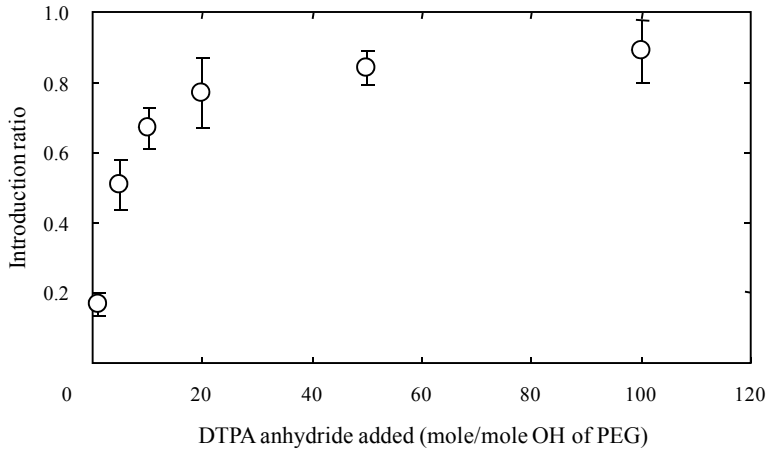

Figure 1. Introduction of DTPA residues to PEG as a function of the amount of DTPA anhydride added in reaction.

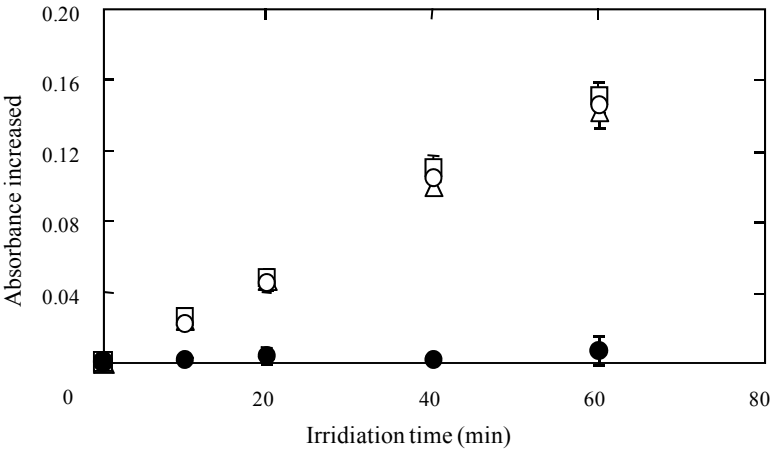

Figure 2. Absorbance increment of cytochrome C solution after light irradiation in the present of C_{60}-PEG (○), C_{60}-PEG-DTPA (△), C_{60}-PEG-Gd (□), and PEG-Gd (●)

Superoxide anion generation and photo-induced in vitro antitumor activity of C_{60}-PEG-DTPA conjugates

Figure 2 shows the increase pattern of cytochrome C absorbance for different C_{60}-PEG conjugates after light irradiation. In the present of C_{60}-PEG conjugates, the solution

absorbance increased with the irradiation period, in marked contrast to that of PEG-Gd solution. The similar increase pattern was observed for both of the C_{60}-PEG and C_{60}-PEG-Gd conjugates. Solutions without any light irradiation did not show the time change of absorbance.

Figure 3 shows the photo-induced in vitro cytotoxicity of different C_{60}-PEG conjugates with or without light irradiation. Combination of the conjugates and light irradiation exhibited significant cytotoxicity, while light irradiation alone or the conjugates alone under the dark condition did not decrease the cell number. Neither DTPA introduction nor additional Gd^{3+} chelation affected the cytotoxicity. In all the groups with C_{60}, the number of alive cells decreased to about 40 % of control number by light irradiation for 20 min while more cells died by 40 min irradiation.

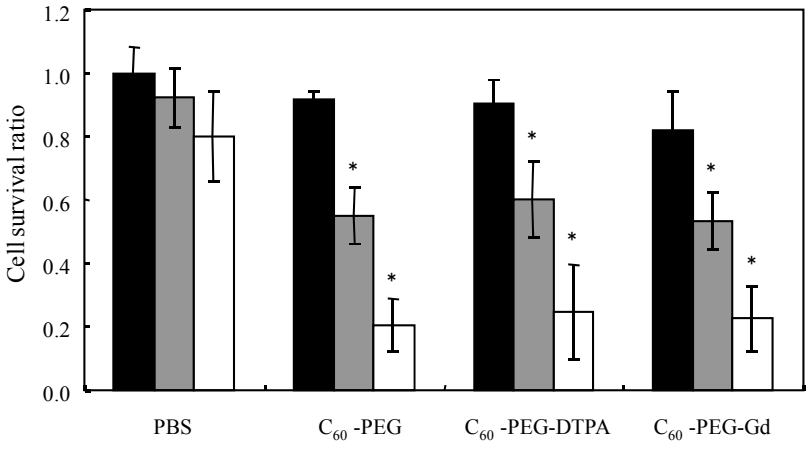

Figure 3. The number of MethAR1 cells grown 3 days after culturing in the presence of different C_{60}-PEG conjugates in dark (black bars), or with light irradiation for 20 (gray bars) and 40 min (white bars). The C_{60} concentration is 100 μM. *, $p<0.05$: significance against the number ratio of cells cultured in dark for the same conjugate.

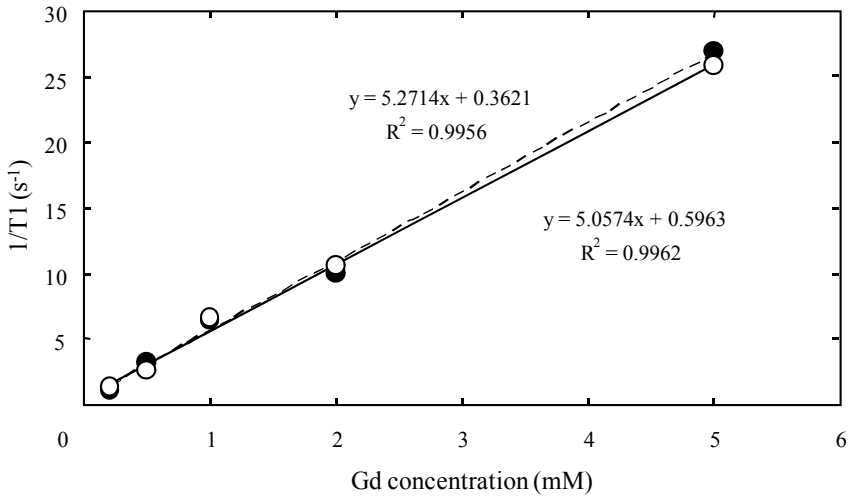

Figure 4. T1 inversion recovery time of C_{60}-PEG-Gd (○) and Magnevist® (●) at pH 7.4 and 25 ˚C.

In vitro and in vivo MRI studies

Figure 4 shows the T1 inversion recovery time of C_{60}-PEG-Gd and Magnevist® solution with different amounts of Gd^{3+} at pH 7.4 and 25 ˚C. Both of the C_{60}-PEG-Gd and Magnevist® solutions exhibited a dose-dependent change of T1 inversion recovery time for water proton. **Table 1** shows the R1 values calculated from the slope. There was no significant difference in the *R*1 relaxivity between the C_{60}-PEG-Gd and Magnevist®. This indicates that the C_{60}-PEG-Gd has T1 signal enhancement ability necessary enough for clinical MRI diagnosis.

Table 1. The *R*1 relaxivity of MRI for C_{60} -PEG-Gd and Magnevist®

Contrast agent	R_1 relaxivity ($mM^{-1} \cdot sec^{-1}$)
C_{60}-PEG-Gd	5.1
Magnevist®	5.3

Figure 5 shows T1 weighted images across tumor at different time intervals after intravenous injection of C_{60}-PEG-Gd and Magnevist® to the tumor-bearing mice. Both of the C_{60}-PEG-Gd and Magnevist® enhanced the MRI signal intensity in the tumor. However, the enhanced level of C_{60}-PEG-Gd at the tumor tissue maintained for a longer time period than that of Magnevist®.

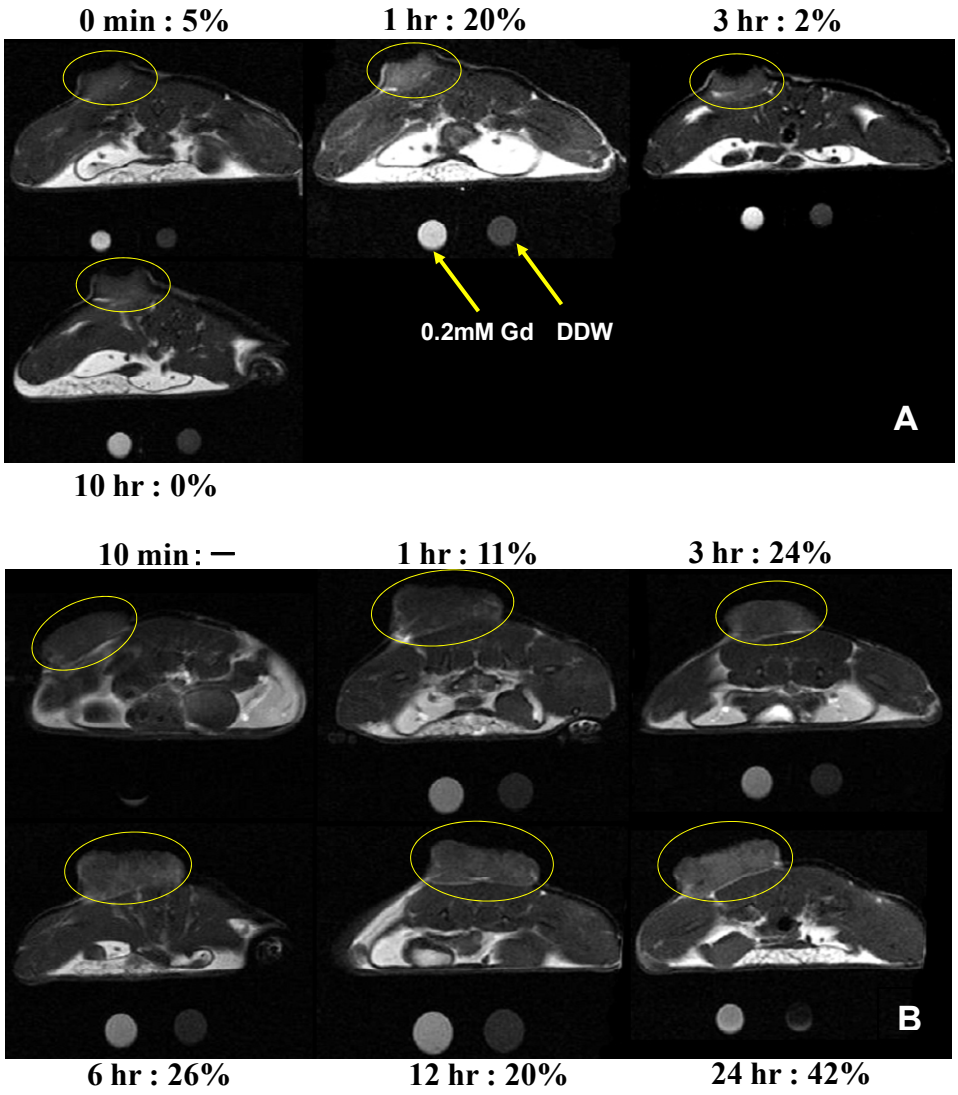

Figure 5. The T1 weighted MRI photographs at different time periods after intravenous injection of Magnevist® (A) and C_{60}-PEG-Gd (B) into the tumor-bearing mice. The signal intensity of tumor tissue was shown in percentage (outside of the figures) and the signal intensity of Gd^{3+}-free DDW and 0.2 mM Gd^{3+} of DDW was defined as 0 and 100%, respectively. The tumor mass is indicated by a circle.0

For clinical MRI diagnosis, it is interesting to enhance the signal contrast between the tumor tissue and the background. This can be expressed as the following formula in Contrast Enhancement = $(I_t-I_m) / (I_{100}-I_0) \times 100$ where I_t, I_m, and I_{100} or I_0 are the signal intensity of tumor tissue, the signal intensity of normal muscle tissue, and the signal intensity of 0.2 mM Gd^{3+} DDW or Gd^{3+}-free DDW, respectively. **Figure 6** shows the time course of MRI signal at the tumor tissue after the intravenous injection of C_{60}-PEG-Gd and Magnevist® into the tumor-bearing mice. For the C_{60}-PEG-Gd, the contrast between the tumor tissue and normal muscle increased after administration, reached a peak about 3 hr later, and kept in a high level even after 24 hr. On the contrary, Magnevist® showed the contrast enhancement only within 1 hr.

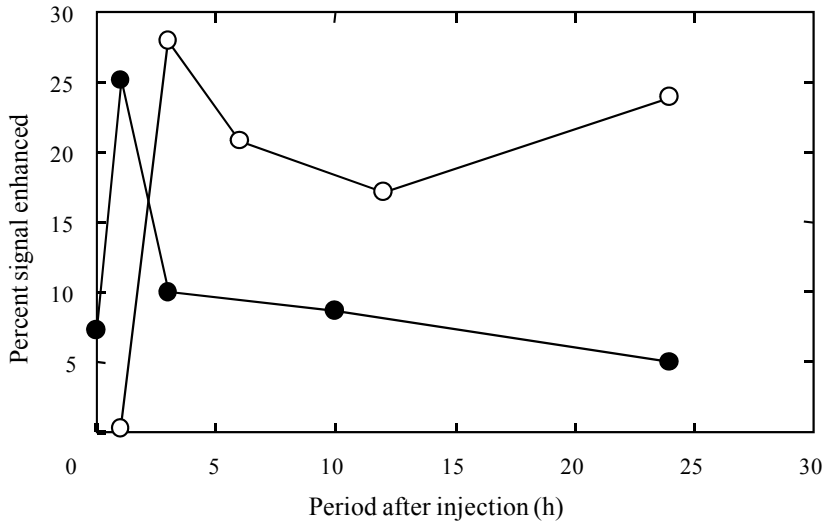

Figure 6. The time course of MRI signal at the tumor tissue after the intravenous injection of (○) C_{60}-PEG-Gd and (●) Magnevist® into the tumor-bearing mice. The enhancement is expressed as the percentage of signal intensity at the tumor tissue to that of muscle tissue.

Tumor targetability of C_{60}-PEG-DTPA conjugates

Figure 7 shows the time course of radioactivity accumulated in the tumor and normal muscle of tumor-bearing mice after intravenous injection of ^{59}Fe-labeled C_{60}-

PEG-DTPA conjugate. After intravenously injected to tumor-bearing mice, ^{59}Fe-labeled C_{60}-PEG-DTPA was accumulated in the tumor tissue with time and significant difference in the percent accumulation against the normal tissue was detected even 1 hr after injection. The conjugate was retained in the tumor tissue in a significantly larger amount and for a longer time period than in the normal tissue. The time profile of remaining radioactivity well correlated with that of the MRI signal intensity shown in **Figure 6**.

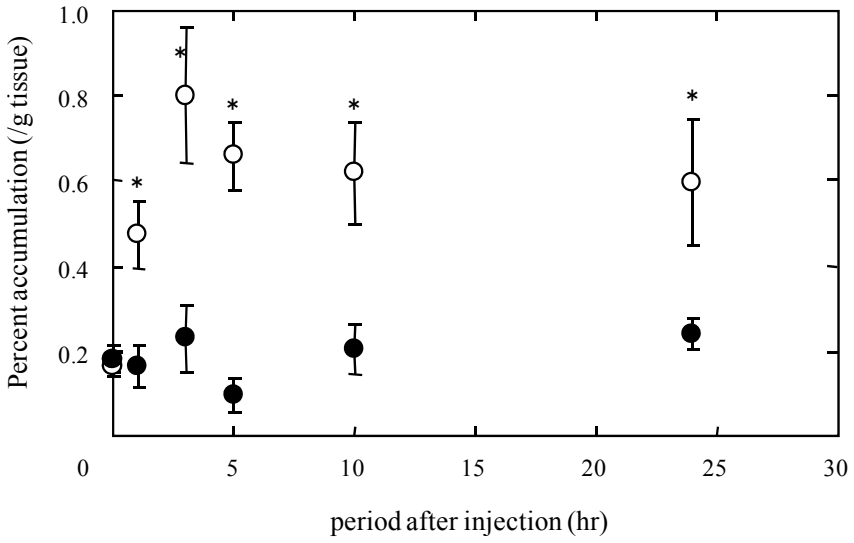

Figure 7. Time course of radioactivity accumulation in the tumor (○) and normal muscle (●) of tumor-bearing mice after intravenous injection of the ^{59}Fe-labeled C_{60}-PEG-DTPA conjugate. *, $p<0.05$: significance against the percent radioactivity of the normal muscle at the corresponding time period.

Photodynamic effect of C_{60}-PEG-DTPA conjugates on tumor

Figure 8 shows the photodynamic effect of C_{60}-PEG-Gd on tumor in different light irradiation manners. When the C_{60}-PEG-Gd was intravenously injected to tumor-bearing mice without light irradiation, the tumor size increased with time similarly to that of the saline injection. On the contrary, light irradiation induced the in vivo anti-tumor activity of C_{60}-PEG-Gd although the extent greatly depended on the time schedule of

light exposure. The PDT effect of C_{60}-PEG-Gd was significant when light irradiation was performed 3 hr or longer after injection, whereas no effect was observed 1hr after injection.

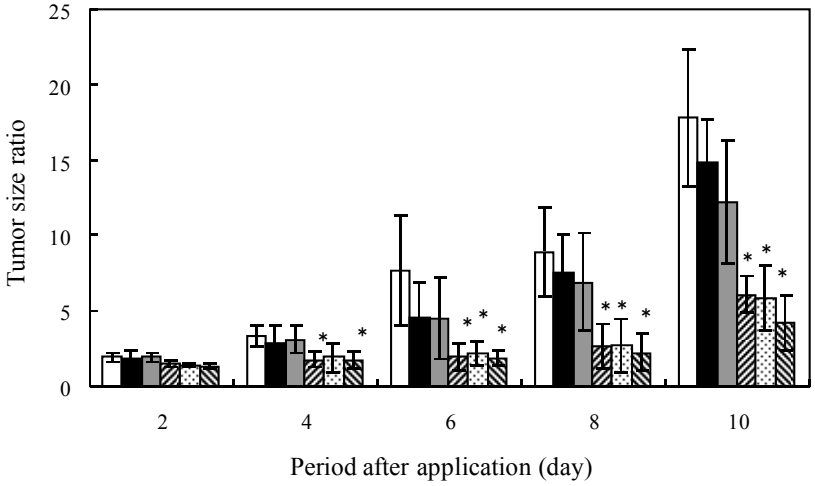

Figure 8. The photodynamic effect of C_{60}-PEG-Gd on the in vivo tumor growth after intravenous injection plus light exposure at different time points: (□) saline, (■) C_{60}-PEG-Gd without light exposure, or (▨, ▨, ▨, and ▨), C_{60}-PEG-Gd plus light exposure 1, 3, 6, and 12 hr after injection, respectively. * $p<0.05$: significant against the tumor size ratio of saline-injected group at the corresponding time point.

DISCUSSION

The present paper clearly demonstrates with experimental data that tumor PDT effect was significantly promoted by giving a photosensitizer tumor targetability and MRI activity. The key steps of PDT include the accumulation of a nontoxic photosensitizer in the tumor after administration, the photo-chemical activation by light irradiation, and the local generation of cytotoxic ROS by the activated photosensitizer. Thus, to enhance the PDT efficacy, every step should be improved. For a successful PDT system, firstly, it is necessary to develop a photodynamic agent with higher light-induced ROS generation. Most of researches have focused on this point to design and create new photosisitizers. C_{60} is one of the attractive materials for the viewpoint of its photochemical characters.

Secondly, to effectively deliver the photosensitizer to the proper site, an effective drug delivery system (DDS) is required. Due to the short lifetime of ROS [13], only the photosensitizer delivered in the tumor tissue can contribute to the tumor PDT effect. The delivery will be achieved by DDS technology. Chemical modification by PEG with an appropriate molecular weight and terminal structure enables water-insoluble C_{60} to dissolve in water and automatically accumulate in the tumor based on a passive targeting mechanism: EPR effect. The third important factor is the timing of light irradiation to maximalize the efficiency of ROS generation at the tumor. This is because the highest PDT effect can be obtained just when the irradiation was performed at the optimal time period when the concentration of photosensitizer accumulated in the tumor tissue become maximum. However, it is practically impossible to predict the optimal treatment timing because the tumor accumulation pattern of photosensitizer greatly depends on the type, size, site and malignancy of tumor. To break through the problem, combination of diagnostic technology will be promising. For example, MRI is a non-invasive and nonradiative dynamic imaging method with both high spatial and time resolution.

In this study, the MRI activity was introduced into the C_{60}-PEG of PDT photosensitizer. The chelate incorporation of Gd^{3+} ions could convert the C_{60}-PEG-DTPA to a photosensitizer with both the diagnostic and therapeutic functions. MRI gave us a non-invasive way to detect the time course of C_{60}-PEG accumulated in the tumor tissue. The C_{60}-PEG-Gd was not accumulated in the tumor 1 hr later, but 3 hr or longer after injection (**Figure 6**). On the other hand, significantly high tumor PDT effect was observed only by light irradiation 3 hr or longer after C_{60}-PEG-Gd injection, but not 1 hr after injection (**Figure 8**). There was a good accordance of the time profile between the PDT effect and the detection of positive MRI signal. This finding strongly indicates that

diagnosis is powerful to determine the optimal timing of light irradiation at the tumor after the photosensitizer injection.

Heterofunctional PEG with amino and hydroxyl terminal groups could be conjugated to C_{60} based on the high coupling reactivity of amines to C_{60} [10]. The unreacted hydroxyl group of the other PEG terminal was used for the chemical introduction of DTPA residue. The DTPA anhydride reacts with the hydroxyl group to form an ester bond between the DTPA and the PEG chain. The DTPA residue of C_{60}-PEG can chelate one Gd^{3+} ion. It is possible that the Gd^{3+} ions chelated contact with the surrounding water molecules easily, resulting in enhanced MRI signal intensity similarly to Magnevist®. On the other hand, introduction of Gd^{3+}-chelated DTPA residue into the terminal of PEG did not change the physicochemical nature of C_{60} molecule to generate superoxide anions upon light irradiation and consequently kill tumor cells (**Figures 3** and **4**). When the stability of C_{60}-PEG-Gd in PBS was examined in terms of Gd^{3+} dissociation, no considerable dissociation was observed (date not shown). Since the enhanced MRI intensity and the prolonged time period of intensity enhancement were observed, it is likely that Gd^{3+} ions are chelated even in the blood circulation.

Both the superoxide anion generation of conjugates and the in vitro cytotoxicity were observed only by the light irradiation while they depended on the time period of light irradiation. This suggests that the cytotoxicity is mainly due to the superoxide anion generated by the C_{60}-PEG-Gd light irradiated. The slight decrease of the cell survival rate in the PBS-treated control group after light irradiation (**Figure 3**) may result from the low temperature and shaking during light irradiation.

For the isotope tracer experiment, $^{59}Fe^{3+}$ was selected for radiolabeling in place of ^{125}I used in our previous studies. This is due to the chelate stability. Since the $\log K_{ML}$ of DTPA-Gd^{3+} and DTPA-Fe^{3+} is 22.5 and 28.6, respectively, it is highly expected that Fe^{3+}

ions are chelated with DTPA residue as stably as Gd^{3+} ions. In addition, radio labeling with $^{59}Fe^{3+}$ does not need another chemical reaction which may change the original structure of photosensitizer. Taken together, it is possible that $^{59}Fe^{3+}$ labeling reflects the body distribution pattern of C_{60}-PEG-Gd correctly. The time profile of remaining radioactivity in the tumor tissue well correlated with that of MRI signal intensity (**Figures 6** and **7**). The finding strongly indicates that the MRI pattern accurately reflected the accumulation pattern of C_{60}-PEG-Gd in the tumor tissue. Conjugation of DTPA residues to macromolecules is a useful approach to prolong the half-life time in the blood circulation and enhance the amount accumulated in the tumor tissue. We have reported that the C_{60}-PEG conjugate showed a high tumor targetability which can be explained by the EPR effect. It is likely that based on the same reason, the C_{60}-PEG-Gd could also be accumulated more in the tumor tissue, resulting in the time period of contrast enhancement longer than that of Magnevist® (**Figures 5** and **6**). Significant enhancement of radioactivity remaining in the tumor was observed 1 hr after intravenous injection. Contrary to this, no positive MRI signal was detected then. In addition, no significant PDT effect was achieved even upon light irradiation. The reason of this time difference is not clear at present. However, it showed be noted that the MRI is more suitable to determine the optimal timing of tumor therapy than the conventional radiotracer technology.

Some normal tissues were highlighted in MRI images (**Figure 5a** and **5b**). Most of them were fat tissue, because it is known that the fat itself normally shows a strong signal in the T1 weighted image even without any contrast agents. Sometimes, a stronger MRI signal intensity was detected in the bladder. It is possible that the C_{60}-PEG-Gd conjugates were excreted in urine, resulting in a higher MRI signal in bladder. The RI tracing study revealed that the conjugates were detected in the urine. Although the liver

was not seen in **Figure 5**, the RI tracing study demonstrated that the C_{60}-PEG-Gd conjugates were accumulated in the liver at about 5% of the dose injected. This can be explained in terms of the entrapment of macromolecules by the reticuloendothelial system.

The in vivo tumor PDT activity of C_{60}-PEG-Gd greatly depended on the timing of light exposure (**Figure 8**). It is clearly that the time pattern of anti-tumor activity was in remarkable accordance with that of MRI signal intensity in the tumor tissue (**Figure 6**). The tumor tissue was highlighted in the MRI photograph. This implies that Gd^{3+} ions are accumulated in the tumor. Considering that the C_{60}-DTPA-Gd is stable under physiological conditions, the extent of C_{60}-PEG-Gd accumulated in the tumor tissue can be easily estimated by MRI method: the higher the MRI signal intensity was observed, the higher concentration of C_{60} conjugates accumulated in the tumor. The PDT effect will be very low if light irradiation did perform in the time period when a sufficient concentration of C_{60} is not present in the tumor tissue (for example, 1 hr after injection). By monitoring the time change of signal contrast, we can find an optimal timing of light irradiation to maximize the superoxide anion-induced tumor killing, resulting in the most efficient tumor PDT.

In conclusion, chemical incorporation of Gd^{3+} ions enabled the C_{60}-PEG with tumor targetability to perform the tumor diagnosis and photodynamic therapy simultaneously. In this DDS system, the therapeutically acceptable time range for the tumor PDT can be diagnostically detected to achieve the most effective tumor therapy. This therapeutic and diagnostic hybrid system is a promising tool to enhance the PDT efficacy for tumor.

REFERENCES

[1] J.W. Arbogast, A.P. Darmanyan, C.S. Foote, F.N. Diederich, R.L. Whetten, Y. Rubin, M.M. Alvarez, S.J. Anz, Photophysical properties of sixty atom carbon molecule (C60). The Journal of Physical Chemistry 95(1) (1991) 11-12.

[2] Y. Tabata, Y. Murakami, Y. Ikada, Photodynamic effect of polyethylene glycol-modified fullerene on tumor. Jpn J Cancer Res 88(11) (1997) 1108-1116.

[3] T. Tsuchiya, I. Oguri, Y.N. Yamakoshi, N. Miyata, Novel harmful effects of [60]fullerene on mouse embryos in vitro and in vivo. FEBS Lett 393(1) (1996) 139-145.

[4] Y. Matsumura, H. Maeda, A new concept for macromolecular therapeutics in cancer chemotherapy: mechanism of tumoritropic accumulation of proteins and the antitumor agent smancs. Cancer Res 46(12 Pt 1) (1986) 6387-6392.

[5] V.P. Torchilin, Drug targeting. Eur J Pharm Sci 11 Suppl 2 (2000) S81-91.

[6] D.S. Lawrence, S.L. Gibson, M.L. Nguyen, K.R. Whittemore, D.G. Whitten, R. Hilf, Photosensitization and tissue distribution studies of the picket fence porphyrin, 3,1-TPro, a candidate for photodynamic therapy. Photochem Photobiol 61(1) (1995) 90-98.

[7] I. Zupko, A.R. Kamuhabwa, M.A. D'Hallewin, L. Baert, P.A. De Witte, In vivo photodynamic activity of hypericin in transitional cell carcinoma bladder tumors. Int J Oncol 18(5) (2001) 1099-1105.

[8] D. Sosnovik, R. Weissleder, Magnetic resonance and fluorescence based molecular imaging technologies. Prog Drug Res 62 (2005) 83-115.

[9] J.P. Basilion, S. Yeon, R. Botnar, Magnetic resonance imaging: utility as a molecular imaging modality. Curr Top Dev Biol 70 (2005) 1-33.

[10] N. Manolova, I. Rashkov, F. Beguin, H. Vandamme, Amphiphilic Derivatives Of Fullerenes Formed By Polymer Modification. Chem Comm (1993) 1725-1727.

[11] B.M. Babior, R.S. Kipnes, J.T. Curnutte, Biological defense mechanisms. The production by leukocytes of superoxide, a potential bactericidal agent. J Clin Invest 52(3) (1973) 741-744.

[12] H. Winn, Journal of the National Cancer Institute Monographs 2 (1959) 113.

[13] J. Moan, K. Berg, The photodegradation of porphyrins in cells can be used to estimate the lifetime of singlet oxygen. Photochem Photobiol 53(4) (1991) 549-553.

Chapter 5

A hydroxyapatite-associating agent of pamidronate-modified pullulan for bone regeneration imaging

INTRODUCTION

With the recent development of molecular or cell biology and tissue engineering, it has been practically possible to treat diseases based on the natural-healing potential of patients themselves. This is called the therapy of regeneration medicine and has been expected as a new medical treatment. Some animal and clinical trials have been successfully performed to regenerate and repair injured or defection tissues, such as bone, cartilage, skin, and nerve tissues by making use of cells and biomaterials for the DDS of growth factors and cell scaffolds [1-6]. However, the technology and methodology to evaluate the tissue regeneration and repairing still depend on histological [7], biochemical [8], and morphological examinations [9] of conventional diagnosis and the clinical availability of examination methods were limited in terms of their invasiveness and reliability. In addition, they cannot be always applied to observe the change with the passage of time which is important to accurately evaluate the process of tissue regeneration. Under these circumstances, it is necessary to develop a new diagnosis system for the non-invasive evaluation of tissue regeneration in the time sequence fashion.

Noninvasive imaging technologies, such as MRI, PET, SPECT, NIRF imaging, and CT, have been widely used in clinical diagnosis. However, each imaging modality is based on quite different principles and has the advantages and disadvantages. Generally, a single technique does not always correspond to all the requirements for diagnosis imaging [10]. As one trial to tackle the issue, it is practically possible to design a multimodal imaging system. A combinational imaging system composed of different imaging

modalities may compensate the deficiencies of single imaging modality, while it gives useful and new tools to biomedical researches and clinical diagnosis. Currently, some prototypes of multimodal imaging system including MRI–optical, NIRF–SPECT, PET-CT, and SPECT-MRI, have been introduced [11-14]. However, the research and development of multimodal imaging probes are still in an early stage although they are highly required to realize the idea of multimodal imaging.

Generally, bone healing and repairing have been diagnosed so far by CT, X-ray, and MRI to obtain the clinical reliability. However, the convention imaging methods cannot always provide detailed information about soft and bone tissues regenerated even in the early stage [15, 16] and there have been a few studies on bone-specific imaging probes [17]. If a multimodal imaging system based on new material, technology, and methodology can be developed to evaluate the bone tissue regenerated, bone repairing achieved by the idea of regeneration therapy will be more reliably diagnosed and become a new therapeutic strategy. In addition, the system can also give a diagnostic way to evaluate whether or not the process of bone tissue regeneration takes place properly. For this purpose, the combination of MRI with a superior property of seeing through as well as a high spatial resolution and optical imaging with a high sensitivity and specificity would be a promising choice. To design and prepare such a multimodal imaging system, it is also of prime necessity to make use of DDS technology to enhance the accumulation of imaging agents in the target tissue, resulting in the increased S/N ratio.

In this study, pamidronate (PA), which is one type of bisphosphonates with a high affinity for the hydroxyapatite (HA) of bone tissues [18, 19], was introduced to pullulan with different molecular weights (PA-pullulan). Next, fluorescence and MR imaging probes were introduced to prepare PA-pullulan conjugates containing two imaging probes (PA-pullulan-F/M). The affinity of PA-pullulan-F/M conjugates to the HA and the in vivo

fluorescence imaging of bone tissue ectopically formed were evaluated in terms of the molecular weight of pullulan conjugated. The in vitro MRI activity of PA-pullulan-F/M conjugates was also examined.

EXPERIMENTAL

Materials and reagents

Pullulan with weight-average molecular weights of 6,000, 12,000, and 23,000 were purchased from Hayashibara Biochemical Laboratories, Inc., Okayama, Japan. Pamidronic acid sodium salt (PA) was purchased from Toronto Research Chemicals Inc., North York, ON, Canada. CDI and ethylenediamine were purchased from Wako Pure Chemical Industries, Ltd., Osaka, Japan. HA beads (Type II, the average diameter=40 μm) was purchased from Bio-Rad Laboratories, Inc., Hercules, CA. Cy5.5 and Cy5 mono-functional N-hydroxysuccinimidyl esters (Cy5.5-NHS and Cy5-NHS) were purchased from GE Healthcare, Ltd., Buckinghamshire, UK, BMP-2 was kindly obtained from Yamanouchi Pharmaceutical Co., Japan. Buckinghamshire, UK. DTPA anhydride and TNBS were purchased from Sigma-Aldrich Co., St Louis, MO and Nakalai Tesque Inc., Kyoto, Japan, respectively. All the chemicals were used as obtained and without further purification.

Chemical conjugation of pullulan to PA

PA was introduced to the hydroxyl groups of pullulan by a CDI activation method [20]. Briefly, various molar amounts of CDI were added to 10 ml of dehydrated DMSO containing 100 mg of pullulan. The molar ratio of CDI initially added to the hydroxyl groups of pullulan was defined as a [CDI]/[OH] ratio. Following agitation using a magnetic stirrer at room temperature for 3 hr, the reaction mixture was precipitated by

absolute ethanol. The precipitate was washed several times with absolute ethanol and redissolved in 10 ml of 0.1 M carbonate buffer (pH 9.4) containing 20 mg PA, followed by agitation for 24 hr at room temperature. The reaction mixture was purified by a gel filtration of a PD-10 column (GE healthcare UK ltd., Buckinghamshire, UK) with DDW, and then freeze-dried to obtain the PA-introduced pullulan (PA-pullulan). The unreacted PA was determined by the TNBS method [21] to assess the percentage of PA introduced.

Introduction of imaging probes to PA-pullulan

Ethylenediamine was similarly introduced to the hydroxyl groups of pullulan by the CDI activation method as described above. Briefly, CDI and ethylendiamine were added to 10 ml of dehydrated DMSO containing 100 mg of PA-pullulan. Following agitation at room temperature for 24 hr, the reaction mixture was precipitated by absolute ethanol, washed with absolute ethanol, and redissolved in 10 ml of DDW. After freeze-drying, the aminized PA-pullulan (PA-pullulan-NH_2) was obtained and the percentage of amino groups introduced was determined by the TNBS method.

The PA-pullulan-NH_2 was dissolved in 1 ml of dehydrated DMSO, and then to the DMSO solution, Cy5.5-NHS and DTPA anhydride were added in various addition ratios. After reaction in room temperature for 6 hr, the reaction mixture was precipitated by absolute ethanol. The precipitate was redissoved in DDW, and the solution pH was adjusted to 6.5 by the addition of 1N NaOH aqueous solution. Then, 100 μg of gadolinium acetate was added to the solution, followed by 1 hr leaving for Gd^{3+} chelation to obtain Gd^{3+}-chelated PA-pullulan-Cy5.5/DTPA (PA-pullulan-F/M). The PA-pullulan-F/M was purified by a PD-10 column with DDW and the amount of Gd^{3+} ion in each elution fraction was measured by atomic absorption spectrophotometer (AA-6800, Shimazu, Kyoto,. Japan). For the histology examination, Cy5 introduced PA-pullulan-

F/M was prepared under the same conditions except to use Cy5-NHS in place of Cy5.5-NHS.

Evaluation of binding affinity of PA-pullulan-F/M for HA

The affinity of PA-pullulan-F/M to HA was evaluated according to a binding experiment reported previously [22, 23]. Briefly, 50 mg HA beads were suspended in 0.5 ml of saline and mixed with 0.2 ml of PA-pullulan-F/M saline solution. The mixture was placed at room temperature for 30 min with continuous mixing by vortex (1,000 rpm, Eppendorf thermomixer, Eppendorf AG, Hamburg, Germany) and then centrifuged at 4 ºC for 10 min at 20,000G (Eppendorf centrifuge 5417R, Eppendorf AG, Hamburg, Germany). The supernatant was carefully transferred to each well of 96-well assay plate (COSTAR® 3915, Corning Inc, NY, USA) and the fluorescent intensity of unbonded PA-pullulan-F/M in the solution form was measured by SpectraMax Gemini EM Fluorescence Microplate reader (Molecular Devices, sunnyvale CA, USA). Each experimental group is composed of 3 samples.

Preparation of mouse model of ectopic bone formation

A biodegradable hydrogel with a water content of 97.8 % was prepared through the chemical crosslinking of aqueous gelatin solution with glutaraldehyde according to the method described previously [24]. Briefly, 3 wt% gelatin aqueous solution containing 0.16 wt% glutaraldehyde was cast into a polypropylene dish (138×138 mm^2, BIO-BIK) , followed by crosslinking reaction at 4°C for 12 hr. The crosslinked hydrogel prepared was punched out to obtain the discs in 6 mm diameter. The hydrogel discs were stirred in 100 mM aqueous glycine solution at 37°C for 1 hr to block the residual aldehyde groups of glutaraldehyde. Following washing three times with DDW, the hydrogels were freeze-dried and sterilized with ethylene oxide gas.

To prepare a gelatin hydrogel incorporating BMP-2, 20 μl of aqueous solution containing 5 μg of BMP-2 was dropped onto the freeze-dried hydrogel, followed by leaving them at 4°C overnight. Then, the gelatin hydrogels incorporating BMP-2 was implanted into the back subcutis of ddY mice (male, 6W, Japan SLC, Inc, Shizuoka, Japan) to prepare a mouse model of ectopic bone formation. The mice prepared were used in the following imaging and histochemistry studies.

Fluorescence imaging of ectopic bone formation and calcification evaluation

To fluorescently evaluate the process of bone regeneration in the time-sequential fashion, the PA-pullulan-F/M conjugates prepared from pullulan with molecular weights of 6,000, 12,000, and 23,000 were injected intravenously into the mouse model of ectopic bone formation prepared at different time intervals for 4 weeks. The PA-pullulan-F/M was injected to the mice though the tail vein 0, 1, 2, 3, and 4 weeks after the hydrogel implantation, and 6 hr later, the mice were observed by an optical imaging system (LAS-4000, Fujifilm, Inc., Tokyo, Japan). After the fluorescence imaging experiment, the mice were sacrificed and the hydrogel implanted plus the surrounding soft tissues were taken out. The tissues obtained were cut into small pieces and digested in 1 N HCl solution in DDW for 1 week at room temperature with occasional mixing. After neutralization with 1 N NaOH, the supernatant solution was tested by a Calcium C kit (Wako Pure Chemical Industries, Ltd., Osaka, Japan) to determine the amount of calcium ions as a measure of bone formation. The experimental group is composed of 3 mice.

Histochemistry evaluation of bone tissue ectopically formed

Histological examination was performed for tissue around the hydrogel implanted of mice receiving various PA-pullulan-F/M conjugates. For mice 4 weeks after the hydrogel implantation, PA-pullulan-F/M conjugate was injected intravenously and 6 hr later, the mice were sacrificed and the skin tissue including the hydrogel implanted was

taken out. After the confirmation of bone generation by soft X-ray photography, the subcutaneous tissue including the gelatin hydrogel incorporating BMP-2 was embedded into Tissue-Tek (Sakura, Co., Ltd., Aichi, Japan), followed by freezing in liquid nitrogen. After fixation with ethanol, serial cryo-sections of the tissues (5 μm thickness) were prepared for the following staining and microscopic viewing.

The calcium deposition of tissues was visualized by the von Kossa staining according to the method described by Drury et al. [25]. Briefly, the sections were stained with silver nitrate with the irradiation of UV light for 20 min, followed by washing with sodium thiosulphate and DDW. The sections prepared were counter-stained by nuclear fast red and histologically viewed on a light microscope (AX-80, Olympus, Japan). In addition, the conventional hematoxylin and eosin (H&E) stain was also performed. On the other hand, the tissue sections of mice receiving the injection of PA-pullulan-F/M conjugate were viewed by using a confocal laser scanning microscopy system (LSM-510, Carl Zeiss, Jena, Germany) for the localization of conjugates while the control experiment was done for the tissue of saline-injected mice.

In vitro MRI studies of PA-pullulan-F/M

The contrast enhancement activity of PA-pullulan-F/M for MRI was evaluated by a 4.7 T horizontal MRI apparatus (Biospec, Bruker, Germany). The T1 relaxation time of PA-pullulan-F/M saline solution (0.2mM Gd^{3+} ion, room temperature) and Magnevist® of a MRI contrast agent commercially available (Japan Schering Inc., Osaka, Japan) was calculated under the following conditions: TR = 5000 ms, TE = 28 ms, FOV = 32 mm, matrix size = 256 × 256, slice thickness = 1.2 mm, number of slices = 1, number of average = 1, RARE factor = 4, TI = 62, 100, 300, 500, 800, 1000, 2000, 3000. Each experimental group is composed of 3 samples.

Statistical analysis

All the values were shown as the mean value±the standard deviation of the mean. The pairwise comparisons of individual group means were conducted based on the Tukey test. The value of $P<0.05$ was considered to be statistically significant.

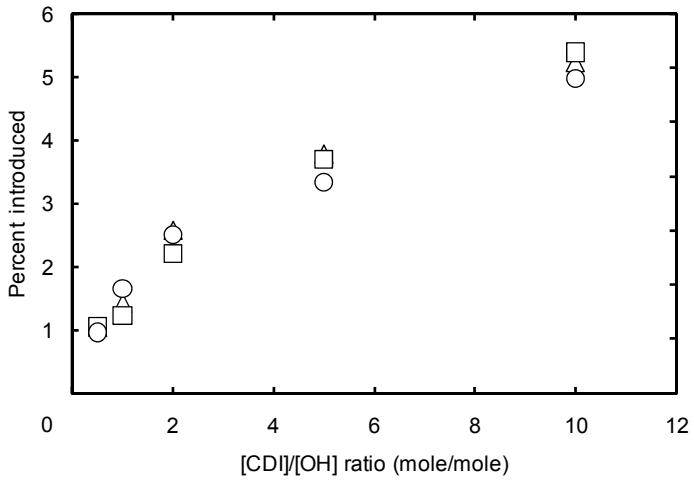

Figure 1. Effect of the initial addition ratio of CDI to OH groups on the percentage of PA introduced to pullulan with molecular weights of 6,000 (○), 12,000 (△), and 23,000 (□).

RESULTS

Preparation and characterization of PA-pullulan-F/M

PA was introduced to the hydroxyl groups of pullulan by the CDI activation method (**Figure 1**). The percentage of PA introduced could be changed by altering the amount of CDI added initially, irrespective of the pullulan molecular weight. **Figure 2A** shows the change of amino groups introduced in PA-pullulan before and after the introduction of ethylenediamine and Cy5.5/DTPA residues. Ethylenediamine was introduced to pullulan while Cy5.5 and DTPA residues were introduced into the amino groups of PA-pullulan. No effect of pullulan molecular weight on the percentage of amino groups and the subsequent Cy5.5 and DTPA residues introduced was observed (**Figure 2A**). On the other hand, the relative ratio of Cy5.5 and DTPA residues introduced

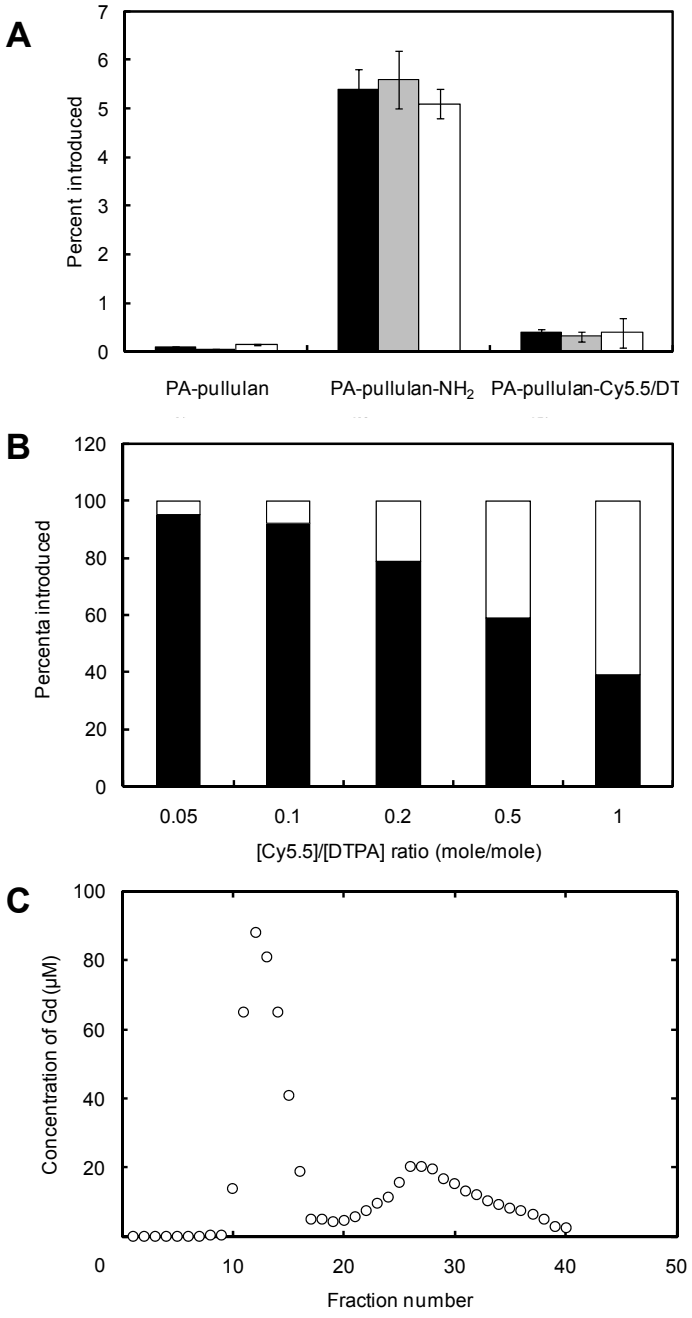

Figure 2. **A)** Change of amino groups introduced in PA-pullulan before and after the introduction of ethylenediamine (PA-pullulan-NH_2) and Cy5.5/DTPA residues of imaging probes (PA-pullulan-Cy5.5/DTPA). The molecular weight of pullulan used is 6,000 (black bars), 12,000 (gray bars) or 23,000 (white bars). The percentage of PA introduced is 3.8 mole%. **B)** Percentage of Cy5.5 (white area) and DTPA residues (black area) introduced to PA-pullulan in different ratios of Cy5.5 to DTPA anhydride added initially. The molecular weight of pullulan used is 6,000. The percentage of PA introduced is 3.8 mole%. **C)** The elution curve of Gd^{3+} ions for PA-pullulan-F/M prepared by mixing of PA-pullulan-Cy5.5/DTPA and Gd^{3+} ions. The molecular weight of pullulan used is 6,000. The percentage of PA introduced is 3.8 mole%.

to PA-pullulan could be controlled by changing the ratio of Cy5.5-NHS and DTPA anhydride added initially (**Figure 2B)**.

Figure 2C shows the elution curve of Gd^{3+} ions for mixed solution of PA-pullulan-Cy5.5/DTPA and Gd^{3+} ions. Two peaks were detected. One was attributed to Gd^{3+}-chelated PA-pullulan (high molecular weight fraction) and the other was for free Gd^{3+} ions (low molecular weight fraction). The similar elution pattern was observed for PA-pullulan-Cy5.5/DTPA prepared from pullulan different molecular weights (date not shown).

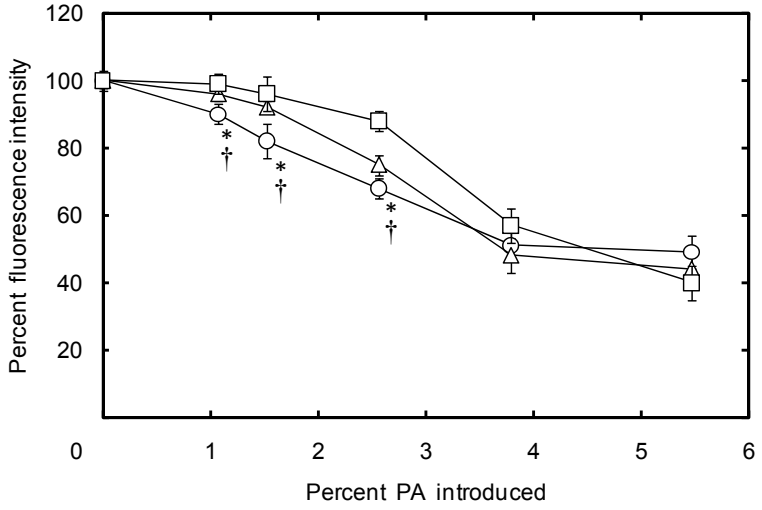

Figure 3. The binding profiles of PA-pullulan-F/M with different percentage of PA introduced to HA beads. The molecular weight of pullulan used is 6,000 (○), 12,000 (△) or 23,000 (□). The percentage of PA introduced is 3.8 mole% and the [Cy5.5]/[DTPA] ratio is 0.1. *, $p<0.05$: significance against the percent fluorescence of PA-pullulan-F/M prepared from pullulan with the molecular weight of 12,000. †, $p<0.05$: significance against the percent fluorescence of PA-pullulan-F/M prepared from pullulan with the molecular weight of 23,000.

Evaluation of binding affinity of PA-pullulan-F/M for HA

Figure 3 shows the binding profiles of PA-pullulan-F/M with different molecular weights and percentage of PA introduced to HA beads. The binding affinity of PA-pullulan-F/M increased with the increase of PA introduced, irrespective of the pullulan molecular weight while PA-free pullulan-F/M had no affinity for HA. When the

introduction percentage was less than 3.8 mole%, the binding affinity of PA-pullulan-F/M prepared from pullulan with the molecular weight of 6,000 was significantly higher than that of PA-pullulan-F/M prepared from pullulan with higher molecular weights. At the PA introduction ratio of 3.8 mole % or higher, the HA affinity of conjugates saturated to a certain level irrespective of the pullulan molecular weight. Therefore, the percentage of PA introduced was fixed at 3.8 mole % otherwise mentioned.

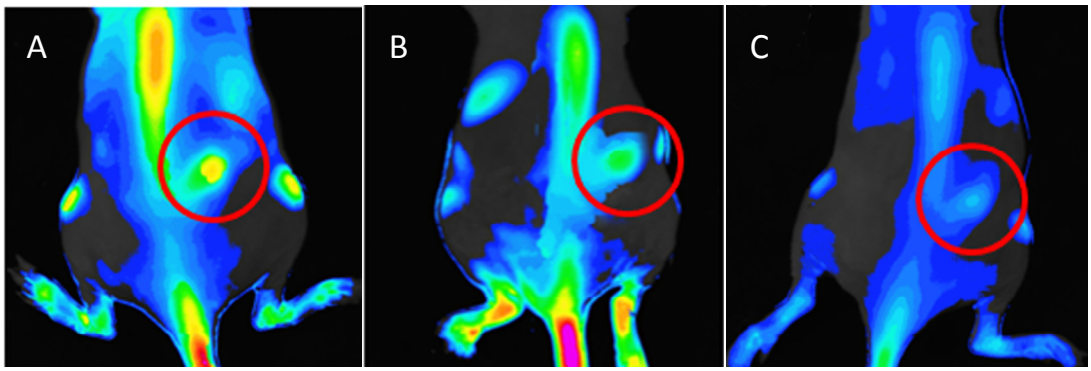

Figure 4. Fluorescence images of mice 6 hr after the intravenous injection of PA-pullulan-F/M prepared from pullulan with different molecular weights of 6,000 (A), 12,000 (B), and 23,000 (C). The injection was performed for mice 4 weeks after the hydrogel implantation. The percentage of PA introduced is 3.8 mole% and the [Cy5.5]/[DTPA] ratio is 0.1. The site implanted with hydrogel incorporating BMP-2 is indicated by a red circle.

Bone regeneration imaging by PA-pullulan-F/M

Figure 4 shows the fluorescence images of mice 6 hr after the intravenous injection of PA-pullulan-F/M prepared from pullulan with different molecular weights. It is apparent that the PA-pullulan-F/M prepared from pullulan with the molecular weight of 6,000 shows the strongest imaging around the site of bone tissue newly formed. **Figure 5** shows the fluorescent intensity of site around the hydrogel incorporating BMP-2 implanted 6 hr after the intravenous injection of PA-pullulan-F/M. The fluorescent

intensity of bone tissue of mice receiving the injection of PA-pullulan-F/M with the lowest molecular weight was significantly higher than that of other conjugates.

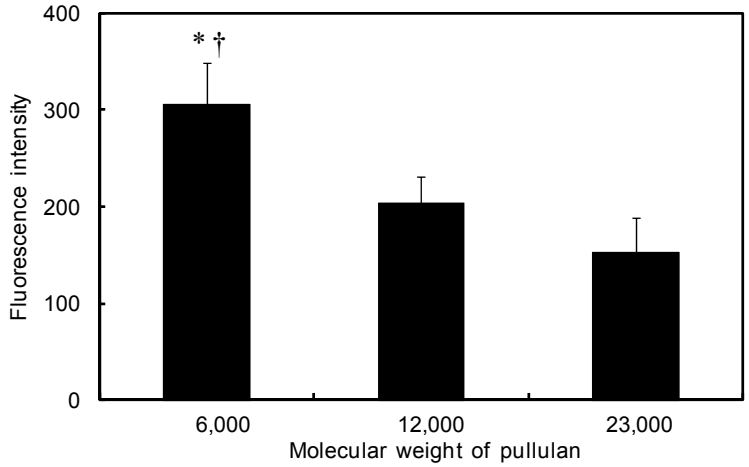

Figure 5. Fluorescent intensity of site around the hydrogel incorporating BMP-2 implanted 6 hr after the intravenous injection of PA-pullulan-F/M prepared from pullulan with different molecular weights of 6,000 (A), 12,000 (B), and 23,000 (C). The injection was performed for mice 4 weeks after the hydrogel implantation. The percentage of PA introduced is 3.8 mole% and the [Cy5.5]/[DTPA] ratio is 0.1. *, $p<0.05$: significance against the fluorescence intensity after the injection of PA-pullulan-F/M prepared from pullulan with the molecular weight of 12,000. †, $p<0.05$: significance against the fluorescence intensity after the injection of PA-pullulan-F/M prepared from pullulan with the molecular weight of 23,000.

Figure 6A shows the time profile of calcium concentration of subcutaneous tissues around gelatin hydrogels incorporating BMP-2 implanted. The calcium amount of bone tissue newly formed increased with time to reach a maximum level 3 weeks after implantation of hydrogel. **Figure 6B** shows the time profiles of fluorescent intensity of vertebral bone and the site around gelatin hydrogels incorporating BMP-2 implanted. The similar increase pattern was observed for the fluorescent intensity at the bone tissue ectopically formed, while the normal bone tissue showed a constant fluorescent intensity. In addition, the fluorescent intensity of bone tissue ectopically formed tended to increase with time to that of vertebral bone.

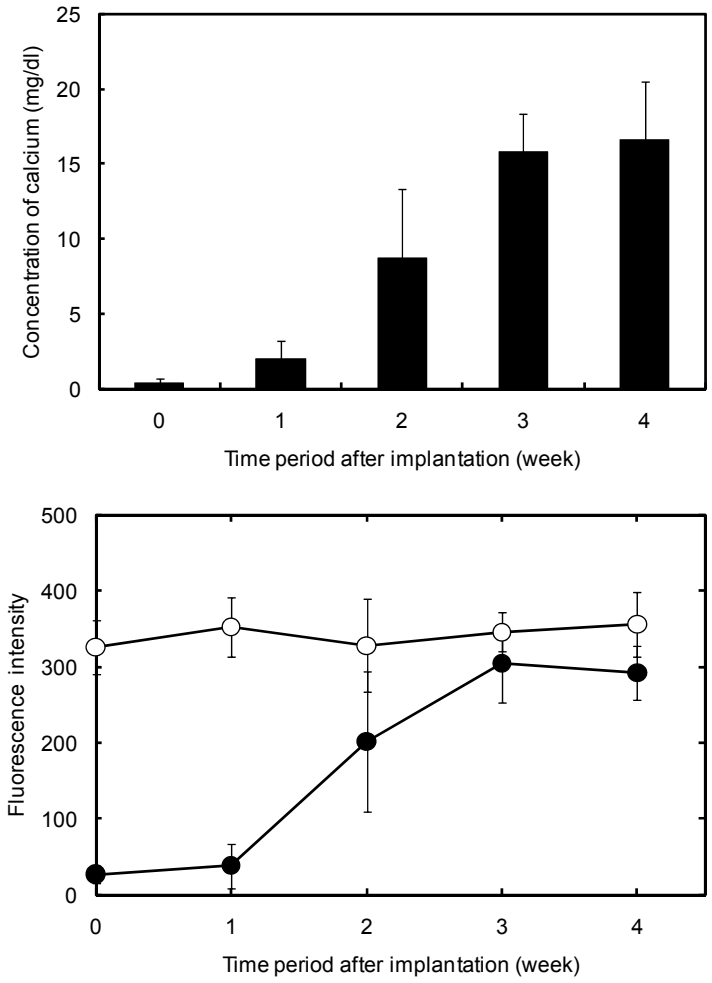

Figure 6. **A)** Time profile of calcium concentration of subcutaneous tissues around gelatin hydrogels incorporating BMP-2 implanted. **B)** Time profile of fluorescent intensity of normal vertebral bone (○) and the site around gelatin hydrogels incorporating BMP-2 implanted (●) 6 hr after the intravenous injection of PA-pullulan-F/M. The molecular weight of pullulan used is 6,000. The percentage of PA introduced is 3.8 mole% and the [Cy5.5]/[DTPA] ratio is 0.1.

Histochemical evaluation of bone tissue ectopically formed

Figure 7 shows the microscopic images of subcutaneous tissues 4 weeks after the implantation of gelatin hydrogel incorporating BMP-2. By using the hydrogel incorporating BMP-2, the bone formation around the hydrogel was observed histochemically. The calcium-deposited tissue area well corresponded to the bone tissue recognized by the H&E staining. Interestingly, the area of bone tissue newly formed was

clearly superposed with that of fluorescence contributing to the PA-pullulan-F/M conjugate intravenously injected. For the saline injection, such a fluorescent imaging was not observed around the site of hydrogel implanted.

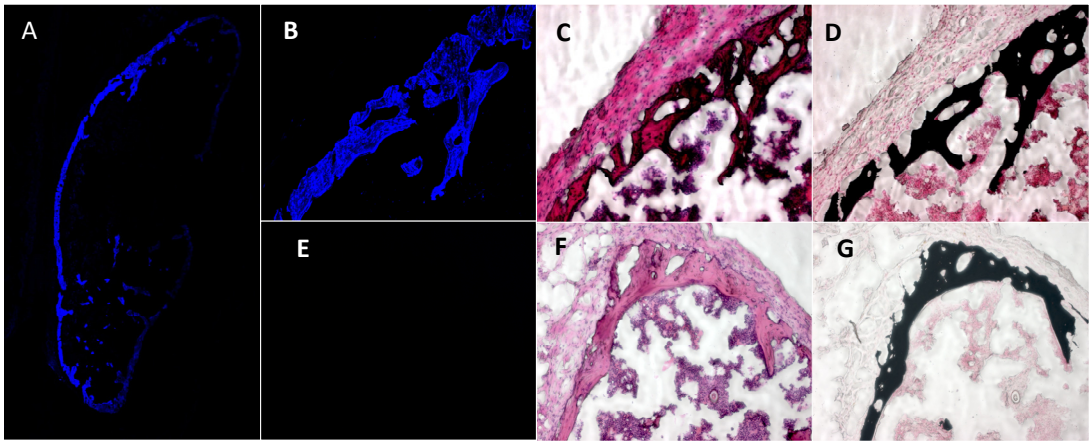

Figure 7. Microscopic images of subcutaneous tissue sections around gelatin hydrogel incorporating BMP-2 implanted. The tissues were taken out 6 hr after the intravenous injection of PA-pullulan-F/M (A-D) and saline (E-G) to mice 4 weeks after hydrogel implantation: fluorescence (A, B and E), H&E stained (C and F), and von Kossa stained sections (D and G). The molecular weight of pullulan used is 6,000. The percentage of PA introduced is 3.8 mole% and the [Cy5.5]/[DTPA] ratio is 0.1.

In vitro MRI studies of PA-pullulan-F/M

Table 1 shows the MRI contrast enhancement activity of PA-pullulan-F/M prepared from pullulan with different molecular weights. Irrespective of the pullulan molecular weight, every conjugate showed T1 relaxation times lower than DDW. The T1 relaxation time of PA-pullulan-F/M was even higher than that of Magnevist® in the same Gd^{3+} concentration. This result indicated the high contrast enhancement activity of PA-pullulan-F/M prepared.

Table 1. MRI contrast enhancement activity of PA-pullulan-F/M

Contrast agent	Molecular weight of pullulan	T1 relaxation times (ms)
None	-	1565
Magnevist®	-	289
[a)]PA-pullulan-F/M	6,000	159
[a)]PA-pullulan-F/M	12,000	128
[a)]PA-pullulan-F/M	23,000	132

[a)] The percentage of PA introduced is 3.8 mol% and the [Cy5.5]/[DTPA] ratio is 0.1.

DISCUSSION

The main objective of this study is to develop a DDS of non-invasive multimodal imaging for bone regeneration. For this purpose, we selected pamidronate which has a high affinity for the hydroxyapatite of bone tissues, as a targeting moiety for bone tissue regenerated. As expected, the pamidronate functioned well to enhance the hydroxyapatite affinity of pullulan. This was experimentally confirmed by the in vitro binding assay (**Figure 3**) and the in vivo accumulation at the site of bone tissue newly formed (**Figures 5**, **6**, and **7**).

The CDI method was effective in the chemical introduction of PA to pullulan as well as an intermediate derivative of ethylenediamine for the subsequent reaction with fluorescent (Cy5.5 and Cy5) and MR imaging probes (**Figures 1** and **2A**). It is apparent from **Figure 2A** that most of amino groups introduced were converted to the imaging probes and the relative ratio could be controlled by changing the ratio of imaging probes added initially (**Figure 2B**). It is well known that the detection sensitivity of fluorescence probes is much higher than that of MRI probes [26, 27]. However, for the combination imaging system, it is highly conceivable that the concentration of every probes in the target site to show the imaging activity can be anticipated based on the imaging

sensitivity. Therefore, in this study, the [Cy5.5]/[DTPA] ratio of 0.1 was selected (**Figure 2B**). It is not doubt that the ratio may affect the multimodal imaging ability. Further investigation should be done to optimize the sensitivity for a fluorescence-MR combination multimodal imaging.

The percentage of PA introduced and the molecular weight of pullulan affected the binding affinity of PA-pullulan-F/M conjugates for hydroxyapatite (**Figure 3**). When the amount of PA conjugated in one pullulan molecule enhanced, it is possible that the binding site of conjugates to hydroxyapatite increases, resulting an enhanced affinity of PA-pullulan-F/M. However, when the percent PA introduced was 3.8 mole% or higher, the binding affinity of PA-pullulan F/M became constant. It is apparent that the PA introduction increased with the [CDI]/[OH] ratio (**Figure 1**). Taken together, this finding indicates that the PA density contributing to the binding affinity has a threshold. The molecular weight of pullulan also affected the binding affinity of PA-pullulan-F/M. When the percentage of PA introduced was low, an increase in the molecular weight of pullulan decreased the binding affinity of PA-pullulan-F/M conjugates. However, at the higher percentage of PA introduced, the affinity became a similar level, irrespective of the molecular weight of pullulan. The reason may be explained by the steric hindrance of pullulan molecules. Longer chain of pullulan with higher molecular weight may result in many and long loops of polymer chains which cause steric hindrance to decrease the contact probability of PA with hydroxyapatite at the low percentage of PA introduced. On the other hand, when the percentage increased, the steric hindrance will be no longer essential and consequently the binding affinity was similar for any PA-pullulan-F/M conjugate. To achieve a high targetability to bone tissues, higher PA introduction ratio may be favorable. However, an excess of PA may cause some side effects because PA itself also has bioactivity [28, 29]. For these reasons, a balanced PA introduction ratio is

needed. Considering that the PA introduction ratio higher than 3.8 mol% do not contribute to their binding activity to HA any more, the percentage of PA introduced was selected at 3.8 mole% for all experiments.

For the in vivo fluorescent imaging, the PA-pullulan-F/M prepared from pullulan with the molecular weight of 6,000 showed significantly higher imaging ability than the others (**Figures 4 and 5**). Therefore, further in vivo imaging experiments were performed by using this conjugate. It is highly conceivable that the PA-pullulan-F/M prepared from pullulan with the low molecular weight has a smaller molecular size, which allows the conjugate to reach the bone tissue regenerated. It is well known that the new formation of blood vessels needs the formation of bone tissue [30]. The process is normally accompanied with inflammation reactions [31]. Considering the EPR effect [32] of blood vessels formed in inflammation, it is possible that the conjugate of small size tends to accumulate to a high extent compared with that of too large size. This is one of the reasons why the bone tissue accumulation of PA-pullulan-F/M conjugates had an influence on the molecular weight of pullulan. This type of molecular size selection by the wall of blood capillaries may take place around the bone tissue newly formed by BMP-2. In addition, the bone tissue composed of HA and organic substances may have a complex structure where the large-size imaging agent cannot reach to the HA component of tissue. Further investigation is needed to make clear the mechanism of molecular weight dependence.

After the implantation of gelatin hydrogel incorporating BMP-2 to the subcutis of mice, the ectopic bone regeneration was achieved. The ectopic model was selected in this study by the reason that bone tissue newly formed can be readily recognized histologically. We have demonstrated that the controlled release of BMP-2 effectively induced ectopically bone formation [2]. The calcium assay revealed that bone tissue was

formed over the time period of 4 weeks (**Figure 6A**). The similar time profile was observed for fluorescent intensity of PA-pullulan-F/M accumulated. The good correspondence of time profile between the calcium amount and fluorescent intensity strongly indicates the possibility that the progress of bone regeneration can be fluorescently evaluated by the PA-pullulan-F/M. This is also confirmed by histological examinations (**Figure 7**). The area of calcium deposited which is confirmed by the von Kossa and H&E staining overlayed that of fluorescence emission from the PA-pullulan-F/M. For the saline injection, no fluorescence was detected at the area of calcium deposited. Taken together, it is clearly that the PA-pullulan-F/M was specifically bound to the calcium in the bone tissue regenerated, resulting in the achievement of fluorescence imaging thereat. The PA-pullulan-F/A had a high MRI contrast enhancement activity similar to the Magnevist® of clinical use (**Table 1**). This allows us to imagine that the PA-pullulan-F/M also functions as the MRI system to evaluate the process of bone regeneration. In addition, it is well known that DTPA has high chelate stability to many metal ions, this character make it possible to readily introduce another radioactive isotope for the scintigraphy, PET and SPECT imaging. These possibilities are now under investigation.

REFERENCES

[1] Y. Tabata, S. Hijikata, M. Muniruzzaman, Y. Ikada, Neovascularization effect of biodegradable gelatin microspheres incorporating basic fibroblast growth factor. J Biomater Sci Polym Ed 10(1) (1999) 79-94.

[2] M. Yamamoto, Y. Takahashi, Y. Tabata, Controlled release by biodegradable hydrogels enhances the ectopic bone formation of bone morphogenetic protein. Biomaterials 24(24) (2003) 4375-4383.

[3] M. Itoh, Y. Hiraoka, K. Kataoka, N.H. Huh, Y. Tabata, H. Okochi, Novel collagen sponge reinforced with polyglycolic acid fiber produces robust, normal hair in murine hair reconstitution model. Tissue Eng 10(5-6) (2004) 818-824.

[4] K. Kojima, R.A. Ignotz, T. Kushibiki, K.W. Tinsley, Y. Tabata, C.A. Vacanti, Tissue-engineered trachea from sheep marrow stromal cells with transforming growth factor beta2 released from biodegradable microspheres in a nude rat recipient. J Thorac Cardiovasc Surg 128(1) (2004) 147-153.

[5] S. Bajada, I. Mazakova, J.B. Richardson, N. Ashammakhi, Updates on stem cells and their applications in regenerative medicine. J Tissue Eng Regen Med 2(4) (2008) 169-183.

[6] A. Marui, Y. Tabata, S. Kojima, M. Yamamoto, K. Tambara, T. Nishina, Y. Saji, K. Inui, T. Hashida, S. Yokoyama, R. Onodera, T. Ikeda, M. Fukushima, M. Komeda, A novel approach to therapeutic angiogenesis for patients with critical limb ischemia by sustained release of basic fibroblast growth factor using biodegradable gelatin hydrogel: an initial report of the phase I-IIa study. Circ J 71(8) (2007) 1181-1186.

[7] K. Lysiak-Drwal, M. Dominiak, L. Solski, B. Zywicka, S. Pielka, T. Konopka, H. Gerber, Early histological evaluation of bone defect healing with and without guided

bone regeneration techniques: experimental animal studies. Postepy Hig Med Dosw (Online) 62 (2008) 282-288.

[8] E. Daglioglu, M.S. Dike, K. Kilinc, D. Erdogan, G. Take, F. Ergungor, O. Okay, Z. Biyikli, Neuroprotective effect of melatonin on experimental peripheral nerve injury: an electron microscopic and biochemical study. Central European neurosurgery. Central European neurosurgery 70(3) (2009) 109-114.

[9] X.B. Fu, T.Z. Sun, X.K. Li, Z.Y. Sheng, Morphological and distribution characteristics of sweat glands in hypertrophic scar and their possible effects on sweat gland regeneration. Chin Med J (Engl) 118(3) (2005) 186-191.

[10] T.F. Massoud, S.S. Gambhir, Molecular imaging in living subjects: seeing fundamental biological processes in a new light. Genes Dev 17(5) (2003) 545-580.

[11] K. Chtourou, M. Maloul, F. Kallel, S. Charfedine, F. Hamza, F. Guermazi, SPECT and MRI fusion for an extended bilateral osteonecrosis. Eur J Nucl Med Mol Imaging 35(12) (2008) 2343.

[12] V. Ntziachristos, A.G. Yodh, M. Schnall, B. Chance, Concurrent MRI and diffuse optical tomography of breast after indocyanine green enhancement. Proc Natl Acad Sci U S A 97(6) (2000) 2767-2772.

[13] T. Beyer, D.W. Townsend, T. Brun, P.E. Kinahan, M. Charron, R. Roddy, J. Jerin, J. Young, L. Byars, R. Nutt, A combined PET/CT scanner for clinical oncology. J Nucl Med 41(8) (2000) 1369-1379.

[14] O. Veiseh, C. Sun, J. Gunn, N. Kohler, P. Gabikian, D. Lee, N. Bhattarai, R. Ellenbogen, R. Sze, A. Hallahan, J. Olson, M. Zhang, Optical and MRI multifunctional nanoprobe for targeting gliomas. Nano Lett 5(6) (2005) 1003-1008.

[15] D. Berthoty, P. Haghighi, D.J. Sartoris, D. Resnick, Osseous invasion by soft-tissue sarcoma seen better on MR than on CT. AJR Am J Roentgenol 152(5) (1989) 1131.

[16] J.J. Peterson, L.W. Bancroft, M.J. Kransdorf, Principles of bone and soft tissue imaging. Hand Clin 20(2) (2004) v, 147-166.

[17] J. de Boer, C. van Blitterswijk, C. Lowik, Bioluminescent imaging: emerging technology for non-invasive imaging of bone tissue engineering. Biomaterials 27(9) (2006) 1851-1858.

[18] D. Wang, S.C. Miller, P. Kopeckova, J. Kopecek, Bone-targeting macromolecular therapeutics. Adv Drug Deliv Rev 57(7) (2005) 1049-1076.

[19] R. Graham, G. Russell, Determinants of structure-function relationships among bisphosphonates. Bone 40 (2007) S21-S25.

[20] G.T. Hermanson, Bioconjugate techniques, Academic Press, 1996.

[21] T.G.M. Schalkhammer, Analytical biotechnology Springer, 2002.

[22] H. Uludag, N. Kousinioris, T. Gao, D. Kantoci, Bisphosphonate conjugation to proteins as a means to impart bone affinity. Biotechnol Prog 16(2) (2000) 258-267.

[23] M.F. Jarvis, C.J. Burns, H.W. Pauls, A. Assal, J.S. Kim, D.L. Cheney, R.D. Youssefyeh, Characterization of the bisphosphonate recognition site on hydroxyapatite using radioligand binding techniques with [14C]citric acid. Calcif Tissue Int 52(5) (1993) 372-377.

[24] M. Yamamoto, Y. Tabata, L. Hong, S. Miyamoto, N. Hashimoto, Y. Ikada, Bone regeneration by transforming growth factor beta1 released from a biodegradable hydrogel. J Control Release 64(1-3) (2000) 133-142.

[25] R. Drury, E. Wallington, Demonstration of calcium salts. In: Carleton's Histological Techniques, 5th ed., Oxford University Press, 1980.

[26] V.M. Runge, J.W. Wells, Update: safety, new applications, new MR agents. Top Magn Reson Imaging 7(3) (1995) 181-195.

[27] W. Mason, Fluorescent and luminescent probes for biological activity, Academic Press, London, 1999.

[28] M.C. Lodder, P.A. Van Pelt, W.F. Lems, P.J. Kostense, C.H. Koks, B.A. Dijkmans, Effects of high dose IV pamidronate on disease activity and bone metabolism in patients with active RA: a randomized, double-blind, placebo-controlled trial. J Rheumatol 30(9) (2003) 2080-2081.

[29] E. Terpos, J. Palermos, K. Tsionos, K. Anargyrou, N. Viniou, P. Papassavas, J. Meletis, X. Yataganas, Effect of pamidronate administration on markers of bone turnover and disease activity in multiple myeloma. Eur J Haematol 65(5) (2000) 331-336.

[30] L.R. Amir, A.G. Becking, A. Jovanovic, F.B. Perdijk, V. Everts, A.L. Bronckers, Formation of new bone during vertical distraction osteogenesis of the human mandible is related to the presence of blood vessels. Clin Oral Implants Res 17(4) (2006) 410-416.

[31] C.H. Rundle, H. Wang, H. Yu, R.B. Chadwick, E.I. Davis, J.E. Wergedal, K.H. Lau, S. Mohan, J.T. Ryaby, D.J. Baylink, Microarray analysis of gene expression during the inflammation and endochondral bone formation stages of rat femur fracture repair. Bone 38(4) (2006) 521-529.

[32] H. Maeda, J. Wu, T. Sawa, Y. Matsumura, K. Hori, Tumor vascular permeability and the EPR effect in macromolecular therapeutics: a review. J Control Release 65(1-2) (2000) 271-284.

SUMMARY

Chapter 1

The objective of this study is to investigate the effect of molecular size and terminal structure of PEG on the antitumor activity of PEG-modified fullerene (C_{60}). The PEG samples with different terminal structures and molecular weights were covalently coupled to C_{60} and their superoxide anion generation, in vitro or in vivo antitumor activity, and body distribution were assessed for the photosensitizer of PDT on tumor. Irrespective of the molecular weight and terminal structure of PEG used, the C_{60}-PEG conjugates exhibited the similar ability of superoxide anion generation ability and in vitro antitumor activity. On the contrary, the strong activity to suppress the in vivo tumor growth was observed for the C_{60}-PEG conjugates prepared by methyl-terminated PEG with the highest molecular weight, which showed the longest half-life period of blood circulation and the highest tumor accumulation among all the conjugates used. It is concluded that a superior tumor targetability of C_{60}-PEG conjugates is one of the keys to enhance the PDT activity.

Chapter 2

To design a novel cytospecific photosensitizer for photodynamic antitumor therapy, a fullerene (C_{60}) was chemically modified with pullulan which is a water-soluble polysaccharide with a high affinity for asialoglycoprotein receptors. Ethylene diamine was introduced to the terminal aldehyde groups of pullulan by the reductive amination reaction. Pullulan was coupled to C_{60} through the terminal amine group. The C_{60} end-group conjugated with pullulan was water-soluble and generated superoxide anion upon light irradiation. The C_{60}-pullulan conjugates significantly suppressed the in vitro growth

of HepG2 hepatoma cells with asialoglycoprotein receptors, while less suppression activity was observed for HeLa cells without the receptors. The conjugates have a high binding affinity for HepG2 cells, in contrast to HeLa cells. When C_{60} was conjugated with PEG with the similar molecular weight to compare the in vitro cell binding and antitumor activities with the C_{60}-pullulan conjugate, the dependence of cell type on their activities was not observed. Following the intravenous injection of C_{60}-pullulan conjugates to mice carrying a subcutaneous mass of HepG2 cells, significant stronger photodynamic effect on tumor was observed than the intravenous injection of C_{60}-PEG conjugates and saline. It is concluded that the pullulan conjugation gave C_{60} the targetability to HepG2 cells, resulting in enhanced photodynamic tumor therapy effect.

Chapter 3

To design a novel cytospecific photosensitizer for photodynamic antitumor therapy, a fullerene (C_{60}) was chemically modified with pullulan which is a water-soluble polysaccharide with a high affinity for ASGPR. The effect of pullulan molecular weight and the modification manner to C_{60} on the photodynamic antitumor activity of C_{60} modified with pullulan was evaluated. In this study, two modification manners were selected. First, ethylene diamine was chemically introduced to the hydroxyl groups of pullulan with different molecular weights. Then, C_{60} was coupled to pullulan through the amino group introduced (pendant type). Second, ethylene diamine was introduced to the terminal aldehyde group of pullulan by the reductive amination reaction, and then the pullulan with the terminal amino group was coupled to C_{60} (terminal type). Irrespective of the pullulan molecular and the modification manner, the C_{60}-pullulan conjugates exhibited the similar ability to generate superoxide anions upon the irradiation of light. When compared between the C_{60}-pullulan conjugates of pendant and terminal types, a

high lectin affinity was observed for the latter conjugates. The conjugates showed a high affinity for HepG2 cells with ASGPR and the consequent strong in vitro antitumor activity on the cells. It is conclude that the manner of pullulan modification is a key factor contributing to the photodynamic antitumor activity of C_{60} modified.

Chapter 4

A novel photosensitizer with MRI activity was designed from fullerene (C_{60}) for efficient PDT of tumor. After chemical conjugation of PEG to C_{60} (C_{60}-PEG), DTPA was subsequently introduced to the terminal group of PEG to prepare PEG-conjugated C_{60} (C_{60}-PEG-DTPA). The C_{60}-PEG-DTPA was mixed with gadolinium acetate solution to obtain Gd^{3+}-chelated C_{60}-PEG (C_{60}-PEG-Gd). Following intravenous injection of C_{60}-PEG-Gd into tumor-bearing mice, the PDT anti-tumor effect and the MRI tumor imaging were evaluated. The similar $O_2^{\bullet-}$ generation was observed with or without Gd^{3+} chelation upon light irradiation. Both of the C_{60}-PEG-Gd and Magnevist® aqueous solutions exhibited a similar MRI activity. When intravenously injected into tumor-bearing mice, the C_{60}-PEG-Gd maintained an enhanced MRI signal at the tumor tissue for a longer time period than Magnevist®. Injection of C_{60}-PEG-Gd plus light irradiation showed significant tumor PDT effect although the effect depended on the timing of light irradiation. The PDT efficacy of C_{60}-PEG-Gd was observed at the time when the tumor accumulation was detected by the enhanced intensity of MRI signal. This therapeutic and diagnostic hybrid system is a promising tool to enhance the PDT efficacy for tumor.

Chapter 5

The objective of this study is to design a new multimodal imaging system to evaluate the process of bone regeneration. Pamidronate, one type of bisphosphonates with a high affinity for hydroxyapatite, was introduced to pullulan with molecular weights of 6,000, 12,000, and 23,000 (PA-pullulan). Then, two probes for fluorescence and MR imagings were introduced into the PA-pullulan to prepare the PA-pullulan conjugates containing both the imaging probes (PA-pullulan-F/M). The PA-pullulan-F/M conjugates had an affinity for hydroxyapatite and the extent increased with the amount of PA conjugated. A gelatin hydrogel incorporating BMP-2 was prepared and implanted subcutaneously into mice to obtain an animal model of bone regeneration. The calcium amount around the site implanted increased with time. When intravenously injected into mice with the bone tissue ectopically formed by the BMP-2 incorporated hydrogel to fluorescently evaluate their body distribution, the PA-pullulan-F/M conjugates were accumulated in the bone tissue regenerated. The highest amount of tissue accumulation was observed for the PA-pullulan-F/M conjugate prepared from pullulan with the molecular weight of 6,000. The time profile of fluorescent intensity well corresponded with that of calcium amount in the bone tissue newly formed. In addition, the PA-pullulan-F/M conjugates showed a MRI activity similar to Magnevist® of MRI agent clinically used. It is concluded that the PA-pullulan-F/M conjugate is a useful multimodal agent of DDS to evaluate the process of bone regeneration.

LIST OF PUBLICATIONS

Chapter 1

Jian. Liu and Yasuhiko Tabata, Photodynamic antitumor activity of fullerene modified by polyethylene glycol with different molecular weights and terminal structures, Journal of Biomaterials Science: Polymer Edition, in press.

Chapter 2

Jian. Liu and Yasuhiko Tabata, Photodynamic therapy of fullerene modified with pullulan on hepatoma cells, Journal of Drug Targeting, in press.

Chapter 3

Jian. Liu and Yasuhiko Tabata, Effect of modification manner on photodynamic antitumor activity of C_{60} modified with pullulan, submitted.

Chapter 4

Jian Liu, Shin-ichi Ohta, Akinaga Sonoda, Masatoshi Yamada, Masaya Yamamoto, Norihisa Nitta, Kiyoshi Murata, and Yasuhiko Tabata, Preparation of PEG-conjugated fullerene containing Gd^{3+} ions for photodynamic therapy. Journal of Controlled Release 117(1) (2007) 104-110.

Chapter 5

Jian. Liu, Masaya Yamamoto, Jun-ichiro Jo, and Yasuhiko Tabata, A Hydroxyapatite-associated agent of pamidronate-modified pullulan for bone regeneration imaging, submitted.

ACKNOWLEDGEMENT

This research was carried out under the guidance of Dr. Yasuhiko Tabata, profesor of Institute for Frontier Medical Science, Kyoto University. The author is deeply indebted to professor Tabata for his constant guidance, encouragement, valuable discussion, informative advice, and rational criticism on whole experiments as well as the manuscript through the present work. The author also likes take an opportunity to extend his heartily to thank for Prof. Tabata not only in the present research, but also in his whole overseas life. The completion of the present research has been an exciting project and one which would not have been realized without his guidance and kindly help over the author's daily life.

The author wishes to express his special thanks to Dr. Masaya Yamamoto, Institute for Frontier Medical Science, Kyoto University, for his thoughtful guidance, encouragement, cooperation, valuable advice and discussion and his kindly help over the author's overseas life.

The author wishes to express his deeply thanks to Dr. Kiyoshi Murata, Dr. Norihisa Nitta, Dr. Shin-ichi Ohta, and Dr. Akinaga Sonoda, Department of Radiology, Shiga University of Medical Science, Otsu City, Shiga Japan for their cooperation, advice, and discussion in Chapter 4.

The author wishes to express his deeply thanks to Mr. Masatoshi Yamada, Research and Development Division, Nippon Kayaku Co, Ltd, Tokyo, Japan for his cooperation, advice, and discussion in Chapters 1 and 4.

The author wishes to express his deeply thanks to Dr. Ichio Aoki, Molecular Imaging Center, National Institute of Radiological Sciences, Chiba, Japan and Dr. Yuko

Kawai, Meiji University of Integrative Medicine, Nantan-shi, Kyoto, Japan for their cooperation, advice, and discussion in chapter 5.

The author is much indebted to Dr. Jun-ichiro Jo for his contribution to the present studies and great help for preparation of this manuscript.

The author wishes to express his thanks to Dr. Yu Kimura and Dr. Sachiko Inoue for their help to his experiment and life in Tabata Lab.

The author wishes to express his deeply thanks to Mrs. Miyuki Fukuma, Ms. Hisako Yoshida and Ms. Kyoko Bamba, secretary to professor Tabata, for their help and kindness.

The author would like to take an opportunity to extend his heart thanks to his perients, Shude Liu and Feng Gao. The author also wishes to express his sincere appreciation to his wife, Yifei Sun, who give his a warm family and always encouraged him in his study.

Finally, the author is thankful to JASSO of Ministry of Education, Culture, Sports, Science and Technology, Japan and Nitori International Scholarship Foundation, for providing the scholarship to pursue the author's doctoral course.

January, 2010

Kyoto, Japan

Jian Liu